Climbing Quantum Ladder Systems by Ultrashort Infrared Laser Pulses

Het Beklimmen van Quantum Ladder-Systemen met behulp van Ultrakorte Infrarode Laserpulsen

Climbing Quantum Ladder Systems by Ultrashort Infrared Laser Pulses

Het Beklimmen van Quantum Ladder-Systemen met behulp van Ultrakorte Infrarode Laserpulsen

Academisch Proefschrift

ter verkrijging van de graad van doctor
aan de Universiteit van Amsterdam,
op gezag van de Rector Magnificus
prof.dr. J. J. M. Franse ten overstaan
van een door het college voor promoties
ingestelde commissie in het openbaar te
verdedigen in de Aula der Universiteit
op vrijdag 27 maart 1998 te 9:00 uur

door

Diederik Jan Maas

geboren te Utrecht

Promotiecommissie

Promotor	prof.dr.ir. H. B. van Linden van den Heuvell
Copromotores	dr. L. D. Noordam
	prof.dr. W. J. van der Zande
Overige leden	prof.dr. A. W. Kleyn
	prof.dr. C. A. de Lange
	dr. A. F. G. van der Meer
	prof.dr. S. Stolte
	dr. G. H. Wegdam

Faculteit der Wiskunde, Informatica, Natuur- en Sterrenkunde

Cover design in co-operation with Susan Ketelaars and Armando Cairo

The work described in this thesis was performed at the following institutes:

FOM Institute for Atomic and Molecular Physics,
Kruislaan 407, 1098 SJ Amsterdam, the Netherlands.

FOM Institute for Plasma Physics “Rijnhuizen”,
Edisonbaan 14, 3439 MN Nieuwegein, the Netherlands.

This work is part of the research program of the Stichting voor Fundamenteel Onderzoek der Materie (Foundation for Fundamental Research on Matter) and was made possible by financial support from the Nederlandse Organisatie voor Wetenschappelijk Onderzoek (Netherlands Organization for the Advancement of Research).

aan mijn ouders
aan Susan

This thesis is based on the following publications:

Chapter 1	D. J. Maas, D. I. Duncan, A. F. G. van der Meer, W. J. van der Zande, and L. D. Noordam, *Vibrational ladder climbing in NO by ultrashort infrared laser pulses*, Lambropoulos and Walter, *ed.* Multiphoton Procces 1996, Institute of Physics Conference Series No. **154**, 308 (1997) Institute of Physics Publishing, Bristol and Philadelphia
	R. B. Vrijen, G. M. Lankhuijzen, D. J. Maas, and L. D. Noordam, *Adiabatic population transfer in multiphoton processes*, Comments At. Mol. Phys. **33**, 6 (1996).
Chapter 2	P. Balling, D. J. Maas, and L. D. Noordam, *Interference in climbing a quantum ladder system with frequency-chirped laser pulses*, Phys. Rev. A **50**, 4276 (1994).
Chapter 3	D. J. Maas, C. W. Rella, Ph. Antoine, E. S. Toma, and L. D. Noordam, *Total population transfer on the rubidium* $5s$-$5p$-$5d$-ϵ_p/ϵ_f *ladder*, Phys. Rev. A. **59**, 1374 (1999).
Chapter 4	D. J. Maas, D. I. Duncan, A. F. G. van der Meer, W. J. van der Zande, and L. D. Noordam, *Vibrational ladder climbing in NO by ultrashort infrared laser pulses*, Chem. Phys. Lett. **270**, 45 (1997).
Chapter 5	D. J. Maas, D. I. Duncan, R. B. Vrijen, W. J. van der Zande, and L. D. Noordam, *Vibrational ladder climbing in NO by (sub)picosecond frequency-chirped infrared laser pulses*, Chem. Phys. Lett. **290**, 75 (1998).
Chapter 6	D. J. Maas, M. J. J. Vrakking, and L. D. Noordam, *Rotational interference in vibrational ladder climbing in NO by chirped infrared laser pulses*, Accepted for: Phys. Rev. A**60**, (1999)

Contents

CHAPTER 1

INTRODUCTION

1.1 Motivation

The fields of physics and chemistry have emerged from the more general domain of Philosophy and Science during the 19^{th} century. Subject of interest of both fields is the interaction between the various manifestations of “dead matter”. The approach of this subject has been different for each field. Crudely put, chemistry poses the more pragmatic “How. . . ?”-questions, while physics deals with “Why. . . ?”. Each of these classes of questions and both fields have their own merits and have contributed to progress in the understanding of nature and the control over the outcome of chemical processes. Chemist investigate how the different building bricks of matter can recombine with each other, creating new forms of matter. This has lead to a wealth of knowledge on reaction control by handles like mixture, temperature, dopants, catalysts, acidity and many more, enabling the production of the desired final product [1–3]. The reason why a specific environment is so well suited for making a specific form of matter should be explicable from the basic properties of the reactants and reaction circumstances. The study of the fundamental attributes of matter is the field of physicists, who have developed a high degree of the understanding of interactions on the molecular, atomic or even sub-atomic level. This achievement has yielded a stunning degree of control over the exact quantum state of a particle (e.g., see [4–6], to name just a few among many other stunning discoveries). Of course the bi-partition in “How. . . ?” and “Why. . . ?” is much too crude, but it illustrates the general notion of the pragmatic attitude of chemists, versus the philosophical angle of attack of physicists.

The progress that has been made in physics and chemistry during the last two centuries is enormous, and the Top-Down approach of chemistry, that started with exploring the macroscopic attributes of matter, begins to meet the Bottom-Up advancements in understanding interactions at a microscopic scale made in physics. Nowadays, the common interest in reaction dynamics, one of the shared subjects of study, is reflected in the rapid growth of fields like Physical Chemistry and Chemical Physics. Especially advances in present day laser technology and computational methods have enabled many chemists to perform detailed studies of problems that were too complex to deal with in earlier days. So far chemists have succeeded in gaining more and more control over the rate of reactions and the quality of the final products by improving catalyst technology, which lowers the energy barrier of a certain reaction. Still, the selected outcome is determined by the laws of thermodynamics. Present day laser technology offers the possibility to alter the precise quantum state of the initial reactants by adding extra energy and hence lower the barrier for specific states only, enabling state-selective chemistry. Vibrational ladder climbing by ultrafast laser pulses can develop itself as a valuable tool in achieving active control over the population distribution over the internal states of one or more reactants. In the next section a state-of-the-art example illustrating the current state of affairs is discussed, which introduces the main concepts of state-selective chemistry to the reader.

One of the goals in (physical) chemistry is to achieve control over chemical reactions [7–9]. Since most chemical reactions are accelerated by heating, catalysts, dopants, acidity, et cetera, control over these parameters of the reactants is the most commonly used handle to retrieve the desired reaction products. For example, raising the temperature allows a larger fraction of the molecules to occupy an excited vibrational state. Although manipulation of the reactants with the above mentioned handles directs the reaction and increases the reaction rates, it does not provide selectivity on the microscopic scale of *individual* molecules. It is often the specific vibrational state of a molecule that determines what type of reaction occurs, and that greatly influences reaction rates (chemical activation). Hence excitation of a selected vibrational mode, or even the dissociation of a specific molecular bond, is a major ingredient of state-selective chemistry. The relatively simple gas-phase reaction of a hydrogen atom with a water molecule is an illustrative example showing many features of state-selective chemistry. Nowadays a rather complete study has been made of the family of chemical reaction of $H + H_2O$ and its isotopically substituted analogs, $H + HOD$ and $H + D_2O$,

$$\mathrm{H} + \mathrm{H_2O} \rightarrow \mathrm{H_2} + \mathrm{OH}\ , \tag{1.1a}$$

$$\mathrm{H} + \mathrm{HOD} \rightarrow \mathrm{H_2} + \mathrm{OD}\ , \tag{1.1b}$$

$$\mathrm{H} + \mathrm{HOD} \rightarrow \mathrm{HD} + \mathrm{OH}\ , \tag{1.1c}$$

$$\mathrm{H} + \mathrm{D_2O} \rightarrow \mathrm{HD} + \mathrm{OD}\ . \tag{1.1d}$$

All these reactions are endothermic with a typical activation energy of 0.93 eV [10]. The excess energy to activate the reaction has to come from either the kinetic energy of the reactants or the internal vibrational excitation of the HOD molecule. The high spectral brightness makes lasers outstanding tools to excite a large fraction of an ensemble of molecules bond-specifically or mode-selectively. Using laser light having a well defined frequency, it is possible to activate this reaction with bond-specifically vibrationally excited HOD. The shifts in the transition frequencies induced by the difference in the nuclear masses are used to select a bond [11–15]. These experiments show one or more features that motivate the current interest in state-selective chemistry. Firstly, as shown by Sinha *et al.* [11, 12], for specific excitation of the $OH(v = 4)$ vibration in the HOD molecule, the reaction with the H atoms produces two orders of magnitude more OD than OH fragments, i.e. favors reaction 1.1b over reaction 1.1c. A few years later Metz *et al.* [15] showed that excitation of the OD($v = 5$) results in a similar amount more OH than OD fragments. In both cases the bond that was initially excited reacted preferentially. Intuitively, this is understood in terms of motion of the stretch-excited proton (H or D), which approaches the free proton more and therefore is more likely to react than the proton (D or H) in the non-activated bond. This shows that vibrational excitation can speed up reactions *and* direct the reaction path. Secondly, experiments in the same system for lower vibrational states in the local v_{OH} and v_{OH} modes by Bronikowski *et al.* [13] show the general trend that with less excitation energy available a smaller enhancement is achieved, combined with less selectivity. Surprisingly, exciting the bending mode of the molecule does not increase the rate of reaction (1.1d) of H with D_2O, despite the availability of the same amount of excess energy [14]. The much higher reactivity of the states with all the vibrational energy in the reaction coordinate is a clear demonstration of mode-selective chemistry.

The experiments on these example reactions elucidate a few general notions on state-selective chemistry:

1. state-selective excitation of at least one of the reactants must be possible,
2. the prepared state must enhance the reactivity of that part of the molecule,
3. the excess energy must remain localized.

The experiments on water described above involved narrow-band laser light and were only feasible because of the rare coincidence of an excitation frequency of a vibrational mode ($\nu_{\mathrm{OH}} \approx 3{,}800$ cm^{-1} (2.65 μm) [16], $\nu_{\mathrm{OD}} \approx 2{,}800$ cm^{-1} (3.57 μm) [16]) with the output of a powerful laser operating in the mid infrared. In addition, only one resonant photon was involved in the excitation process, restricting the final state to the lowest vibrational states since the Franck-Condon Factors [17, 18] are negligibly small for single-photon excitation to high vibrational states. For consecutive excitation to higher vibrational states the photons were off-resonant due to the anharmonicity of the vibrational ladder. However, highly selective and strong enhancement of reactivity demands excitation of high vibrational states of a molecular bond. A possible solution is the stepwise excitation of the vibrational ladder. Such bond-selective vibrational ladder climbing involves a series of vibrational excitations. The anharmonic nature of vibrational ladders requires as many narrow-band lasers as the number of steps to be resonantly climbed. The number of lasers needed can be reduced if one uses lasers with larger bandwidths. In order to be resonant with a large number of vibrational steps, several authors have suggested the use of broadband radiation [19, 20]. An ultrashort laser pulse necessarily has the large bandwidth containing the frequencies required to climb several steps of the ladder. Although the large bandwidth of such pulses might frustrate isotope selectivity, both mode-selectivity and bond-specificity can still be achieved since the different vibrational modes in a molecule are generally well separated in frequency. Moreover, since the large bandwidth sustains short pulses, intra-molecular vibrational relaxation to other modes will not have time to occur during the pulse, keeping the energy localized in the selected bond. This aspect of short-pulse excitation is of importance in preserving mode-selectivity or bond-specificity in vibrational excitation of poly-atomic molecules. So far, the lack of experiments demonstrating vibrational ladder climbing stems from the absence of tunable ultrashort sources in the infrared. The construction of Free-Electron Lasers (FEL) has made a tunable coherent radiation source available that operates at the required wavelengths in the infrared at high power. Ultrashort laser pulses produced by a FEL contain sufficient spectral width to cover several steps of a vibrational ladder.

In this thesis experimental results and calculations are presented on ladder climbing using laser pulses in two types of ladder systems:

I. the electronic ladder in the rubidium atom using frequency chirped laser pulses with a wavelength of $\lambda=780$ nm,
II. The vibrational ladder in the electronic ground state of the nitric oxide molecule using mid infrared radiation ($\lambda=5.4$ μm) from a free-electron laser.

1.2 How to reach 100% transfer in climbing ladder systems

Before considering the climbing of a multi-level ladder, it is useful to review a way to achieve robust population transfer in a 2-level system. To achieve complete inversion, the transition will have to be strongly driven by the excitation field. Take, for example, a strong coherent light field of frequency ω, and a constant intensity, switched on at t_0 and off at t_1, that is (almost) resonant with the transition. Starting at t_0 the population will be driven from the ground to the upper state, as the light is absorbed by the system. Due to the coherence of the excitation field, this leads to complete inversion, after which the system is stimulated to emit photons and decay to the ground state. These cycles of excitation and de-excitation are known as Rabi cycles. The frequency of the Rabi oscillations are determined by the coupling strength (μ) between the two levels, and the field strength (E)

$$\Omega_{\mathrm{Rabi}} = 2\frac{\mu E}{\hbar}\ . \tag{1.2}$$

Population inversion is obtained most efficiently by irradiating the system with the laser fluence (i.e. the time integrated intensity) corresponding to half a Rabi cycle. The amount of energy required to invert the population with half a Rabi cycle is determined by the strength of the coupling between ground and upper state. If this coupling is not well-known, or if the fluence of the laser pulse can not be accurately controlled, the degree of excitation is undetermined and may range from exciting all the population to the upper state to no excitation at all. In a multi-step process the transfer per step must be close to 100% to achieve considerable population in the upper state. Hence, the sensitivity of the degree of inversion on the laser parameters makes Rabi pumping a non-robust method to climb a multi-level ladder with 100% efficiency.

The transfer process in the Rabi-cycling limit is an example of Chirped Adiabatic Passage (CAP, for a general review see [21, 22]). The latter is easily explained using a dressed-level

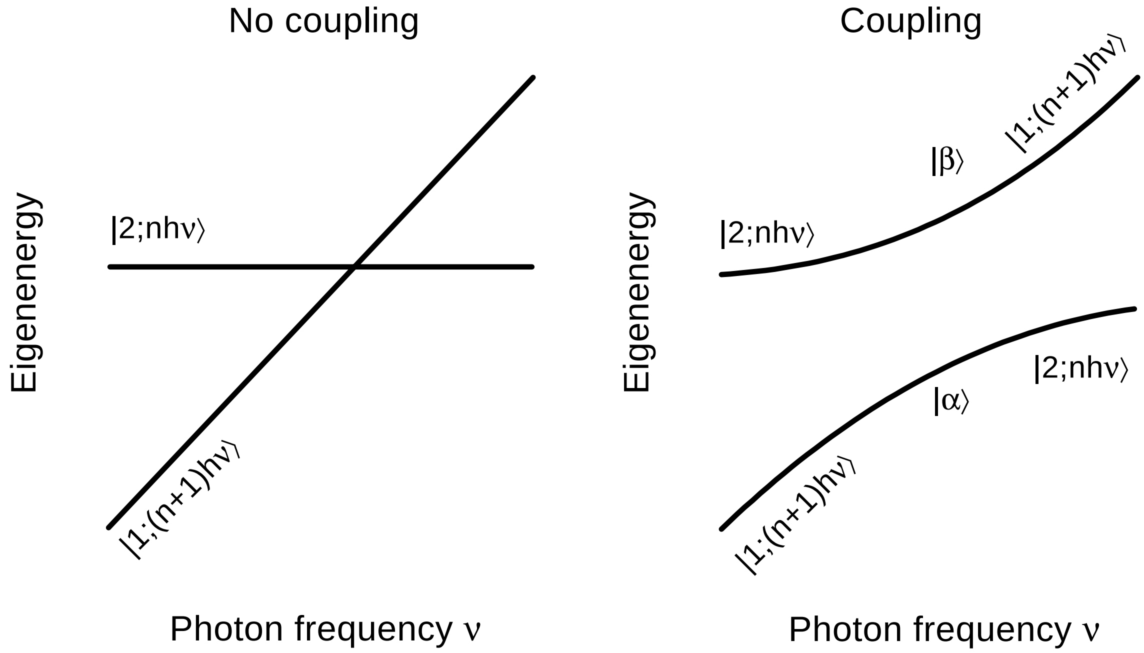

Figure 1.1*: The eigenenergy of a 2-level system with the ground state dressed by one photon as a function of the photon frequency. For the left panel the levels* $|1;(n+1)h\nu\rangle$ *and* $|2;nh\nu\rangle$ *are not coupled by the field and they cross at the resonance. The energies of the eigenstates* $|\alpha\rangle$ *and* $|\beta\rangle$ *of the system strongly interacting with the laser field are sketched in the right panel. The degeneracy at the resonance is lifted by the coupling between the two levels. Slow sweeping of the photon frequency over the resonance transfers the complete ground state population to the upper level.*

picture of a 2-level system [23]. The left panel of Fig. 1.1 shows the eigenenergy of the dressed states $|1;(n{+}1)h\nu\rangle$ and $|2;nh\nu\rangle$ (i.e. the ground state $|1\rangle$ dressed with one photon more than the excited state $|2\rangle$) as a function of the photon frequency. If there is no interaction between the levels (no coupling), the dressed states cross at the resonance and no population is transferred. For strong interaction however, the eigenstates of the system in the field $|\alpha\rangle$ and $|\beta\rangle$ are a linear combination of the dressed ground and upper state, *lifting the degeneracy at the resonance* (right panel of Fig. 1.1). The character of the eigenstates in the field $|\alpha\rangle$ ($|\beta\rangle$) changes from (to) $|1;(n{+}1)h\nu\rangle$ to (from) $|2;nh\nu\rangle$, for increasing (decreasing) photon frequency. This dressed-level picture becomes more interesting if one considers excitation by a chirped ultrashort laser pulse with a large spectral width (see Fig. 1.2), tuned around the resonance. The frequency the system is exposed to now changes in time: $\Delta\nu \sim t/\alpha$, where α is the linear chirp, with dimension T^2: the inverse of the change of the frequency in Hz per s. If this frequency variation is sufficiently slow, and many Rabi cycles are made during the sweep (i.e. large chirp, the adiabatic limit), the system has time to follow the perturbed eigenstates $|\alpha\rangle$ or $|\beta\rangle$. After crossing the resonance all population is transferred to the upper level $|2;nh\nu\rangle$. Or, more formally put, the probability

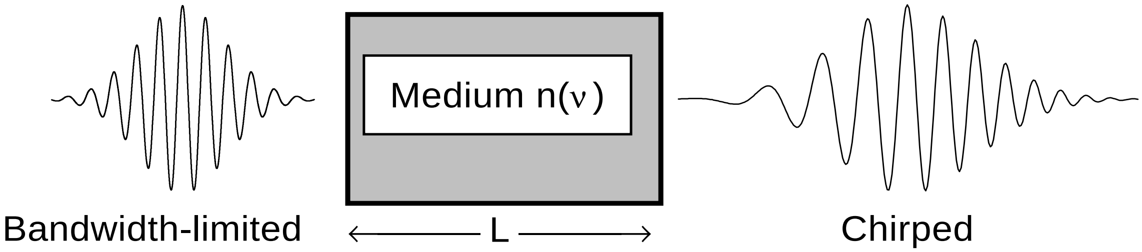

Figure 1.2: *The time evolution of a compressed laser pulse with a Gaussian shape (left panel) and for the same pulse when it is strongly chirped (right panel). The chirp can, for example, be generated by propagation of the pulse through a medium with a refractive index* $\mathsf{n}(\nu)$ *that is a non-linear function of the photon frequency* ν.

to make the adiabatic transition is given by the Landau-Zener transition probability [24–27]:

$$P_{\text{adiabatic}} = 1 - \exp\left(\frac{-\pi\Omega^2_{\text{Rabi}}}{2|\partial\Delta/\partial t|}\right) \ , \tag{1.3}$$

where $\Delta = (E_2 - E_1)/\hbar - \omega$ is the detuning of the laser from the resonance and the sweep rate is $\partial\Delta/\partial t = 1/\alpha$, for a chirped Gaussian pulse (see Fig. 1.2). For an excellent review see the book of Shore [28]. Obviously total inversion of the population is obtained when the argument of the exponential is very negative, or

$$-\frac{\pi|\alpha|\Omega^2_{\text{Rabi}}}{2} \ll -1 \ . \tag{1.4}$$

This sets the following "adiabaticity condition" on the chirp

$$|\alpha| \gg \frac{2}{\pi\Omega^2_{\text{Rabi}}} \ . \tag{1.5}$$

In this regime of slow sweeping and high fluence, the amount of population transferred to the excited state is relatively insensitive to fluctuations in the fluence or unknown matrix elements.

Recent experiments on anharmonic electronic ladder systems in atomic rubidium [29, 30] and sodium [31] have shown that, by frequency chirping an intense laser pulse, the transfer can be controlled by the direction of the frequency chirp (i.e. blue-to-red or red-to-blue). In the weak pulse regime the transfer efficiency is significantly enhanced if the chirp of the laser pulse follows the anharmonicity of the ladder system so that the different spectral components of the laser pulse pump the consecutive steps of the ladder sequentially (see chapter 2). In the strong pulse regime (Rabi-cycling limit), the transfer approaches 100% and becomes rather insensitive to the fluctuations of parameters like bandwidth, pulse fluence or uncertainties in dipole moments (see [29, 31, 32] and chapter 2).

1.3 The rubidium atom, a three-level system

Turning to ladder climbing in three-level ladder systems, the power of CAP is demonstrated by experiments presented in chapter 3 and those of Broers *et al.* [29], where 100% of the population

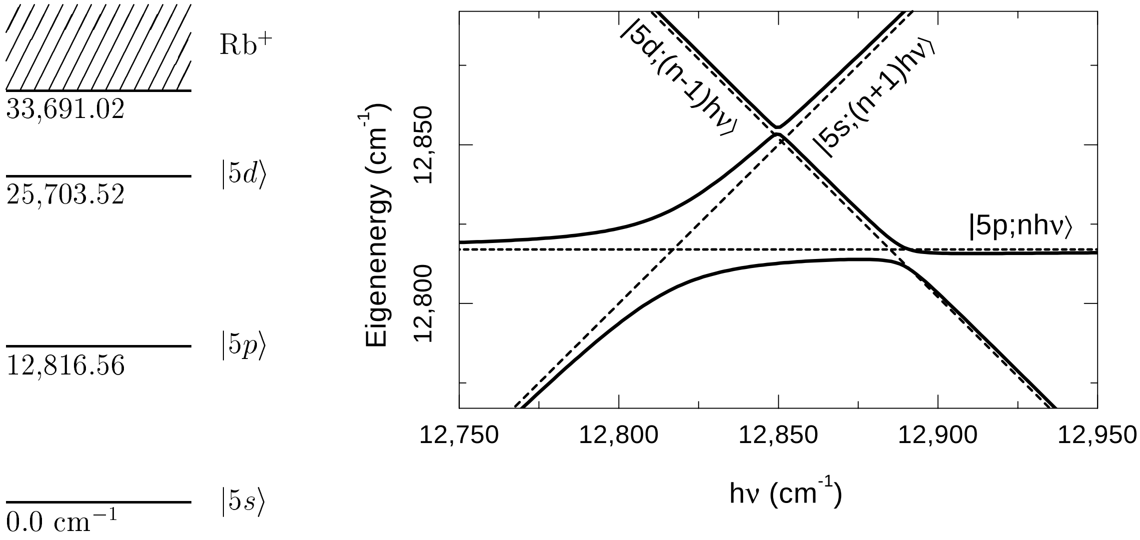

Figure 1.3: *The left panel shows a simplified energy level diagram of the relevant electronic states of rubidium. The right panel displays a dressed-level or Floquet diagram of the same three-level ladder system. The full curves show the dressed-level energies as a function of the photon energy of dressed states* $|5s;(n{+}1)h\nu\rangle$, $|5p;nh\nu\rangle$ *and* $|5d;(n{-}1)h\nu\rangle$.

is put in the upper level. The left panel of Fig. 1.3 shows the electronic 5s→5p→5d ladder in the rubidium atom. The energy levels of the $5s$, $5p$ and $5d$ states of the Rb atom form a ladder system with $(E_{5p}-E_{5s})=12{,}816.6$ cm^{-1} and $(E_{5d}-E_{5p})=12{,}886.9$ cm^{-1}. The ladder anharmonicity δ is defined as

$$\delta=[\nu_{i+2}-\nu_{i+1}]-[\nu_{i+1}-\nu_i]\ , \tag{1.6}$$

with the ν_i the eigenfrequencies of state i. For the rubidium ladder system the anharmonicity is $\delta=70.34$ cm^{-1}. In the experiment Rb atoms interact with laser pulses having a bandwidth large enough to contain the photon energies corresponding to both transitions of the ladder. The population of the upper level is, after the initial excitation, easily probed with ionization by a low-intensity high fluence pulse (with duration of 5 ns) of the second harmonic of a Nd:YAG laser ($\lambda=532$ nm). The right panel of Fig. 1.3 shows a dressed-level diagram of the Rb atom as a function of the photon frequency. The single-photon transitions from $|5s\rangle$ to $|5p\rangle$ respectively from $|5p\rangle$ to $|5d\rangle$ are found at the crossings of the curves of the dressed states $|5s;(n{+}1)h\nu\rangle$ with $|5p;nh\nu\rangle$ and $|5p;nh\nu\rangle$ with $|5d;(n{-}1)h\nu\rangle$, respectively. In between these transitions the two-photon transition is located at the crossing of $|5s;(n{+}1)h\nu\rangle$ and $|5d;(n{-}1)h\nu\rangle$.

However, as shown in chapter 2, at intermediate intensities all level crossings in the right panel of Fig. 1.3 are traversed partly adiabatically. Consequently, for a blue-to-red chirp, there are two paths contributing to the final population of the excited state $|5d\rangle$. The first contribution is from the path that follows the adiabatic curves for the two single-photon transitions. The second part stems from the population that follows the adiabatic curve for the two-photon transition. The wavefunction of each contribution has its own phase evolution. When the

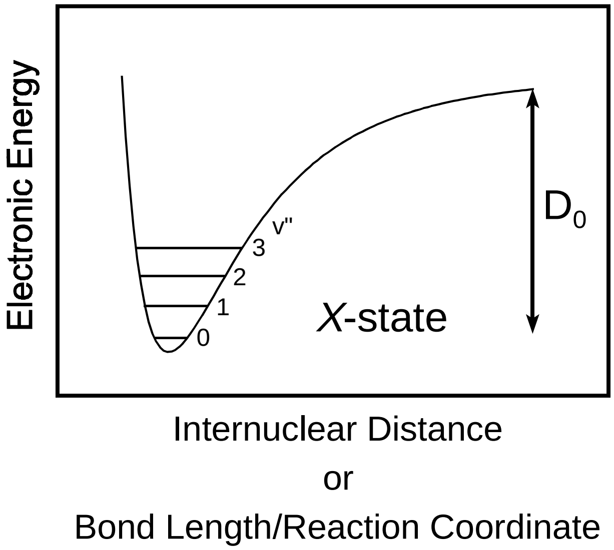

Figure 1.4: *A typical molecular potential energy diagram, showing the electronic energy of a diatomic molecule as a function of internuclear distance for the electronic ground state. Vibrational states are indicated by the horizontal dashes. For simplicity, the rotational splitting of each vibrational state in many rotational levels is not shown. A similar graph can be drawn for a poly-atomic molecule, by replacement of the X-axis coordinate* "Internuclear Distance" *with* "Bond Length". *For state-selective chemistry such a bond should be identified with a reaction coordinate.*

pathways recombine, these two contributions to the top-level population can interfere either constructively or destructively [33]. The acquired phase $\Delta\phi$ difference depends both on the energy difference of the paths and on the duration of the separation:

$$\Delta\phi = \int \frac{\Delta E(t)}{\hbar} dt \ . \tag{1.7}$$

Notice that $\Delta\phi$ is a function of the chirp, since the time it takes to sweep the frequency from the first to the second single-photon transition is proportional to the chirp. Therefore oscillations in the population of the upper state as a function of chirp are to be expected. In the high-intensity limit the population follows, for a sufficiently large chirp, the adiabatic paths, resulting in total transfer of the population to the top level (chapter 3).

These results achieved in the Rb three-level system provide a promising outlook for multi-level ladder climbing in molecules using CAP.

1.4 The nitric oxide (NO) molecule, a multi-level ladder system

The last part of this thesis (chapters 4, 5 and 6) deals with two ways of climbing the vibrational ladder in the electronic ground state $X\ ^2\Pi$ of the nitric oxide (NO) molecule. The vibrational transitions of the $X\ ^2\Pi$-state are pumped by a broadband IR laser. The resulting population distribution over the ro-vibrational states is probed by Resonantly Enhanced Multi-Photon

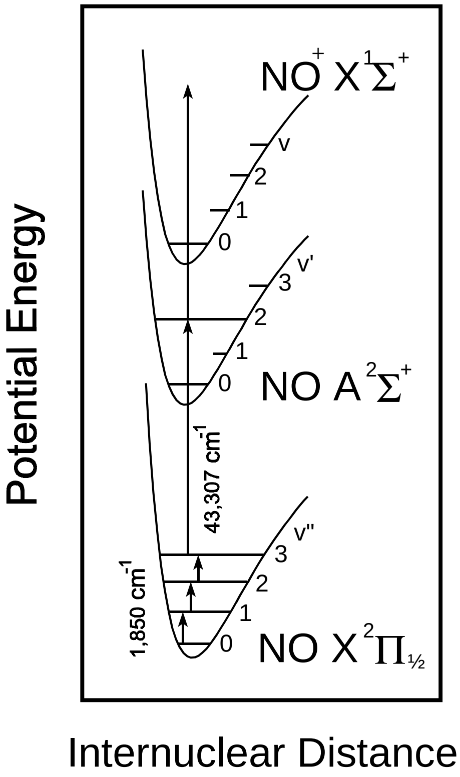

Figure 1.5: *Simplified energy level diagram of NO showing the* $X\ ^2\Pi$ *electronic ground state and the first* $A\ ^2\Sigma^+$ *electronic excited Rydberg state with their first few vibrational levels (denoted by* v'' *and* v'*) and the ionic* $X\ ^1\Sigma^+$ *ground state. The arrows indicate the types of driven transitions: vibrational excitation of the electronic ground at* $h\nu = 1{,}850\ \mathrm{cm}^{-1}$, *electronic excitation to the* $A\ ^2\Sigma^+$ *Rydberg state by a UV photon [the NO(*v',v''*)* γ*-band], and subsequent ionization by a UV photon. For clarity neither the rotational splitting of the vibrational levels nor the spin-orbit splitting of the* $X\ ^2\Pi$ *electronic ground state is displayed.*

Ionization (REMPI) via the $A\ ^2\Sigma^+$-state. Below, diatomic molecules are briefly introduced, followed by a discussion of the two relevant electronic states ($X\ ^2\Pi$ and $A\ ^2\Sigma^+$) of the NO molecule. The chapter concludes with an overview of the complications that arise when the ladder system under study is extended from the simple three-level system in the rubidium atom to the complex multi-level system of the vibrational ladder in NO.

1.4.1 Diatomic molecules

A diatomic molecule consists of two atoms that share some of their electrons to form a bond (see Fig. 1.4). The total energy of the molecule, that is the sum of its electronic, vibrational and rotational energy, is lower than the sum of the energy of the separated atoms. This energy difference is the dissociation energy. The complete wavefunction is very complex, hence some simplifications have to be made to enable a simple description of the molecule. In general the nuclear motion is much slower that the motion of the electrons. Vibrational motion can often be separated from rotational motion by similar time-scale arguments. In the Born-Oppenheimer approximation these notions are used by proposing a wave function that is written as the product of three independent wavefunctions $\psi_e\psi_v\psi_r$ which depend on the electron coordinates, the internuclear separation and the rotation, respectively. This yields the following approximation for the total energy

$$E_{\text{total}} = E_e + E_v + E_r \ . \tag{1.8}$$

More detailed descriptions of (diatomic) molecules can be found in the books of Herzberg [34–36], Lefebvre-Brion [37] and Thorne [38], and the monograph by Hougen [39]. A useful summary and explanation of the spectroscopic symbols of diatomic molecules is given in [40] and for polyatomic molecules in [41].

1.4.2 The $X\,^2\Pi$- and $A\,^2\Sigma^+$-states of the NO molecule

Fig. 1.5 shows a simplified potential energy diagram of the $X\,^2\Pi$ and $A\,^2\Sigma^+$ states of the NO molecule.

The $X\,^2\Pi$-state of the NO molecule

The lower part of the energy level diagram of NO (Fig. 1.6) shows the energy of the lowest vibrational states of the electronic ground $X\,^2\Pi_{\frac{i}{2}}(v'', J'')$-states of the NO molecule. The energy of the vibrational levels is given by the expansion in Dunham coefficients:

$$E_v(v'') = \omega_e(v'' + \tfrac{1}{2}) - \omega_e x_e(v'' + \tfrac{1}{2})^2 + \omega_e y_e(v'' + \tfrac{1}{2})^3 + \dots \ , \tag{1.9}$$

where for the $X\,^2\Pi$-states $\omega_e = 1{,}904.405$ cm^{-1}, $\omega_e x_e = 14.187$ cm^{-1} and $\omega_e y_e = 0.0240$ cm^{-1}. The dissociation energy of the N-O bond is $D_0 = 52{,}403$ cm^{-1} [42], from which the highest bound vibrational state in the $X\,^2\Pi$-state can be calculated: $v_{\max} = 37$. The $X\,^2\Pi$-states of NO belong to the intermediate coupling case between Hund's cases (a) and (b). In this intermediate coupling case neither N, the total rotational quantum number exclusive spin, nor Ω, the absolute value of $|\Lambda + \Sigma|$, i.e. the sum of the projection of the resultant orbital angular momentum and the resultant spin on the molecular axis, is a good quantum number. Each rotational level is split into two sublevels, labeled 1 and 2, with $\Omega = \frac{1}{2}$ and $\Omega = \frac{3}{2}$, respectively. The relative magnitude of the level splitting depends on the ratio $\lambda(v'') = A(v'')/B_e(v'')$ of the spin-orbit coupling constant $A(v'')$ and the rotational constant $B_e(v'')$, with

$$A(v'') = 123.26 - 0.1906(v'' + \tfrac{1}{2}) - 0.0108(v'' + \tfrac{1}{2})^2 \ , \tag{1.10}$$

and

$$B_e(v'') = 1.70427 - 0.01728(v'' + \tfrac{1}{2}) + 0.000037(v'' + \tfrac{1}{2})^2 \ , \tag{1.11}$$

taken from Mallard *et al.* [43] and Engleman *et al.* [44]. This gives the following expressions $E_{\rm rot1}$, $E_{\rm rot2}$ for the rotational energy E_r of the two sublevels of each rotational level[1]:

$$E_{\rm rot1}(v'',J'') = B_e(v'')\left[(J''+\tfrac{1}{2})^2 - 1 - \tfrac{1}{2}\sqrt{\lambda^2(v'') - 4\lambda(v'') + 4(J''+\tfrac{1}{2})^2}\right] \; , \qquad (1.12a)$$

$$E_{\rm rot2}(v'',J'') = B_e(v'')\left[(J''+\tfrac{1}{2})^2 - 1 + \tfrac{1}{2}\sqrt{\lambda^2(v'') - 4\lambda(v'') + 4(J''+\tfrac{1}{2})^2}\right] \; . \qquad (1.12b)$$

From each initial state $|v\Omega J m_J\rangle$ there are multiple couplings[2]: to $|(v\pm1)\Omega(J-1)m_J\rangle$ by a $\mathsf{P}_{v\pm1,v}$-type transition, or to $|(v\pm1)\Omega J m_J\rangle$ by a $\mathsf{Q}_{v\pm1,v}$ or $|(v\pm1)\Omega(J+1)m_J\rangle$ by a $\mathsf{R}_{v\pm1,v}$ transition. As an example, the transitions from rotational state $X\,^2\Pi_{\frac{1}{2}}(0,1\frac{1}{2})$ to $X\,^2\Pi_{\frac{1}{2}}(1,J'')$ are indicated in Fig. 1.6 by the short arrows with labels P_{10}, Q_{10} and R_{10}.

The $A\,^2\Sigma^+$-state of the NO molecule

The $A\,^2\Sigma^+$-state of the NO molecule is the lowest Rydberg state of the NO molecule with $n'=3$, with electronic energy $\mathrm{T}_e = 43{,}906.37$ cm^{-1}. The vibrational energy of this state is given by Eq. (1.9) as well, where the parameters for the $A\,^2\Sigma^+$-state are $\omega_e = 2{,}374.307$ cm^{-1}, $\omega_e x_e = 16.106$ cm^{-1} and $\omega_e y_e = -0.04645$ cm^{-1}. The rotational constant $B_e(v')$ is

$$B_e(v') = 1.99478 - 0.018328(v'+\tfrac{1}{2}) \; , \qquad (1.13)$$

and the rotational energies of the sublevels F_1 and F_2 are

$$F_1(v',J') = B(v')(J'-\tfrac{1}{2})(J'+\tfrac{1}{2}) \; , \qquad (1.14a)$$

$$F_2(v',J') = B(v')(J'+\tfrac{1}{2})(J'+1\tfrac{1}{2}) \; , \qquad (1.14b)$$

where the energy difference between $F_1(v',J')$ and $F_2(v',[J'-1])$, the two sublevels that have the same N rotational quantum number but opposite spin, is neglected, as is indicated with the curly braces in Fig. 1.6.

REMPI via the NO $A\,^2\Sigma^+ - X\,^2\Pi$ transition [the NO$(v',v'')\gamma$-band]

The ionization potential (I.P.) of the electronic ground state of NO is I.P. = 74,721.7 cm^{-1} [45, 46]. Hence two-photon ionization is energetically allowed if the photon energy $h\nu \geq 37{,}381$ cm^{-1}. When the photon energy is such that it is resonant with an intermediate state the process is a Resonantly Enhanced Multi Photon ionization (or REMPI) process. The ionization yield at a certain photon energy is proportional to the transition strength of the $A\,^2\Sigma^+ - X\,^2\Pi$ (the NO(v',v'') γ-band) and the $A\,^2\Sigma^+$-continuum transitions, and, more importantly, to the population that is present in the $X\,^2\Pi$ ground state. Since the spectroscopic constants ω_e, $\omega_e x_e$, B_e etc. for the $A\,^2\Sigma^+$-state are different than the constants for the $X\,^2\Pi$-state, the photon

---

[1] For clarity, neither the (negligible) splitting of each rotational level by Λ-doubling nor the corresponding parity of the wavefunction is indicated in Fig. 1.6.

[2] Dipole allowed transitions are called P, Q and R, for $\Delta J = -1$, 0, +1, respectively.

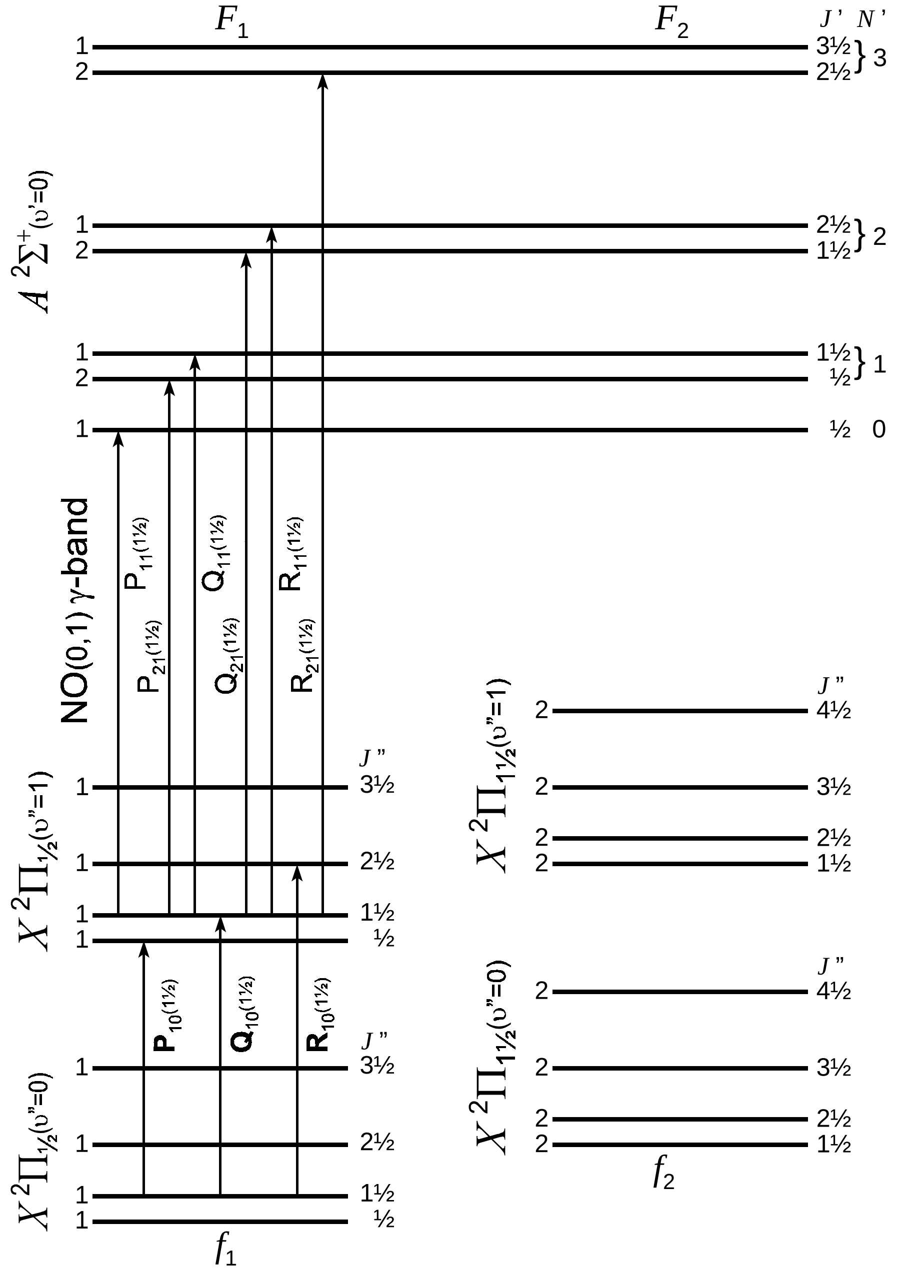

Figure 1.6: *A schematic energy level diagram of NO, showing the rotational and vibrational levels of both components* $X\,^2\Pi_{\frac{1}{2}}$ *and* $X\,^2\Pi_{\frac{3}{2}}$ *of the electronic ground state and the* $A\,^2\Sigma^+$ *first excited electronic state. The electronic ground state in* $X\,^2\Pi_{\frac{1}{2}}$ *and* $X\,^2\Pi_{\frac{3}{2}}$ *is split into sublevels* f_1 *and* f_2 *due to spin-orbit interaction. The* $A\,^2\Sigma^+$*-state is split in sublevels* F_1 *and* F_2 *in a similar fashion, but the effective splitting is negligible. The arrows with labels* P_{fi}*,* Q_{fi} *and* R_{fi} *indicate the relevant transitions in the* $X\,^2\Pi - X\,^2\Pi$ *vibrational ladder, where the subscript* fi *denotes the final and initial vibrational level. The arrows with labels* $\mathsf{P}_{FI}(J'')$*,* $\mathsf{Q}_{FI}(J'')$*,* $\mathsf{R}_{FI}(J'')$ *indicate the relevant branches used in the probing of the excited state population by the 1+1 REMPI process via the NO*(v', v'') γ*-band, where the subscript* FI *denotes the final and initial rotational sublevel.*

energy of the resonance is different for every v'' and J''. Hence the population distribution of the ground state can be determined from the 1+1 REMPI-spectra that are recorded by scanning the photon energy over the resonances. Actually there are several branches in the NO(v', v'') γ-band indicated in Fig. 1.6 by the symbols $\mathsf{P}_{FI}(J'')$, $\mathsf{Q}_{FI}(J'')$ and $\mathsf{R}_{FI}(J'')$, where the subscript FI denotes the final and initial rotational sublevel. As an example, the long arrows in Fig. 1.6 indicate the four different photon frequencies corresponding to the six branches $\mathsf{P}_{11}(1\frac{1}{2})$, $\mathsf{P}_{21}(1\frac{1}{2})$+$\mathsf{Q}_{11}(1\frac{1}{2})$, $\mathsf{Q}_{21}(1\frac{1}{2})$+$\mathsf{R}_{11}(1\frac{1}{2})$ and $\mathsf{R}_{21}(1\frac{1}{2})$ that probe the population in the $X\,^2\Pi_{\frac{1}{2}}(v''\!=\!1)$ state via the NO(01) γ-band. The cross-section for the single-photon ionization of the $A\,^2\Sigma^+$ to the electronic ground state of NO$^+$ $X\,^1\Sigma$ is determined by Zacharias *et al.* [47] and found to be structureless for ionization out of the lowest vibrational states of the $A\,^2\Sigma^+$ state.

1.4.3 Complications arising while climbing the vibrational ladder of the $X\,^2\Pi$-state of NO

Compared to the relatively simple three-level system of the rubidium atom, the driving of a vibrational ladder climbing process in NO brings up quite some complications.

From Eq. (1.9) the energy difference between the vibrational states $v''=1$ and $v''=0$ can be estimated at $\Delta E_{10} = 1{,}876$ cm^{-1}. For the lowest vibrational levels, the anharmonicity per vibrational quantum an be estimated using Eq.'s (1.6) and (1.9):

$$\begin{aligned}\delta_{\mathrm{vib}} &= [E_{\mathrm{vib}}(v+2) - E_{\mathrm{vib}}(v+1)] - [E_{\mathrm{vib}}(v+1) - E_{\mathrm{vib}}(v)] \\ &\cong -\omega_e x_e\{[(v+2\tfrac{1}{2})^2 - (v+1\tfrac{1}{2})^2] - [(v+1\tfrac{1}{2})^2 - (v+\tfrac{1}{2})^2]\} \\ &= -2\omega_e x_e \ , \end{aligned} \tag{1.15}$$

where the terms of order $(v+\frac{1}{2})^3$ and higher are neglected. For the vibrational ladder of the electronic ground state of NO the anharmonicity is $\delta_{\mathrm{vib}} = -28$ cm^{-1}[3]. Consequently, a large bandwidth laser operating in the mid-infrared is required to pump the $X\,^2\Pi - X\,^2\Pi$ transitions for a reasonably large range of v'''s. Such an ultrafast, femtosecond (1 fs$=10^{-15}$ s) laser is not as ubiquitary available as the table-top Ti:sapphire laser system that is used for the rubidium experiments. The only laser capable of producing fs MIR laser pulses in the Netherlands is the Free-Electron Laser for Infra-red eXperiments FELIX [48, 49]. Due to the relatively small transition dipole moment of the NO $X\,^2\Pi - X\,^2\Pi$ transitions, for the first transition $X\,^2\Pi(1) - X\,^2\Pi(0)$ the dipole moment is only $\mu_{10} = 2.48\times 10^{-31}$ Cm [50], whereas the dipole moment for the $5p-5s$ transitions in Rb is $\mu_{\mathrm{5p-5s}} = 2.03\times 10^{-29}$ Cm [51]. To obtain a similar Rabi frequency for NO the reduced dipole moment must be compensated by a two orders larger electric-field strength. Hence four orders higher intensities are required to drive a vibrational ladder in NO rather than an electronic ladder in Rb. Given the considerably reduced laser pulse energies compared to the Rb experiment ($\mathrm{E_{FELIX}} = 1$ μJ while $\mathrm{E_{Ti:sapphire}} \geq 10$ mJ), the

---

[3] Note that this anharmonicity is negative, whereas for the Rb ladder the anharmonicity is $\delta_{\mathrm{Rb}} = 70.38$ cm^{-1}. Consequently the sign of the chirp corresponding to the following of the ladder by the laser frequency is $\alpha_{\mathrm{Rb}} > 0$ while $\alpha_{\mathrm{NO}} < 0$.

experiments on NO could only be performed in the low-Rabi-cycling limit[4]. Once the population is transferred to excited states by the MIR laser, the next step is to measure the population of the vibrationally excited molecules. The role of "upper state" (the $|5d\rangle$ level that was present in the rubidium experiments) is now taken over by a total of $v_{\max} = 37$ vibrational states and an infinite number of rotational levels J''. In order to learn the most about the nature of the ladder climbing process, it is desirable to retrieve detailed information on the distribution of the population over the ro-vibrational levels. The 1+1 REMPI process, described in the previous subsection, is used as a tool to map out both the initial and final population distribution over the ro-vibrational levels of the electronic ground state of NO.

The output of the free-electron laser FELIX is a train of macro pulses at a repetition frequency of 5 Hz [48]. Each macro pulse has a typical duration of $5 - 7$ μs and consists of a burst of micropulses that have a pulse duration of 0.2–10 ps and a micropulse separation of 1 or 40 ns. In chapter 4 the population is distributed over the vibrational levels of the $X\,^2\Pi(v)$ state by a train of ultrashort bandwidth-limited (i.e. non-chirped) IR pulses. Chapter 5 presents experimental results of ladder climbing in NO exposed to a *single*, chirped, large bandwidth IR pulse.

From Fig. 1.6 it is clear that instead of having all population initially in one state (the $|5s\rangle$ state) for the NO experiment a large set of ro-vibrational states $|v\Omega J m_J\rangle$ is thermally populated[5]. From each initial state there are multiple couplings to other vibrational states by $\mathsf{P}_{v\pm1,v}$-, $\mathsf{Q}_{v\pm1,v}$- and $\mathsf{R}_{v\pm1,v}$-type transitions. Corresponding to this wealth of transitions, a multitude of interfering paths to every high vibrational state is to be expected. The consequences of the presence of rotations in a molecular system are investigated. Because the rotational energy can be of the same order of magnitude as the anharmonicity of the vibrational ladder, the sign of the anharmonicity of a specific sequence of **P**-, **Q**- or **R**-transitions in the excitation process may depend on the specific initial ro-vibrational state. This idea is explored in chapter 6 and confirmed by model calculations. In addition, model calculations are presented that mimic the experimental results presented in chapter 5 very well.

---

[4] Experiments on an other complex ladder system have been performed by Vrijen *et al.* [52, 53]. The ladder system used for their study is subset of the high Rydberg states ($n \geq 18$) in Cs, with transition frequencies around 200 cm^{-1} ($\lambda = 50$ μm). The high peak intensities of the IR laser pulses from FELIX and the large dipole moments between Rydberg states [54] enabled a study of the transport in the high-Rabi-cycle limit. Remarkably, the transfer to the upper level did *not* show any chirp dependency. For the high intensities used in their experiment, states outside the ladder couple with the states of the ladder, resulting in severe distortion of the ladder which frustrates efficient ladder climbing. This puts an upper limit on the intensity range where efficient ladder climbing is possible.

[5] For example, to have 99% of the molecules in the lowest rotational level, the temperature must be as low as 1.55 K.

CHAPTER 2

INTERFERENCE IN CLIMBING A QUANTUM LADDER SYSTEM WITH FREQUENCY-CHIRPED LASER PULSES

Excitation of a quantum ladder system by chirped, i.e. frequency-swept, laser pulses has been investigated by studying an atomic model system, the $5s$-$5p$-$5d$ *ladder of rubidium. The population transfer is significantly enhanced when the frequency is swept such that it follows the spacing of the ladder. At intermediate intensities oscillations in the population transfer to the upper level (*$5d$*) are observed. These oscillations can be attributed to interference between two paths of excitation, sequential transfer and direct two-photon excitation via a virtual intermediate state. The population transfer to the upper level (*$5d$*) and the direct three-photon ionization are determined simultaneously, the ionization signal corresponding to a three step ladder with the final state in the continuum:* $5s$-$5p$-$5d$-$\varepsilon_p/\varepsilon_f$*. The experiments are performed using 100 fs pulses at ~780 nm from a self-mode-locked Ti:*Al_2O_3 *oscillator amplified at 10 Hz.*

The concept of ladder climbing is introduced in section 2.1. Then the experimental set-up is described in section 2.2 and the key experimental findings are discussed qualitatively in section 2.3. Before the quantitative treatment of the results in section 2.6, the experimental realization of chirped pulses is discussed in section 2.4 and a theory based on solving the time-dependent Schrödinger equation is introduced in section 2.5. The chapter ends with some conclusions in section 2.7.

2.1 Introduction

The quest of manipulating quantum systems on a detailed level, thus controlling the exact quantum state of the system, has been long ongoing. The advent of the laser facilitated high selectivity in the interaction with atomic and molecular systems, but it is only through recent theoretical and experimental developments that the goal is becoming realistic for more complicated systems [9]. One important example of quantum manipulation is the attempt to bring an ensemble of molecules into a specific highly excited vibrational state. This facilitates the selective breaking of chemical bonds, thus modifying chemical reactions [55, 56]. Direct single-photon excitation to a highly excited vibrational state is not possible, due to the small overlap between the initial and final states. Thus a step-wise excitation is needed, introducing other complications. The anharmonicity of the chemical bond results in different transition frequencies between sequential vibrational states, demanding the use of several laser frequencies. Furthermore, the time scales for redistribution of vibrational energy within a molecule are very short (picosecond range). Ultrashort laser pulses can potentially present a solution to both of these problems, since the bandwidth of ultrashort pulses may be large enough to contain all the frequency components needed in the vibrational ladder and picosecond time resolution is readily obtained. At a first glance it may seem that the selectivity cannot be sustained with this approach, and even if the purpose is simply multiphoton dissociation it turns out that the intensities needed to dissociate an appreciable fraction of the molecules are far beyond those leading to ionization.

A possible solution to the problem was suggested by Chelkowski, Bandrauk, and Corkum [19]. They proposed to use chirped ultrashort laser pulses. If the laser pulse is blue-to-red chirped, the instantaneous frequency will follow the spacing between the vibrational levels of the anharmonic molecular potential. The suggested process is an example of chirped adiabatic passage. Adiabatic passage is an attractive approach for obtaining efficient population transfer [9,57], primarily because of the insensitivity to inhomogeneities associated with the ensemble of molecules, as compared, for example, to Rabi pumping. Adiabatic passage by chirped pulses has been used to create inversion in a collection of molecules, with more than half of the population transferred to an *excited* electronic and ro-vibrational state [58]. A high degree of selectivity has been proven to be compatible with the large bandwidth of a short laser pulse [59]. Adiabatic passage in a molecular vibrational ladder system has yet to be demonstrated. Chapters 4–6 present the first results obtained on ro-vibrational ladder climbing in the electronic *ground* state of a molecule by (non)-chirped laser pulses. Broers *et al.* have investigated population transfer using adiabatic passage by a chirped pulse and total population inversion has been demonstrated in an atomic model system, the three-state ladder $5s \rightarrow 5p \rightarrow 5d$ in the rubidium atom [29].

In this chapter it will be shown that in the three-level ladder system of rubidium, the actual population transfer at moderate intensities is oscillating as a function of the chirp due to quantum interference [33]. A simplified energy level diagram of Rb is depicted in Fig. 2.1a. The $5s$, $5p$, and $5d$ states are labeled $|1\rangle$, $|2\rangle$, and $|3\rangle$, respectively. In the experiment Rb atoms interact with laser pulses of a bandwidth large enough to contain the photon energies corresponding to both transitions of the ladder system, $5p \leftarrow 5s$ (12,816.56 cm^{-1}) and $5d \leftarrow 5p$ (12,886.94 cm^{-1}). The dependence of the population transfer to the upper level $|3\rangle$ on the frequency chirp of the laser is investigated. It is found that the population transfer is enhanced when the applied pulse is red-to-blue chirped (positively chirped). This is to be expected, since the transition $|2\rangle \leftarrow |1\rangle$ is resonant in the beginning of the pulse, and the $|3\rangle \leftarrow |2\rangle$ transition becomes resonant at a later time during the pulse.

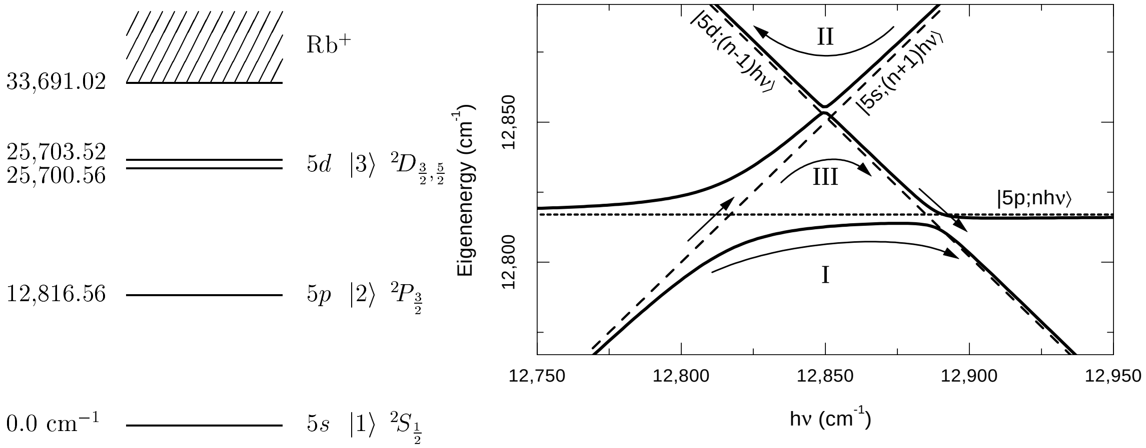

(a) **(b)**

Figure 2.1: **(a)** *A simplified energy-level diagram of rubidium. The* $5s \longleftrightarrow 5p$ *(or* $|1\rangle \longleftrightarrow |2\rangle$*) and the* $5p \longleftrightarrow 5d$ *(*$|2\rangle \longleftrightarrow |3\rangle$*) couplings can be driven by the same ultrashort laser pulse, due to the small difference in the energy spacings.* **(b)** *Dressed-atom diagram of the same levels, dressed as* $|1;(n{+}1)h\nu\rangle$, $|2;nh\nu\rangle$, *and* $|3;(n{-}1)h\nu\rangle$. *The dashed lines show the unperturbed energies as a function of the photon energy of the dressing field. The full lines show the dressed-atom energies, when the dipole coupling is included, and the laser has an intensity of* $1.9\times10^{7}\ \mathrm{W\,cm^{-2}}$. *The arrows indicate different paths of excitation of the upper level (5d), labeled as described in the text.*

The effect of chirping the optical pulses on the population transfer can be visualized using the dressed-atom picture [23]. In Fig. 2.1b the dashed lines show the unperturbed dressed-atom states of $|1;(n{+}1)h\nu\rangle$, $|2;nh\nu\rangle$, and $|3;(n{-}1)h\nu\rangle$, and their energy dependence on the photon energy. Including the dipole coupling between states $|1\rangle \longleftrightarrow |2\rangle$ and $|2\rangle \longleftrightarrow |3\rangle$ the dressed-atom states split up (full lines in Fig. 2.1b). In a chirped pulse the instantaneous frequency changes over the pulse duration, which corresponds to a traversal of the dressed atom diagram from left to right (red-to-blue chirped) or right to left (blue-to-red chirped). Depending on the strength of the dipole coupling (determined by intensity) and the rate of the frequency sweep (determined by the chirp), the avoided crossings of the dressed states are traversed more or less adiabatically. If the frequency chirp is from red-to-blue (left to right in Fig. 2.1b), population transfer from level 1 to level 3 occurs if an atom follows the full (adiabatic) dressed atom curve (path labeled I). This is the so-called intuitive frequency chirp leading to efficient population of the upper state. Note that once the intensity is high enough to traverse the crossings fully adiabatically, the population transfer will still be 100% for all higher intensities, as demonstrated by Broers *et al.* [29] and studied further in chapter 3. This is in contrast to Rabi pumping, where the upper state population keeps oscillating as a function of intensity. Broers *et al.* also discussed that at sufficiently high intensities, even with a counter intuitive chirp (blue-to-red), 100% of the population can be transferred (path II in Fig. 2.1b). Their experiment was performed using very intense pulses with a square power spectrum. In the present experiment only Gaussian pulses with a lower intensity are involved (low-Rabi-cycle limit). As to be expected, no complete population transfer is found at the moderate intensities of the present experiment. The next chapter will present the findings on complete population transfer when the pulse fluence is sufficiently large to reach the high-Rabi-cycle limit.

However, at these low to intermediate intensities a third, new, path leading to population of level 3 is of importance. If an atom is dressed by a red-to-blue chirped light field, it may follow $|1;(n+1)h\nu\rangle$ crossing $|2;nh\nu\rangle$ diabatically, then going adiabatically to $|3;(n-1)h\nu\rangle$ and continuing in this state crossing level $|2\rangle$ a second time (path III in Fig. 2.1b). The relative significance of the paths I and III depends on the experimental parameters (section 2.4). In general a (quantum-mechanical) interference between the two pathways is expected. This interference manifests itself as oscillations in the population transfer as a function of chirp, and is a general feature in most of the present measurements as well as in the calculated results (see section 2.6). The accumulated phase difference between the two paths depends on the difference in energy and the time spent to traverse the paths. For a linearly chirped pulse this time is proportional to the chirp, and the phase change is simply the product of the area between the two paths (Fig. 2.1b) and the chirp, giving regular oscillations as a function of the chirp (see section 2.3).

After the population transfer to level $|3\rangle$ another photon can be absorbed to leave the atom ionized. This process corresponds to a four-level ladder, with the last level in the continuum. The situation is analogous to a molecular ladder ending up in a dissociative state. The three-photon ionization signal is primarily an image of the population in the upper bound state ($5d$), except for small chirp, which corresponds to high IR intensity. There a significant part of the signal seems to originate from direct off-resonant multiphoton ionization.

2.2 Description of the experiment

Rubidium atoms are evaporated into the interaction region of a vacuum system. Across the interaction region a small voltage can be applied to accelerate detached electrons towards a channel electron multiplier. In the interaction region the atomic beam is crossed perpendicularly with the linearly polarized, collimated laser beam (Fig. 2.2). The laser source is based on a homebuilt Ti:Al_2O_3 oscillator [60]. The self-mode-locked oscillator is running at $\lambda \approx 780$ nm with a bandwidth of $\Delta\lambda \approx 10$ nm and a pulse-duration of $\tau_0 \approx 100$ fs, i.e. approximately transform-limited pulses. Following spatial filtering the infrared (IR) laser pulses are amplified at 10 Hz in three Bethune cells containing LDS 765 (2-mm-diameter cell), LDS 798 (3-mm-diameter cell), and LDS 765 (8-mm-diameter cell), respectively. When pumped by the second harmonic of a Q-switched Nd:YAG laser (pulse duration 8 ns), the overall average gain in the three cells is $A \approx 10^5$, leading to amplified pulses of $\Phi \approx 50$ μJ. The amplified pulses are sent through a pulse shaper [61,62], which is used to continuously control the chirp of the IR pulses. A pulse shaper consists basically of two parallel gratings of a variable separation (Fig. 2.3a). In order to be able to apply chirp in both directions, it is, however, necessary to add a $-1\times$ telescope between the two gratings (Fig. 2.3b). In fact, the shaper has been implemented by using just

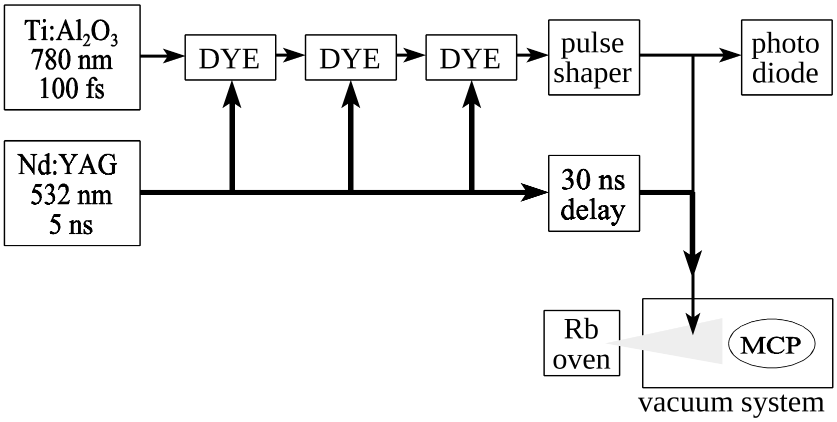

Figure 2.2: *A schematic of the experimental setup showing the laser system, pulse shaper, and the multi channel plate (MCP) detector in the vacuum chamber.*

one grating, an achromatic positive lens and a mirror in the configuration shown in Fig. 2.3c. The distance between the lens and the mirror is fixed at the focal distance of the lens, while the grating can be displaced out of the focus plane. When the grating is moved away from the focus of the lens, the phase shift of a laser pulse is dependent on the frequency, i.e. chirp is induced. In the situation shown in Fig. 2.3, the distance between the grating and the lens is larger than the focus length, and the pulse shaper works like a normal grating compressor, having a phase shift decreasing with frequency, so that an initially unchirped pulse becomes blue-to-red (or negatively) chirped. A thorough description of the actual chirp as a function of the grating-lens distance is given in section 2.4.

The IR laser beam, which is kept collimated through the vacuum chamber, has a diameter of 3 mm. It is overlapped with a 2-mm-diameter green laser beam, which is a fraction of the second harmonic of the Nd:YAG laser, delayed approximately 30 ns. The probe laser post-ionizes Rb atoms which are left in the $5d$ state after interaction with the IR pulse. Since the probe laser has a smaller diameter than the IR beam, it only probes the central region of the IR laser, having approximately constant intensity. The relatively large delay of the post-ionizing laser serves to separate in time the electron signal stemming from direct three-photon ionization by the IR laser and from post-ionization. Since the lifetime of level 3 is 266 ns [51], the decay out of the $5d$ state before the arrival of the probe laser can be neglected. The fluence of the probe laser is generally chosen fairly low ($\Phi_{\text{probe}} \approx 0.3\ \mu\text{J}\,\text{cm}^{-2}$) in order to keep the electron signal from the two different processes on the same order, to facilitate the simultaneous detection, and to avoid direct two photon ionization of atoms in the ground state ($5s$) or the intermediate state ($5p$).

For each IR laser pulse the time-of-flight spectrum of the electron multiplier is recorded on a digital scope and transferred to a computer, and both the direct three-photon ionization and the post-ionization signals are collected. Due to the unseeded nature of the Nd:YAG laser, the intensity and thus the gain in the Bethune cells at the instant of the short pulse fluctuates from shot to shot, leading to similar fluctuations in the pulse energy of the amplified pulses. The

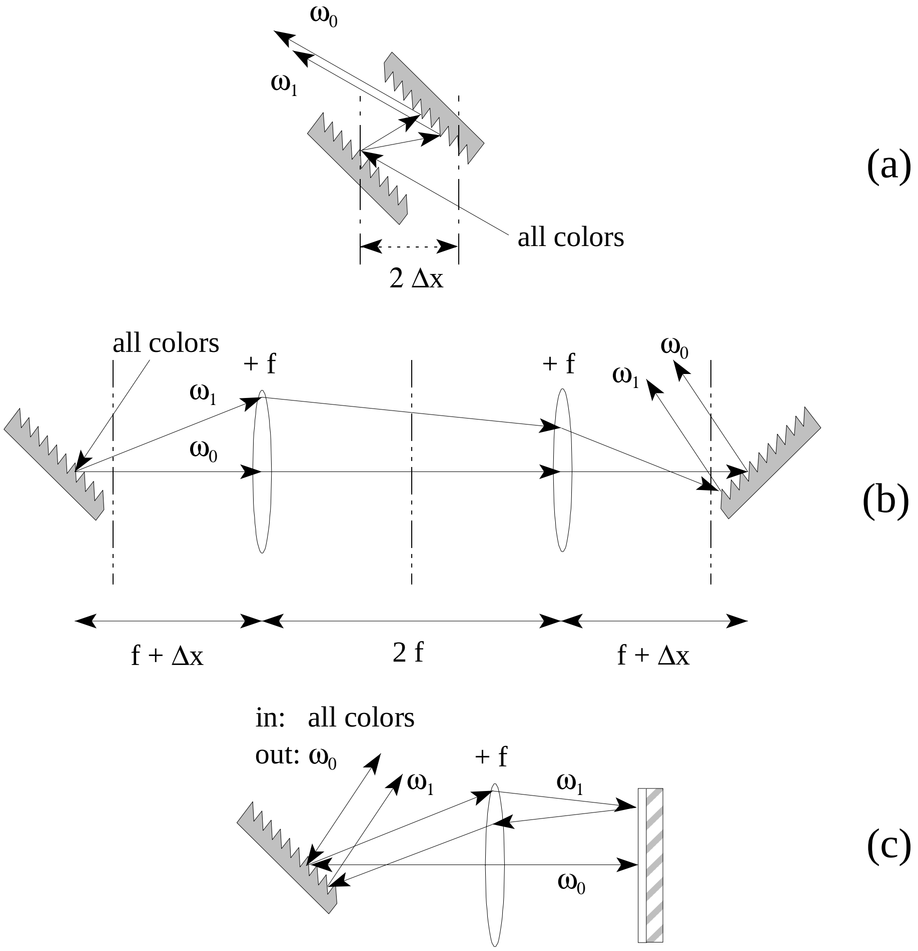

Figure 2.3: *This figure shows the working principle of the pulse shaper. In panel* **(a)** *a grating compressor is shown. The lines symbolize ray traces.* Δx *is the grating displacement. A* $(-1\times)$ *telescope is added in* **(b)***. Focal planes are indicated by* — · · — · · — *lines. Now* Δx *can be negative also. In panel* **(c)** *the mirror images the second grating, thus reducing the setup.*

pulse energy of each shot of the IR laser is monitored on a photo-diode, to serve for binning the two different ionization signals. For each position of the shaper, i.e. for each value of the chirp, typically 500 time-of-flight traces are recorded. The energy of the IR pulses after the shaper are typically a few tens of microjoule, corresponding to fluences of $\Phi_{\text{IR}} \approx 100\ \mu\text{J}\,\text{cm}^{-2}$. The origin of the clearly present oscillations in the transfer as a function of the chirp is discussed in the next section.

Fig. 2.4 shows an example of the signal measured by post-ionization of the Rb atoms upon interaction with an IR laser pulse of the indicated chirp. The chirp is calculated from the displacement of the grating, as described in section 2.4. Strong enhancement in the population transfer is observed when the IR pulse has a positive (red-to-blue) chirp. This agrees with the intuitive picture of having the $|2\rangle \leftarrow |1\rangle$ transition resonant with the chirped laser pulse before the $|3\rangle \leftarrow |2\rangle$ transition.

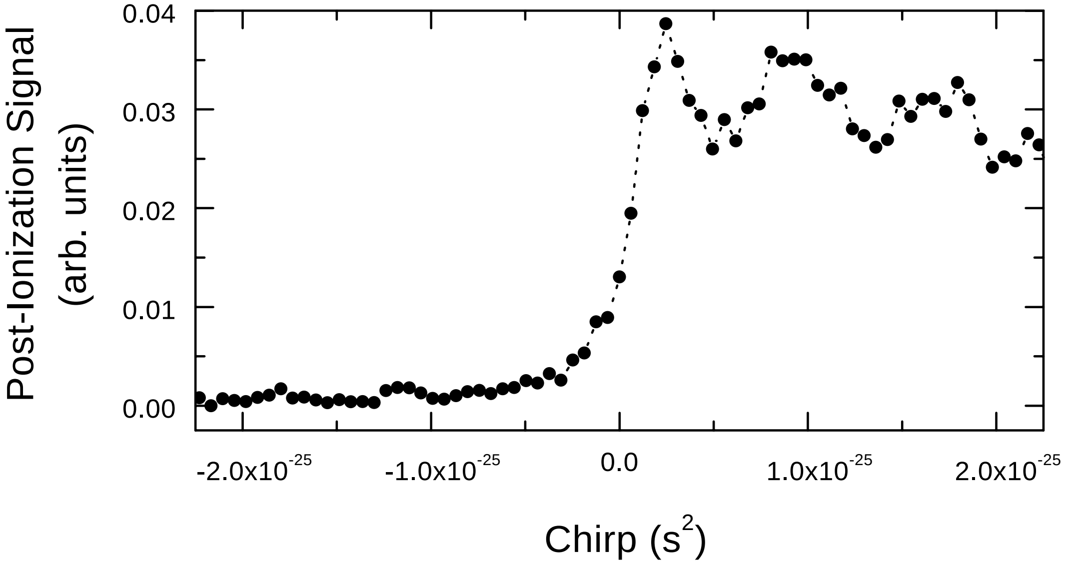

Figure 2.4: *The measured post-ionization signal as a function of the chirp of the IR laser pulse at a fluence of* $\Phi_{\mathrm{IR}} = 120\ \mu\mathrm{J\,cm^{-2}}$ *and a central wavelength of* $\lambda_0 = 780.0$ nm *(*$h\nu = 12{,}821$ cm^{-1}*). This signal is proportional to the population of the upper level (*$5d$*) after the pulse.*

2.3 Interference in the upper state population

In order to understand the quantitative behavior of the interaction of the chirped pulses with the rubidium atoms, are compared with a detailed theoretical model in section 2.5, based on integration of the time dependent Schrödinger equation. The present section, however, is devoted to the explanation of an interesting feature, common to all the measurements. Fig. 2.4 shows that there is an oscillatory dependence of population transfer on the chirp for positive chirp. This is due to quantum interference [33] between the two paths leading to population of the $5d$ level (as shown in Fig. 2.1b). The interference is a result of the low-to-intermediate-intensity regime of this experiment: the avoided crossings are traversed neither fully diabatically, nor fully adiabatically. In chapter 3 will be shown that for higher intensities, where the crossings are passed more and more adiabatically, the amplitude of the oscillations reduces to zero.

The intermediate intensity also results in less than the 100% population transfer reported earlier [29]. The criterion for a passage to be fully adiabatic is (for a two-level system [63]) that

$$\frac{d\theta}{dt} \ll \sqrt{\Omega^2(t) + \Delta^2(t)}\ , \tag{2.1}$$

where $\theta(t) = \frac{\pi}{2} + \arctan[\Omega(t)/\Delta(t)]$ is the polar angle of the Bloch vector, $\Omega(t)$ the Rabi frequency and $\Delta(t)$ the time-dependent detuning. For a linear frequency chirp, the time-dependent detuning has the form $\Delta(t) = \Delta(0) + (d\omega/dt)t$, where $d\omega/dt$ is constant and $\Delta(0)$ is the difference between the central frequency ω_0 of the light pulse, and the transition frequency between the two levels under consideration. If the fluence of the laser pulse with duration τ is high enough to saturate the transition ($\Omega\tau \sim 1$), the adiabatic criterion (2.1) can in principle always be met for a two-level system, provided that the carrier frequency is close to the transition and the chirp is sufficiently large. In the rubidium ladder system, however, the two steps have a slight difference in transition frequencies. The anharmonicity of the ladder is defined as $\delta = (\omega_3 - \omega_2) - (\omega_2 - \omega_1)$ [see Eq. (1.6)], with $h\delta \approx 70.38\ \text{cm}^{-1}$. This leads to fairly large detunings ($\Delta_{1-\text{ph}} = \frac{1}{2}\delta$) for the single-photon transitions $5p \leftarrow 5s$ and $5d \leftarrow 5p$ when the laser is tuned to the two-photon resonance with the $5d \leftarrow 5s$ transition ($\Delta_{2-\text{ph}} = 0$). Therefore the Rabi frequency has to be large, even for non-zero chirp, in order for the adiabatic criterion to be fulfilled. That is not the case in this experiment.

The period of the interference wiggles can be explained by simple phase arguments. The two different paths correspond to different dressed-atom energies $\hbar W$, and since the wavefunction contains a factor $\exp(iWt)$, the phase of the upper-state wavefunction created by the two different paths is different. The period of the interference corresponds to phase changes of 2π. If $\hbar W_{\text{I}}$ and $\hbar W_{\text{III}}$ are used for the dressed-atom energies of the two paths (corresponding to the notation of Fig. 2.1b), the accumulated phase difference is

$$\phi = \int_{t_1}^{t_2} [W_{\text{III}}(t) - W_{\text{I}}(t)]dt \ , \tag{2.2}$$

where t_1 and t_2 are the times of the diabatic crossings going to path III. For a strongly chirped Gaussian pulse the instantaneous frequency varies linearly with time, so changing the variable of integration yields

$$\phi = \frac{1}{d\omega/dt} \int_{\omega(t_1)}^{\omega(t_2)} [W_{\text{III}}(\omega) - W_{\text{I}}(\omega)]d\omega \ , \tag{2.3}$$

where $d\omega/dt$ is constant for a given pulse, but depends on the chirp, called α (see the next section). Eq. (2.3) shows that the phase difference is simply the ratio of the area between the two paths of Fig. 2.1(b) and the rate of change of the instantaneous frequency. The two instants of transition t_1 and t_2 are not really well defined, but at low intensity (e.g. at fairly large chirp), the dressed-atom energies are approximately equal to the unperturbed ones (dashed lines of Fig. 2.1b), and it is a good approximation to assume diabatic crossings at the time of the level crossings. In this case the area in Eq. (2.3) is that of a triangle of height $\delta/2$ and baseline δ, so that a phase change of 2π corresponds to

$$2\pi = \frac{1}{d\omega/dt}\frac{1}{2}\frac{\delta}{2}\delta \ , \tag{2.4}$$

or using the fact that for large chirp $d\omega/dt \approx 1/(2\alpha)$ (see section 2.4),

$$\begin{aligned} \alpha_{2\pi} &= \frac{4\pi}{\delta^2} \\ &= 7.1 \times 10^{-26}\ \text{s}^2 \ . \end{aligned} \tag{2.5}$$

This estimate can now be compared with the experimental results as shown in Fig. 2.4. Quite generally, the first oscillation, which includes the zero-chirp region, has a period which is considerably smaller than the estimate of Eq. (2.5). This is expected, since the derivation was based on large chirp. Using the same picture, however, the fact that the period drops leads us to the conclusion that the enclosed area increases, which can be understood as the dressed-atom levels splitting up in the stronger field. This argument depends, of course, critically on the instants of the diabatic crossings. When the first oscillation is disregarded, the remaining periods of oscillation agree exactly with the estimate of Eq. (2.5), except that there is a tendency that at high fluences the period decreases slightly, in agreement with the above argument.

A more naive look at the interference is that it originates from two different two-photon transition schemes. First, the atom can be excited sequentially by the chirped pulse at the instants where the frequency is resonant with the corresponding transition. Second, there is the possibility of direct two-photon excitation via a virtual state. This will take place when the photon energy is such that two photons match the energy difference between levels $|3\rangle$ and $|1\rangle$. As in the dressed-atom picture, the phase difference between the two transition schemes can be calculated, resulting in the same period as given in Eq. (2.5).

2.4 Chirp introduced by the pulse shaper

The absolute value of the chirp, which is induced by the pulse shaper, can be calculated directly from experimental conditions. If the displacement of the grating from the focal plane is denoted by $\Delta\mathrm{x}$ (with $\Delta\mathrm{x}$ positive if the distance is larger than the focal length, Fig. 2.3), then the distance between the two virtual gratings in the reduced system is $2\Delta\mathrm{x}$. A light beam of wavelength λ approaching the grating under an incident angle i with respect to the normal will be diffracted to the angle r according to the well known grating equation

$$\sin(i) + \sin(r) = m\frac{\lambda}{d} , \tag{2.6}$$

with $5d$ the groove spacing of the grating and m the order of diffraction (in the present case m is 1 and -1 on the first and second gratings, respectively). The total phase shift experienced by the light beam traveling through the shaper is determined by both the (wavelength dependent) path length l as well as by the phase shift which originates from the fact that there is a phase difference $2\pi m$ between consecutive grooves of the grating. The number of grooves to be included depends on wavelength, and is the ratio of the distance that the beam travels along the second grating to the groove spacing, i.e. $2\Delta\mathrm{x}\ \cos(r_0)\ \tan(r)/d$, with r_0 as the fixed angle between the grating normal and the direction perpendicular to the mirror of the shaper. Accordingly, the total phase shift is

$$\varphi(\lambda) = 2\pi\frac{l}{\lambda} + 2\pi m\, 2\Delta\mathrm{x}\ \cos(r_0)\tan(r)/d , \tag{2.7}$$

or using geometrical identities and Eq. (2.6),

$$\varphi(\omega) = \frac{2\cos(r_0)\omega}{c}[\cos(r) + \cos(i)]\Delta\mathrm{x} . \tag{2.8}$$

An incident light pulse of spectrum $E_0(\omega)$ will leave the shaper as $E_0(\omega)\exp[i\varphi(\omega)]$. For a light pulse, which is centered around ω_0 having a reasonably small bandwidth [64], the total phase shift can be expanded around ω_0 to second order in ω:

$$\varphi(\omega) \simeq \varphi(\omega_0) + \frac{1}{1!}\frac{\partial\varphi}{\partial\omega}\bigg|_{\omega=\omega_0}(\omega-\omega_0) + \frac{1}{2!}\frac{\partial^2\varphi}{\partial\omega^2}\bigg|_{\omega=\omega_0}(\omega-\omega_0)^2 \ . \tag{2.9}$$

Here $\varphi(\omega_0)$ is the phase shift of the carrier frequency within the pulse, while $\partial\varphi/\partial\omega$ determines the group velocity of the pulse envelope. The first non-trivial term of Eq. (2.9) is the second-order term, which is responsible for group velocity dispersion. In fact,

$$\alpha = \frac{1}{2!}\frac{\partial^2\varphi}{\partial\omega^2}\bigg|_{\omega=\omega_0}(\omega-\omega_0)^2 \ . \tag{2.10}$$

is the quantity describing the amount of chirp introduced in the pulse shaper. With φ from Eq. (2.8), with r and i depending on ω through the grating Eq. (2.6), we obtain

$$\alpha = -\frac{4\pi^2 c}{d^2}\frac{1}{\omega_0^3}\frac{m^2}{\cos^2(r_0)}\Delta\mathrm{x} \ . \tag{2.11}$$

It appears that α is fixed by the experimental parameters, and for a given light pulse (fixed ω_0) the induced chirp is linear in the displacement of the grating.

In the experiment the incoming pulse has a Gaussian shape with a pulse duration τ_0:

$$E_{\mathrm{in}}(t) = \exp\left[-2\ln 2\left(\frac{t}{\tau_0}\right)^2\right]\exp(i\omega_0 t) \ , \tag{2.12}$$

which, when assumed bandwidth limited, has a bandwidth $\Delta\omega = 4\ln 2/\tau_0$, so that in the frequency domain

$$E_{\mathrm{in}}(\omega) = \exp\left[-2\ln 2\left(\frac{\omega-\omega_0}{\Delta\omega}\right)^2\right] \ . \tag{2.13}$$

If only the second-order phase change is included, the outgoing pulse becomes

$$\begin{aligned} E_{\mathrm{out}}(\omega) &= E_{\mathrm{in}}\exp[i\alpha(\omega-\omega_0)^2] \\ &= \exp\left[-\frac{(\omega-\omega_0)^2}{4,}\right] \ , \end{aligned} \tag{2.14}$$

where , is given by

$$, = \left[\frac{8\ln 2}{\Delta\omega^2} + 4i\alpha\right]^{-1} \ . \tag{2.15}$$

The time dependence of the outgoing pulse is

$$E_{\mathrm{out}}(t) = \exp(-,\, t^2)\exp(i\omega_0 t) \ . \tag{2.16}$$

This pulse is also Gaussian, but with a pulse-duration which depends on chirp:

$$\tau^2 = \tau_0^2 + \left[\frac{8\ln 2\alpha}{\tau_0}\right]^2 \ , \tag{2.17}$$

i.e. for $\alpha \gg \tau_0^2$ the pulse is stretched approximately linearly with chirp. The instantaneous frequency changes linearly in time during the pulse, with the rate of change $d\omega/dt$ approximately inversely proportional to the chirp α:

$$\omega(t) = \omega_0 + \frac{\alpha\left(\frac{\Delta\omega^2}{\ln 2}\right)^2}{8 + 2\alpha^2\left(\frac{\Delta\omega^2}{\ln 2}\right)^2} t \ . \tag{2.18}$$

To summarize, the shaper introduces a chirp which is quadratic in the frequency domain and hence *for Gaussian pulses* linear in the time domain [65].

2.5 Theoretical model

The rubidium three-level ladder system is modeled by solving the time-dependent Schrödinger equation in a truncated basis. Only states that are within the bandwidth of the IR laser are included, i.e. the $5s$ ^2S, the $5p$ $^2P_{\frac{3}{2}}$, and the two fine-structure components of the $5d$ state, $^2D_{\frac{3}{2}}$ and $^2D_{\frac{5}{2}}$. While keeping the notation $|1\rangle$ and $|2\rangle$ for the included $5s$ and $5p$ states, for convenience the $^2D_{\frac{3}{2}}$ and the $^2D_{\frac{5}{2}}$ states are labeled by $|3\rangle$ and $|4\rangle$, and the continuum states are denoted as $|\varepsilon\rangle$. Fig. 2.5a shows the states and couplings included in the model.

The unperturbed atomic system is described by

$$\begin{aligned} H_0|n\rangle &= \hbar\omega_n|n\rangle \ , \\ H_0|\varepsilon\rangle &= \hbar\omega_\varepsilon|\varepsilon\rangle \ , \end{aligned} \tag{2.19}$$

while the full Hamiltonian in the dipole approximation has the form ($\vec{D}=-e\vec{r}$)

$$H = H_0 - \vec{E}\cdot\vec{D} \ , \tag{2.20}$$

to be used in the Schrödinger equation

$$i\hbar\frac{\partial\Psi}{\partial t} = H\Psi \ . \tag{2.21}$$

The wavefunction can be expanded in the above basis as

$$\Psi = \sum_n \exp(-i\omega_n t)a_n(t)|n\rangle + \sum_\varepsilon \exp(-i\omega_\varepsilon t)a_\varepsilon(t)|\varepsilon\rangle \ . \tag{2.22}$$

In the calculations below the sum (integral) over continuum states $|\varepsilon\rangle$ will be eliminated. By substituting the expression (2.22) for into the Schrödinger equation (2.21) and multiplying with $\langle n|$ and $\langle\varepsilon|$, respectively, we obtain

$$\begin{aligned} i\hbar\exp(-i\omega_n t)\dot{a}_n(t) &= \sum_{n'}\exp(-i\omega_{n'}t)a_{n'}(t)\langle n|\vec{E}\cdot\vec{D}|n'\rangle \\ &\quad+\sum_{\varepsilon'}\exp(-i\omega_{\varepsilon'}t)a_{\varepsilon'}(t)\langle n|\vec{E}\cdot\vec{D}|\varepsilon'\rangle \ , \\ i\hbar\exp(-i\omega_\varepsilon t)\dot{a}_\varepsilon(t) &= \sum_{n'}\exp(-i\omega_{n'}t)a_{n'}(t)\langle\varepsilon|\vec{E}\cdot\vec{D}|n'\rangle \\ &\quad+\sum_{\varepsilon'}\exp(-i\omega_{\varepsilon'}t)a_{\varepsilon'}(t)\langle\varepsilon|\vec{E}\cdot\vec{D}|\varepsilon'\rangle \ . \end{aligned} \tag{2.23}$$

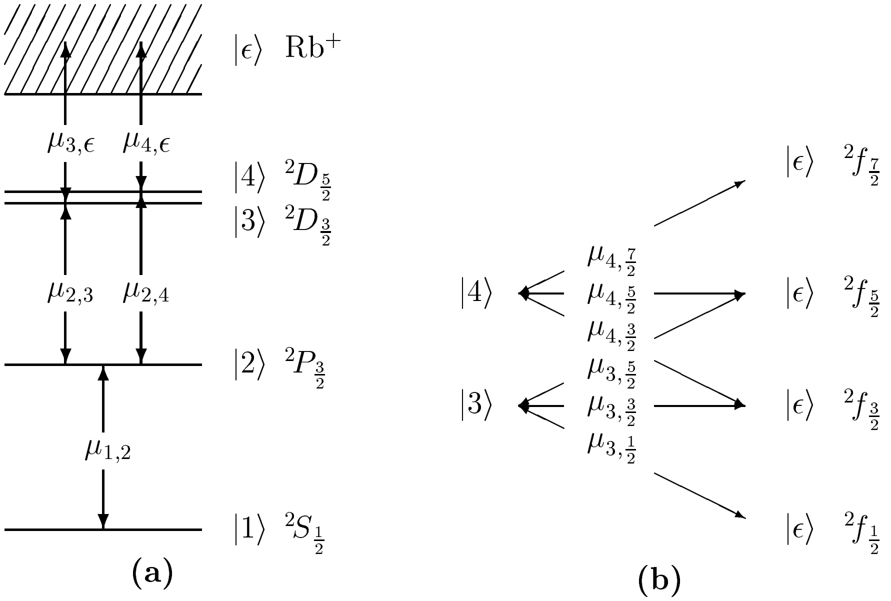

Figure 2.5: **(a)** *Energy-level diagram of rubidium, showing the levels and the couplings included in the model described in the text.* **(b)** *A detailed picture of the coupling of the two* 5*d states to the continuum.*

In the model only levels $|3\rangle$ and $|4\rangle$ couple to the continuum, and furthermore it is reasonable to assume that continuum levels do not couple, since continuum-continuum processes (ATI) only become relevant at much higher intensities (i.e. $I \geq 10^{12}$ W cm^{-2}) [66]. The electric field of the laser pulse is modeled by a Gaussian pulse, linearly polarized in the z direction

$$\vec{E}(t) = E_0 \vec{e}_z \frac{1}{2}\Big[\exp(-,\, t^2)\exp(i\omega_0 t) + \exp(-,\, {}^*t^2)\exp(-i\omega_0 t)\Big]\ . \tag{2.24}$$

Since $\omega_0 \approx \omega_2 - \omega_1 \approx \omega_3 - \omega_2 \approx \omega_4 - \omega_2$, the rotating-wave approximation may be used, which yields

$$\begin{aligned}
\dot{a}_1 &= \frac{eE_0}{2i\hbar}\exp(-,\, t^2)\exp[i(\omega_1 - \omega_2 + \omega_0)t]a_2\langle 1|z|2\rangle\ ,\\
\dot{a}_2 &= \frac{eE_0}{2i\hbar}\Big[\exp(-,\, {}^*t^2)\exp[i(\omega_2 - \omega_1 - \omega_0)t]a_1\langle 2|z|1\rangle\\
&\quad + \exp(-,\, t^2)\exp[i(\omega_2 - \omega_3 + \omega_0)t]a_3\langle 2|z|3\rangle\\
&\quad + \exp(-,\, t^2)\exp[i(\omega_2 - \omega_4 + \omega_0)t]a_4\langle 2|z|4\rangle\Big]\ ,\\
\dot{a}_3 &= \frac{eE_0}{2i\hbar}\Big[\exp(-,\, {}^*t^2)\exp[i(\omega_3 - \omega_2 - \omega_0)t]a_2\langle 3|z|2\rangle\\
&\quad + \exp(-,\, t^2)\sum_{\varepsilon'}\exp[i(\omega_3 - \omega_{\varepsilon'} + \omega_0)t]a_{\varepsilon'}\langle 3|z|\varepsilon'\rangle\Big]\ ,\\
\dot{a}_4 &= \frac{eE_0}{2i\hbar}\Big[\exp(-,\, {}^*t^2)\exp[i(\omega_4 - \omega_2 - \omega_0)t]a_2\langle 4|z|2\rangle\\
&\quad + \exp(-,\, t^2)\sum_{\varepsilon'}\exp[i(\omega_4 - \omega_{\varepsilon'} + \omega_0)t]a_{\varepsilon'}\langle 4|z|\varepsilon'\rangle\Big]\ .
\end{aligned} \tag{2.25}$$

For the continuum states, we have

$$\begin{aligned}\dot{a}_\varepsilon = \frac{eE_0}{2i\hbar}\Big[&\exp(-,\ ^*t^2)\exp[i(\omega_\varepsilon-\omega_3-\omega_0)t]a_3\langle\varepsilon|z|3\rangle\\ &+\exp(-,\ ^*t^2)\exp[i(\omega_\varepsilon-\omega_4-\omega_0)t]a_4\langle\varepsilon|z|4\rangle\Big]\ .\end{aligned}\tag{2.26}$$

This equation can be formally integrated and substituted into the equations for $\dot{a}_3$ and $\dot{a}_4$. If the continuum is assumed to be flat (i.e. $\langle\varepsilon|z|n\rangle$ is independent of ε) and infinitely wide, then the continuum can be adiabatically eliminated to give simply ionization out of the states $|3\rangle$ and $|4\rangle$ in addition to a coupling of the two states through the continuum [67]. The situation is actually slightly more complicated, since there are, in fact, four different continua: ${}^2f_{\frac{7}{2}}$, ${}^2f_{\frac{5}{2}}$, ${}^2p_{\frac{3}{2}}$, and ${}^2p_{\frac{1}{2}}$. Only two of these, ${}^2f_{\frac{5}{2}}$ and ${}^2p_{\frac{3}{2}}$, are accessible from both $|3\rangle$ and $|4\rangle$ (see Fig. 2.5b). As it can be seen, the four continua can be uniquely labeled by their j quantum number, so the following notation is introduced:

$$\begin{aligned}\mu_{n,n'} &= e\langle n|z|n'\rangle\ ,\\ \mu_{n,j'} &= e\langle n|z|\varepsilon j\rangle\ ,\end{aligned}\tag{2.27}$$

which yields the equations

$$\begin{aligned}\dot{a}_3 = {}&\frac{E_0}{2i\hbar}\exp(-,\ ^*t^2)\exp[i(\omega_3-\omega_2-\omega_0)t]\mu_{3,2}\,a_2\\ &-\frac{K}{2}I(t)\Big[(|\mu_{3,\frac{1}{2}}|^2+|\mu_{3,\frac{3}{2}}|^2+|\mu_{3,\frac{5}{2}}|^2)a_3+(\mu_{3,\frac{3}{2}}\mu^*_{4,\frac{3}{2}}+\mu_{3,\frac{5}{2}}\mu^*_{4,\frac{5}{2}})a_4\Big]\ ,\\ \dot{a}_4 = {}&\frac{E_0}{2i\hbar}\exp(-,\ ^*t^2)\exp[i(\omega_4-\omega_2-\omega_0)t]\mu_{4,2}\,a_2\\ &-\frac{K}{2}I(t)\Big[(|\mu_{4,\frac{3}{2}}|^2+|\mu_{4,\frac{5}{2}}|^2+|\mu_{4,\frac{7}{2}}|^2)a_4+(\mu^*_{3,\frac{3}{2}}\mu_{4,\frac{3}{2}}+\mu^*_{3,\frac{5}{2}}\mu_{4,\frac{5}{2}})a_3\Big]\ ,\end{aligned}\tag{2.28}$$

where $I(t)=\frac{1}{2}c\varepsilon_0E_0^2|\exp(-,\ t^2)|^2$ is simply the time-dependent intensity of the Gaussian laser pulse, and the constant K converts the square of the dipole matrix elements to partial cross-sections in units of inverse fluence $\{K=4\pi^2/(3\hbar c)$ for continuum wavefunctions normalized to energy, see [68]$\}$.

If pure LS coupling is assumed, the relative strengths of the different coupling matrix elements to the continuum can be determined using vector algebra [69]. As discussed in [38,68], the cross-section for ionization by a linearly polarized laser beam from state $|\gamma\rangle$ of an atom to the $\varepsilon l'$ continuum leaving an ion in state $|\gamma'\rangle$ can be calculated as

$$\sigma(\gamma,\gamma'\varepsilon l') = K\frac{1}{g_\gamma}|\langle\gamma|\vec{e}_z\cdot\vec{D}|\gamma'\varepsilon l'\rangle|^2\ ,\tag{2.29}$$

where K is defined above and g_γ is the degeneracy of the state $|\gamma\rangle$. Important in this context is the fact that under the assumption of LS coupling, the matrix-element in (2.29) can be decomposed into an angular part and a reduced matrix element. Moreover, when dealing with one electron outside a closed shell, calculations are simplified further. For an atom interacting only with linearly polarized light, the value of the m quantum number is conserved. In the present case, since the ground state is an s state, $m=0$ at all times. Starting out with the (multiplet averaged) cross-sections for ionization of the $5d$ state to the p and f continua, the square of the corresponding reduced matrix elements of the dipole operator (i.e. the linestrengths) are easily calculated, since in this case the Wigner-Eckart theorem yields

$$\begin{aligned}\sigma(\gamma l, \varepsilon l') &= K|\langle \gamma l m=0|\vec{e}_z \cdot \vec{D}|\varepsilon l' m=0\rangle|^2 \\ &= K \begin{pmatrix} l & 1 & l' \\ 0 & 0 & 0 \end{pmatrix}^2 |\langle \gamma l||D||\varepsilon l'\rangle|^2 \ , \end{aligned} \tag{2.30}$$

where $|\gamma'\rangle$ is left out, since the ion is simply left in its closed-shell ground state. In order to obtain the reduced matrix elements for each of the two fine-structure components, the above coupling coefficients and the fact that the dipole matrix element is independent of spin can be used. Then [69]

$$\langle \gamma s l j||D||\varepsilon s' l' j'\rangle = \sqrt{\frac{(2j+1)(2j'+1)}{(2s+1)}} \begin{Bmatrix} l & j & s \\ j' & l' & 1 \end{Bmatrix} \langle \gamma l||D||\varepsilon l'\rangle \delta_{s,s'} \ , \tag{2.31}$$

where the Racah $6j$ symbol is used. Using this equation, the reduced matrix element corresponding to each of the six couplings (Fig. 2.5b) can be calculated. The relative couplings to the continuum can now be obtained by using again the Wigner-Eckart theorem, but now for the fine-structure components (using $m_j=\pm\frac{1}{2}$):

$$\langle \gamma s l j m_j=\pm\tfrac{1}{2}|\vec{e}_z \cdot \vec{D}|\varepsilon s' l' j' m_j=\pm\tfrac{1}{2}\rangle = \begin{pmatrix} j & 1 & j' \\ \mp\frac{1}{2} & 0 & \pm\frac{1}{2} \end{pmatrix} \langle \gamma s l j||D||\varepsilon s' l' j'\rangle \ . \tag{2.32}$$

It is convenient to use the couplings related to the multiplet averaged cross-sections of ionization of $|\gamma\rangle=|5d, m=0\rangle$. So, fixing the phase of these couplings arbitrarily to zero yields:

$$\begin{aligned}\mu_p &= \sqrt{|\langle 5d, l=2, m=0|\vec{e}_z \cdot \vec{D}|\varepsilon, l'=1, m=0\rangle|^2} \ , \\ \mu_f &= \sqrt{|\langle 5d, l=2, m=0|\vec{e}_z \cdot \vec{D}|\varepsilon, l'=3, m=0\rangle|^2} \ , \end{aligned} \tag{2.33}$$

satisfying

$$\begin{aligned}\sigma_p &= K|\mu_p|^2 \ , \\ \sigma_f &= K|\mu_f|^2 \ , \end{aligned} \tag{2.34}$$

in which case the couplings $\mu_{n,j}$ as defined above are as listed in table 2.1. Four coupled differential equations are obtained:

$$\dot{a}_1 = \frac{E_0}{2i\hbar} \exp(-,\ t^2) \exp[i(\omega_1-\omega_2+\omega_0)t]\mu_{1,2}\, a_2 \ ,$$

Table 2.1: *Relative couplings of upper levels to continuum,* $\mu_{n,j}$.

	$n=3$	$n=4$
$j=\frac{1}{2}$	$-\sqrt{5/12}\mu_p$	0
$j=\frac{3}{2}$	$1/(2\sqrt{30})\mu_p$	$-3/(2\sqrt{5})\mu_p$
$j=\frac{5}{2}$	$\sqrt{7/15}\mu_f$	$1/(3\sqrt{70}\mu_f$
$j=\frac{7}{2}$	0	$\sqrt{10/21}\mu_f$

$$
\begin{aligned}
\dot{a}_2 = {} & \frac{E_0}{2i\hbar}\Big[\exp(-,\ {}^*t^2)\exp[i(\omega_2-\omega_1-\omega_0)t]\mu_{2,1}\,a_1 \\
& + \exp(-,\ t^2)\exp[i(\omega_2-\omega_3+\omega_0)t]\mu_{2,3}\,a_3 \\
& + \exp(-,\ t^2)\exp[i(\omega_2-\omega_4+\omega_0)t]\mu_{2,4}\,a_4\ ,\Big] \\
\dot{a}_3 = {} & \frac{E_0}{2i\hbar}\exp(-,\ {}^*t^2)\exp[i(\omega_3-\omega_2-\omega_0)t]\mu_{3,2}\,a_2 \\
& -\tfrac{1}{2}I(t)\Big[(\tfrac{51}{120}\sigma_p+\tfrac{7}{15}\sigma_f)a_3+(\tfrac{3}{20\sqrt{6}}\sigma_p+\tfrac{1}{15\sqrt{6}}\sigma_f)a_4\Big]\ , \\
\dot{a}_4 = {} & \frac{E_0}{2i\hbar}\exp(-,\ {}^*t^2)\exp[i(\omega_4-\omega_2-\omega_0)t]\mu_{4,2}\,a_2 \\
& -\tfrac{1}{2}I(t)\Big[(\tfrac{9}{20}\sigma_p+\tfrac{301}{630}\sigma_f)a_4+(\tfrac{3}{20\sqrt{6}}\sigma_p+\tfrac{1}{15\sqrt{6}}\sigma_f)a_3\Big]\ .
\end{aligned}
\tag{2.35}
$$

The dipole moments $\mu_{n,n'}$ between bound states needed in the calculation can be derived from reported oscillator strengths [51] under the assumption of *LS* coupling. The values are given in table 2.2. In order to calculate the values of the ionization cross-sections, an estimate based on a Yukawa potential [70] is performed. The two potential parameters are adjusted to reproduce reasonably the quantum defects of the p, d, and f series, as well as the position of a few lower-lying states. Based on the wavefunctions of this potential, approximate values for ionization to the p and f continua are obtained (table 2.2). Under the conditions of this experiment the fluence of the IR pulses are in all cases so low that saturation can be ignored. Therefore only the ratio σ_p/σ_f is important. The model potential estimate gives a ratio of $\sim 1/15$, which is in agreement with more advanced calculations performed on sodium at similar photon energies [71].

The set of Eq.'s (2.35) are solved numerically by integration over the duration of the frequency-chirped laser pulse, using Eq. (2.14). For a given chirp the population distribution over the four levels at the end of the IR laser pulse is determined. The three-photon ionization signal by the pulse is given by the population of continuum states, which can be calculated as the loss in the total population of the bound states. In order to facilitate comparison with

Table 2.2: *List of atomic parameters. Dipole moments are derived from oscillator strengths quoted in [51]. Cross-sections are determined by model potential calculations as described in the text.*

$\mu_{1,2}$	2.03×10^{-29}	Cm
$\mu_{2,3}$	6.45×10^{-31}	Cm
$\mu_{2,4}$	4.74×10^{-30}	Cm
σ_p	3.4×10^{-3}	$\mathrm{m^2\,J^{-1}}$
σ_f	4.5×10^{-2}	$\mathrm{m^2\,J^{-1}}$

the signal from the post-ionizing laser, the population in the levels $|3\rangle$ and $|4\rangle$ are weighted by the cross-section for ionizing the respective level with the probe laser. In fact, since the cross-sections predicted by the model calculation at the wavelength of the probe laser are the same within a few percent, the post-ionization signal can be compared with the sum of the population in the two upper levels.

2.6 Results and discussion

Fig. 2.6 shows a comparison of experimental and theoretical results for the post-ionization signal (proportional to the upper-state population) at two different fluences. The experimental chirp is determined from the displacement of the pulse shaper, according to Eq. (2.11). The solid curve shows the signal which is expected, based on integration of the time-dependent Schrödinger equation, as described in the previous section. Only the vertical scale of the experiment has been adjusted. The calculations show the same features as discussed for the experimental results in section 2.3: strong enhancement in the population transfer at positive chirp and interference wiggles. Furthermore, the calculated results show that the population transfer to $|4\rangle$, the upper $5d$ level, is more than an order of magnitude larger than the transfer to $|3\rangle$. This is due to the much stronger dipole coupling to this level, see table 2.2. It is a good approximation at the intermediate fluences of this experiment to disregard level $|3\rangle$, as done in producing the simplified dressed-atom energy level diagram in Fig. 2.1b.

It can be seen from Fig. 2.6 that the relative amplitude of the interference wiggles to the total population transfer depends on the pulse fluence: the higher the fluence the smaller the relative amplitude of the wiggles. This can be explained as an increase in the adiabaticity of the traversal of the dressed-atom diagram at higher fluences. Hence a larger fraction of atoms will go through the fully adiabatic path (labeled I in Fig. 2.1b). So if this path is already dominant (which appears to be the case), the relative amplitude of the wiggles will decrease with increasing fluence. This, in fact, lends us an internal check of the experimental fluences. If the fluence is calibrated to give agreement between measured and calculated ratios of wiggle

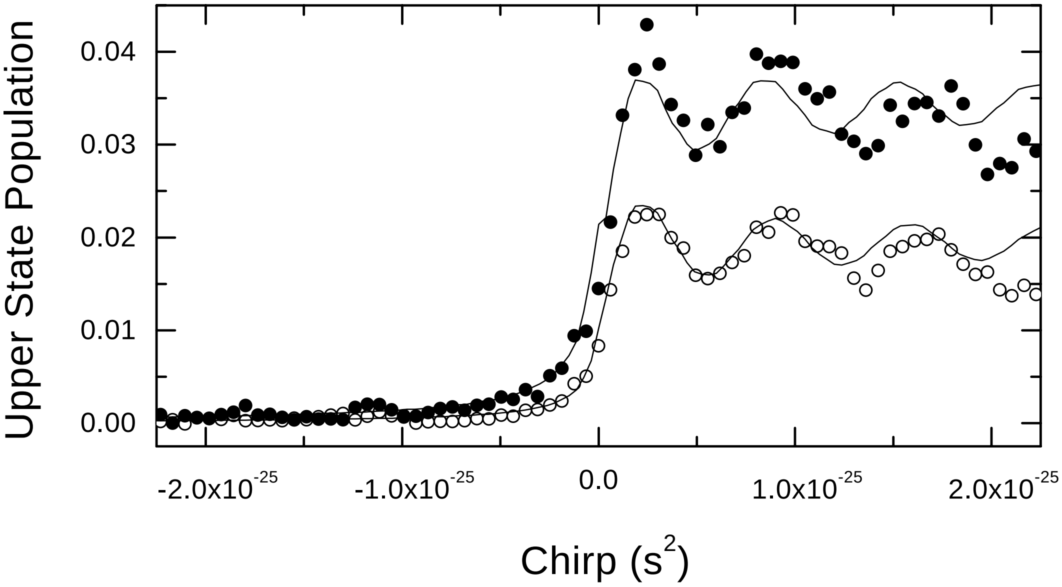

Figure 2.6: *A comparison of the population transfer to the upper level ($|3\rangle$ and $|4\rangle$), as measured by post-ionization (points) and as predicted by the theoretical model (solid curves). Results are shown at two different fluences: $\Phi_{\rm IR} = 75\ \mu{\rm J\,cm}^{-2}$ (lower curve) and $\Phi_{\rm IR} = 120\ \mu{\rm J\,cm}^{-2}$ (upper curve, similar to Fig. 2.4).*

amplitude to peak height, a fluence is found that deviates less than 15% from the experimentally estimated value.

A comparison of the measured three-photon ionization signal and the calculated population loss is shown in Fig. 2.7, again for two different fluences. Both experimental data and the calculated population transfer show oscillations as a function of chirp, reflecting the interference in the upper-state population. This indicates that (for large chirp) the three-photon ionization with the IR laser pulse is dominated by the stepwise process of transfer to the $5d$ level, followed by ionization with the remaining fluence of the pulse. At higher fluences the region of small chirp is apparently not well described by the model. The discrepancy can probably be explained by the limited number of states included in the model, since at high intensities off-resonant contributions from, for instance, the $5p\ ^2P_{\frac{1}{2}}$ (in the $|3\rangle \leftarrow |1\rangle$ transition) or the $7s\ ^2S_{\frac{1}{2}}$ (in the $|\varepsilon\rangle \leftarrow |2\rangle$ transition) may become important. As it appears from the vertical scales of Fig.'s 2.6 and 2.7, only a small fraction of the atoms that are transferred to the upper state is actually ionized. This is due to the small overlap between a bound atomic state and the continuum. For a molecular ladder, however, it is much more probable to transfer a molecule from a highly excited vibrational state to the dissociation continuum.

The possibility of interfering paths is a quite general property of a quantum ladder system. In the dressed atom picture it is easy to see that the number of enclosed areas increases rapidly with the number of levels N, corresponding to many interfering paths. The importance of the interfering paths depends critically on the strength of the interaction between the crossing levels. For a vibrational ladder all possible interferences are discussed in chapter 6. Including the

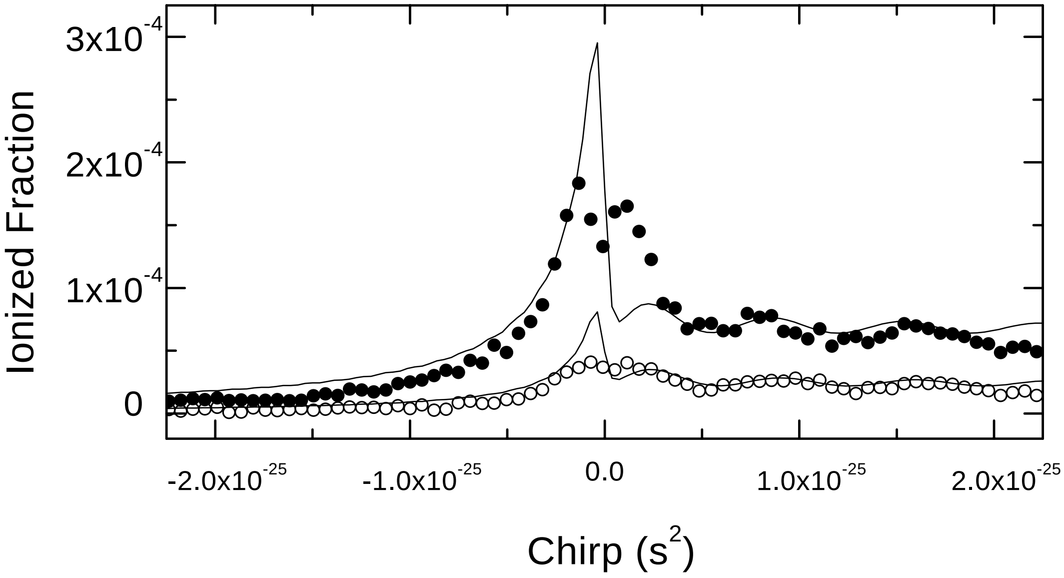

Figure 2.7: *A comparison of the three-photon ionization signal by the IR pulse under the same conditions as in Fig. 2.6.*

rotational structure is shown to possibly invert the sign of the anharmonicity of a ro-vibrational ladder.

It is important to notice that the interference phenomenon is not limited to excitation with Gaussian pulses. If the ladder system interacts with a chirped pulse of arbitrary envelope, interference wiggles will still be present. It is, however, only for a Gaussian pulse that a quadratic phase change corresponds to a linear chirp and hence induces oscillations of a constant period. Presumably the irregular oscillations observed in a previous experiment using square pulses were signatures of the same interference [29]. In the case of Gaussian pulses the interpretation is, however, much simpler, and it is possible to attribute oscillations of a certain period to an enclosed area in the dressed-atom diagram, thus yielding structural information about the ladder system.

2.7 Conclusion

The population transfer in a three-level model system has been investigated. A general interference mechanism is identified, which gives oscillations in the population transfer as a function of chirp. The period of the oscillations is related to structural properties of the ladder system. The situation where the final state of the ladder is in the continuum has been examined by monitoring the direct three-photon ionization of the system.

CHAPTER 3

TOTAL POPULATION TRANSFER IN THE RUBIDIUM $5s$-$5p$-$5d$-$\varepsilon_{p/f}$ LADDER SYSTEM

In this chapter results are presented of an experiment on the rubidium electronic ladder system $5s$-$5p$-$5d$-$\varepsilon_{p/f}$*, in the Rabi-cycling limit where all bound levels are strongly coupled. Transfer to the upper level (defined as the sum of the population in* $|5d\rangle + |\varepsilon_{p/f}\rangle$*) strongly depends on the chirp of the IR laser pulse. Most strikingly, pulses with the highest intensity transfer the least population to the upper level. Calculations based on the model presented in chapter 2 reproduce the behaviour of the transfer efficiency as a function of chirp on an absolute scale, although for* $\alpha \approx 0$ *some deviations are found. These deviations can be attributed to differences in the measured spectrum from the ideal Gaussian spectrum used in the model calculations and/or to the omission of the* $|5p_{\frac{1}{2}}\rangle$ *and* $|7s\rangle$ *states from the basis sets used for the model calculations.*

The criterion on both the Rabi-frequency and the chirp, that characterizes the likelihood of population inversion by Adiabatic Passage (AP), is introduced in section 3.1. A short description of the experiment is given in section 3.2. The results are presented in section 3.3 and compared to model calculations in section 3.4. The chapter ends with a discussion and some conclusions in section 3.5.

3.1 Introduction to Chirped Adiabatic Passage

As discussed in chapter 1, section 1.2, the adiabaticity of a chirped excitation process is determined by the Adiabatic-Passage (AP) criterion R, which is the ratio of the squared Rabi frequency Ω to the sweep rate at zero detuning $|\partial\Delta/\partial t|_{\Delta=0}$:

$$R = \frac{\pi\Omega^2}{2|\partial\Delta/\partial t|_{\Delta=0}} \; . \tag{3.1}$$

As discussed in section 2.4 of the previous chapter, for a Gaussian pulse the duration is proportional to the chirp for large α. Consequently, at constant pulse fluence the field strength E is proportional to the square root of the inverse chirp. For a single photon process, where a radiation field with amplitude E and central frequency ν_c couples level a with level b, the Rabi frequency is given by

$$\Omega_\omega = 2\left|\frac{\vec{\mu}_{ba}\cdot\vec{E}}{\hbar}\right| , \tag{3.2}$$

where $\vec{\mu}_{ba}$ denotes the dipole moment between the states a and b. For a laser pulse with a linear frequency chirp α, the sweep rate is $\partial\Delta/\partial t = 1/\alpha$. The Rabi frequency $\Omega(\alpha)$ is determined by the peak electric field E, which is a function of the chirp, hence $R(\alpha)$ is chirp-dependent as well:

$$R(\alpha) = \frac{\pi}{2}|\alpha|\Omega^2(\alpha) . \tag{3.3}$$

The fact that Ω_ν is proportional to E, $\Omega_\nu(\alpha)\sim\sqrt{1/\alpha}$ gives $R_\nu(\alpha)\sim\alpha\times(1/\sqrt{\alpha})^2$. Hence, the AP criterion of single-photon-transition is chirp-*in*dependent.

For absorption processes of N photons, the corresponding Rabi frequencies $\Omega_{N\nu}$ can be found in Allen *et al.* [72] and Loudon [23]. For a two-photon process from state a to c, these result in

$$\Omega_{2\nu} = 2\left|\frac{(\vec{\mu}_{cb}\cdot\vec{E}_{bc})(\vec{\mu}_{ba}\cdot\vec{E}_{ba})}{2\pi\Delta_{ba}\hbar^2}\right| , \tag{3.4}$$

on the condition that no eigenstate is within a Rabi-frequency of the virtual intermediate state, i.e. $\Delta_{ba}\gg\Omega_{2\nu}$, where $\Delta_{ba}=[(E_b-E_a)/h-\nu_c]$ is the detuning of the photon frequency from the intermediate state. This condition is violated for the resonant ladder climbing processes that are studied in this thesis. However, Eq. (3.4) can be used to derive the general behaviour of $\Omega_{2\nu}(\alpha)$ as a function of α. The two-photon Rabi frequency is quadratically dependent on the field amplitude E. Hence $R_{2\nu}(\alpha)\sim\alpha\times(1/\sqrt{\alpha})^4\sim\alpha^{-1}$. For the counter-intuitive ladder climbing (i.e. the direct two-photon absorption with $\alpha\ll 0$) this implies that, in the Rabi-cycling limit, the population can be efficiently transferred to the upper level only for a small range of α. The transfer efficiency will always drop to zero for more negative chirp.

In this chapter two attributes of population transfer in the rubidium ladder are discussed:

1. Is it possible to observe complete population inversion in the Rb ladder for both signs of the chirp using the same laser pulse?
2. How does the amplitude of the interference between path I and III (as discussed in chapter 2) evolve as a function of the fluence of the laser pulse?

It will be shown that both the appearance of total population inversion for counter-intuitive chirp and the disappearance of the interference can be attributed to meeting the adiabaticity criterion $R(\alpha)$ to enable Chirped Adiabatic Passage (CAP)[1].

---

[1] An earlier study of the efficiency of population transfer in the electronic ladder system $5s$-$5p$-$5d$-$\varepsilon_{p/f}$ in the rubidium atom has shown that complete population inversion is possible by using strong laser pulses and the

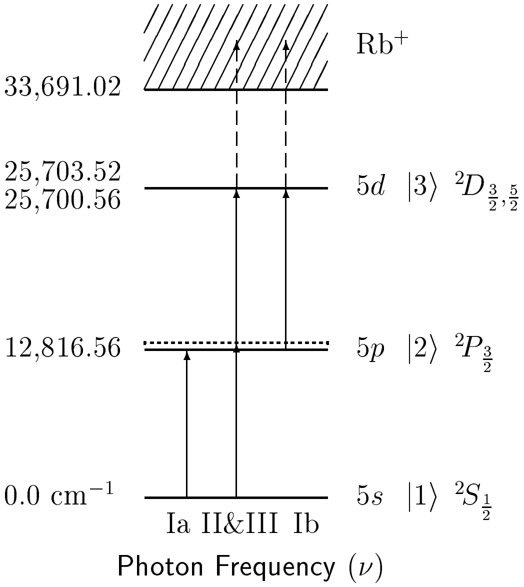

Figure 3.1: *A simplified energy level diagram for the $5s$-$5p$-$5d$-$\varepsilon_{p/f}$-ladder in the rubidium atom. The energy levels of the neutral atom are indicated by the symbols $|5s\rangle$, $|5p\rangle$ and $|5d\rangle$. The ionization continua $|\varepsilon_p\rangle$ and $|\varepsilon_f\rangle$ are represented by the hatched area and the symbol Rb$^+$. The solid arrows represent the couplings between the bound states of the ladder, and the dashed arrows the coupling of the $|5d\rangle$ state with the ε_p- and ε_f-continuum states of the rubidium ion. The one-photon transitions between bound states $5p \leftarrow 5s$ and $5d \leftarrow 5p$ are labeled by* Ia *and* Ib, *respectively. The two-photon transition from $5d \leftarrow 5s$ is labeled by* II&III, *corresponding to the names of the paths in Fig. 3.2.*

Fig. 3.1 shows a simplified[2] energy level diagram of the electronic ladder system $5s$-$5p$-$5d$-$\varepsilon_{p/f}$ in the rubidium (Rb) atom. The bound states in the ladder are coupled by two resonant transitions with slightly different frequencies: $\nu_{5p5s} = 12{,}816.56$ cm^{-1} and $\nu_{5d5p} = 12{,}886.94$ cm^{-1} [74]. The anharmonicity is $\delta = 70.38$ cm^{-1} [see Eq. (1.6)]. When rubidium atoms are irradiated by chirped laser pulses with a bandwidth greater than the anharmonicity, population can be transferred from $|5s\rangle$ to $|5d\rangle$ either by two consecutive single-photon absorptions $5p \leftarrow 5s$ and

---

technique of Chirped Adiabatic Passage [21, 29]. The most striking discovery in the experiment of Broers *et al.* was that 100% transfer to the upper level was also observed for large counter-intuitive chirp (i.e. when the instantaneous laser frequency does *not* follow the anharmonicity of the ladder). Their laser pulse, with a square power spectrum of width $\Delta\nu = 95$ cm^{-1}, was tuned to different central wavelengths to enable observation of total population inversion (at a fluence of $\Phi = 0.5$ mJ cm^{-2}) for each sign of the chirp: $h\nu_c^{\alpha>0} = 12{,}862$ cm^{-1} and $h\nu_c^{\alpha<0} = 12{,}807$ cm^{-1}. Chirped pulses with a square power spectrum have a temporal profile that is described by a sinc-function. For the present experiment the output of a multi-pass Ti:sapphire system is used [73]. Ideally these pulses would have a Gaussian temporal profile (and hence a Gaussian spectral profile as well). Such a temporal profile warrants smooth switching on and off of the laser field, so the adiabaticity criterion for CAP is more easily met than for sinc-pulses.

[2] Both the $5p$ and the $5d$ states are doublets due to LS coupling. For the $5p$ state the splitting is large $(E_{5p_{\frac{3}{2}}} - E_{5p_{\frac{1}{2}}}) = 237.6$ cm^{-1}, and the $5p_{\frac{1}{2}} \leftarrow 5s$ transition is not within the laser bandwidth. Therefore in the rest of this chapter the $5p_{\frac{3}{2}}$ state is meant when we refer to $5p$. The LS-splitting for the $5d$ state is only $(E_{5d_{\frac{5}{2}}} - E_{5d_{\frac{3}{2}}}) = 2.96$ cm^{-1} and both transitions $5d_{\frac{3}{2}} \leftarrow 5p_{\frac{3}{2}}$ and $5d_{\frac{5}{2}} \leftarrow 5p_{\frac{3}{2}}$ are within the laser bandwidth.

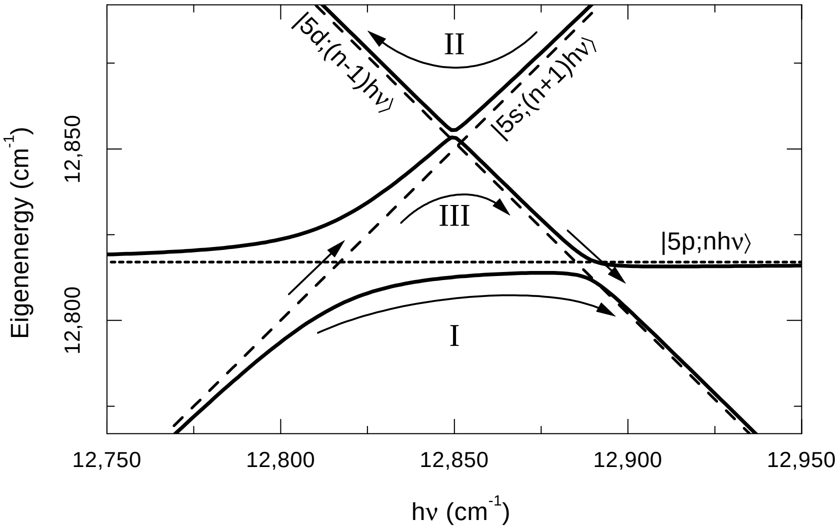

Figure 3.2: *A dressed level-, or Floquet- diagram for the* $5s$-$5p$-$5d$-$\varepsilon_{p/f}$*-ladder in the rubidium atom. The dashed lines show the unperturbed eigenenergies, and the solid curves show the atom+laser field eigenstates for a intensity of* 1.9×10^{7} W cm^{-2}. *For* $\alpha>0$ *the instantaneous field frequency follows the anharmonicity of the ladder. Population is transferred to the* $|5d\rangle$ *state via two paths:* I *sequential absorption of a single photon at the frequencies of the* $5p\leftarrow5s$ *and* $5d\leftarrow5p$ *transition,* III *direct two-photon excitation from* $|5s\rangle$ *to* $|5d\rangle$*. For* $\alpha<0$ *path* II *is followed.*

$5d\leftarrow5p$ or by the direct two-photon transition $5d\leftarrow5s$ via a virtual intermediate state (indicated by the dashed line in Fig. 3.1. The sequential excitation process is indicated by the arrows labeled Ia and Ib in Fig. 3.1. This process can occur only when the instantaneous frequency follows the anharmonicity of the ladder system, i.e. for $\alpha>0$. For the two-photon absorption, on the other hand, the excitation of the $|5d\rangle$ state occurs at the two-photon resonance. Therefore the stacked solid arrows in Fig. 3.1 represent two-photon excitation by a positively *or* negatively chirped laser pulse. Inspection of Fig. 3.2 reveals the distinction between excitation paths II & III: path II contributes only to the final $|5d\rangle$ population for $\alpha<0$ and path III, together with path I, only for $\alpha>0$.

3.2 Description of the experiment

Rubidium atoms were evaporated into the interaction region of a vacuum chamber. A pinhole with diameter $d=3.7$ mm collimated the linearly polarized laser beam. After passing a Berek's polarization compensator [75–78], set at a retardation of $\lambda/2$, the beam passed a dielectric polarizer, enabling easy regulation of the fluence by rotation of the polarization compensator. A lens with focal length $f=20$ cm imaged the pinhole on the interaction region. The magnification factor was $m=\frac{1}{2}$. The atoms were irradiated by the output of a multi-pass Ti:sapphire amplified laser system (see chapter 2 in [73]) tuned to $\nu_c\approx12{,}850$ cm^{-1} and $\Delta\nu\approx150$ cm^{-1}. The chirp of the IR pulse could be controlled by a pulse compressor. The frequency spectrum of the IR laser

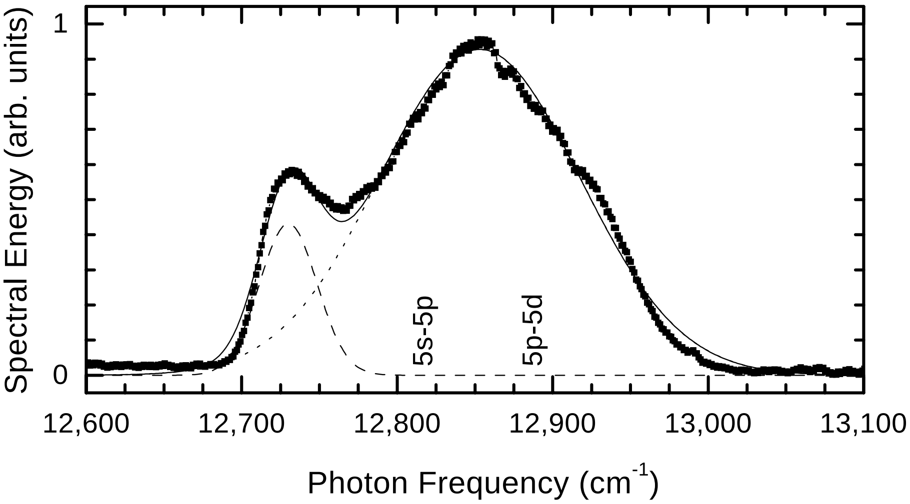

Figure 3.3*: The dots show the normalized recorded spectral energy of the IR pulse from the Ti:sapphire laser. The solid curve is the sum of two Gaussian-shaped spectra, with pulse parameters* $A_1 = 129$, $\nu_{c1} = 12{,}853(10)$ cm^{-1}, $\Delta\nu_1 = 152$ cm^{-1}, *and* $A_2 = 20$, $\nu_{c2} = 12{,}730(10)$ cm^{-1}, $\Delta\nu_2 = 44$ cm^{-1}, *obtained from a fit to the recorded spectrum of two Gaussians of the form* $I_i(\nu) = \frac{A_i}{\Delta\nu\sqrt{\frac{\pi}{2}}}\exp[-2\ln 2(\frac{\nu-\nu_i}{\Delta\nu})^2]$ *(shown as dashed curves).*

pulses was monitored using a monochromator and a photo-diode array during data collection. Ideally the IR pulses have a Gaussian spectral profile. However, as can be seen in Fig. 3.3, the IR pulse spectrum is better fitted with a pair of Gaussians. Both bound-bound transition frequencies of the ladder are resonantly driven within the large width of the IR spectrum. Note that the center frequency of the feature on the low-frequency side of the spectrum is well to the red of any above mentioned ladder transition. A delayed 8 ns long pulse of the second harmonic ($\lambda = 532$ nm) of a Nd:YAG laser had a sufficiently large fluence to ionize all remaining population in the $5d$ state, while its intensity was sufficiently low to prevent ionization from lower lying states. A small voltage accelerated the photo electrons to a multi-channel plate charged particle detector. The fluence of the IR pulses was monitored using a photo diode. Typically 60 shots were recorded for every data point, of which only those with a fluence within 20% of the average were accepted. Summarizing, the photo-electron signal is used to determine the dependency of the population transfer to the upper state as a function of both the fluence and the chirp of the IR laser pulse.

3.3 Experimental results: 100% transfer in the Rb ladder system

The ionization data are measured at six different fluences, spanning over two decades. During data collection only the chirp and the fluence have been changed. The spectrum of the laser remained essentially constant. The relative scaling between the six scans is not adjusted: one vertical multiplication factor is used to normalize the data such that the largest ionization signal

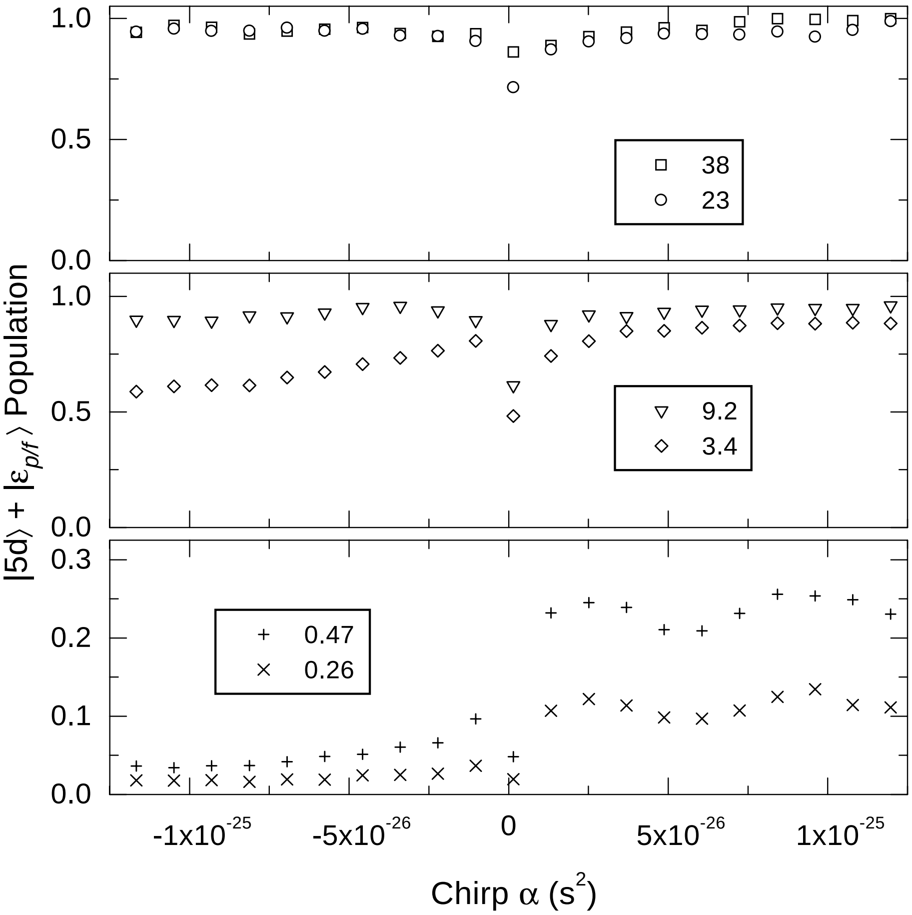

Figure 3.4: *The measured photo-electron yield, probing the population in the* $|5d\rangle+|\varepsilon_{d/f}\rangle$ *states as a function of the chirp of the IR laser pulse for high, intermediate and low IR pulse fluences. The numbers corresponding to the symbols indicate the IR pulse fluence for each data set (in* $\mathrm{mJ\,cm^{-2}}$*). The top panel shows 100% transfer of the population for both intuitive and counter-intuitive chirp. Note that at* $\alpha = 0$*, where the pulse intensity is maximal, the population transfer is the least. The middle panel, measured for slightly lower pulse fluences, shows that for* $\alpha < 0$ *the transfer to the* $|5d\rangle+|\varepsilon_{d/f}\rangle$ *states drops, illustrating the chirp-dependency of the adiabaticity condition for the two-photon process* $R_{2\nu}(\alpha)$*. The one photon CAP-condition is still met, hence the absence of interference for* $\alpha > 0$*. At the lowest fluence, the counter-intuitive transfer strongly reduced. For* $\alpha > 0$ *the interference is present, demonstrating that for these fluences CAP for the one-photon transitions is no longer possible (*$R_\nu \ngtr 1$*).*

among the six data sets is scaled to unity. Fig. 3.4 shows the photo-electron yield, probing the transfer to the $|5d\rangle+|\varepsilon_{d/f}\rangle$ states, as a function of the chirp of the IR laser pulse. The fluences range from 0.26 to 38 $\mathrm{mJ\,cm^{-2}}$ (indicated by the numbers). Obviously for the lowest fluences (lower panel of Fig. 3.4) the presence of the interference wiggles (also found and discussed in chapter 2) demonstrates that transfer occurs by both diabatic and adiabatic paths. For slightly higher fluences (middle panel of Fig. 3.4) the observed decrease of the transfer to $|5d\rangle$ for $\alpha < 0$ indicated that $R_{2\nu}(\alpha) \ngtr 1$. As discussed in section 1.5, the counter-intuitive transfer efficiency is a function of α, showing that the excitation to the $|5d\rangle$ state is a higher-order process. The upper panel of Fig. 3.4 demonstrates 100% transfer to the $|5d\rangle$ state. This total transfer demonstrates that for the highest fluences and large $|\alpha|$ both adiabaticity conditions R_ν and $R_{2\nu}(\alpha)$ (for the single-photon and the two-photon processes) are fully met for both signs of chirp. Note that for all fluences the transfer for $\alpha \neq 0$ is more efficient than for $\alpha = 0$, where the IR pulses are shortest in duration and hence have the highest peak intensity.

Summarizing, the results for $\alpha < 0$ demonstrate how at high intensities a two-photon path can transfer all population to the upper level (via path II). For too negative chirp the intensity no longer sustains the two-photon coupling and the transfer efficiency drops. For $\alpha > 0$ and low intensities the $5d$-state is populated via both paths I and III. At high intensities and sufficiently large chirp the one-photon adiabaticity criterion is met and all the population follows path I.

3.4 Comparison of model calculations with experiments

3.4.1 Population transport as a function of the IR intensity

The transfer to the $|5d\rangle$ state is investigated as a function of the IR intensity both experimentally and theoretically for three values of the chirp. The calculations are performed using the model introduced in chapter 2. Firstly the left panel of Fig. 3.5 is discussed. The symbols $-$ and $+$ represent data recorded for $\alpha = -7\times10^{-26}$ s^2 and $\alpha = +7\times10^{-26}$ s^2, respectively. The lines in the figure show the calculated population at identical chirp values. The agreement is very good. The right panel of Fig. 3.5 shows the data ($\circ$) for $\alpha = 0$ s^2. The calculated populations are shown

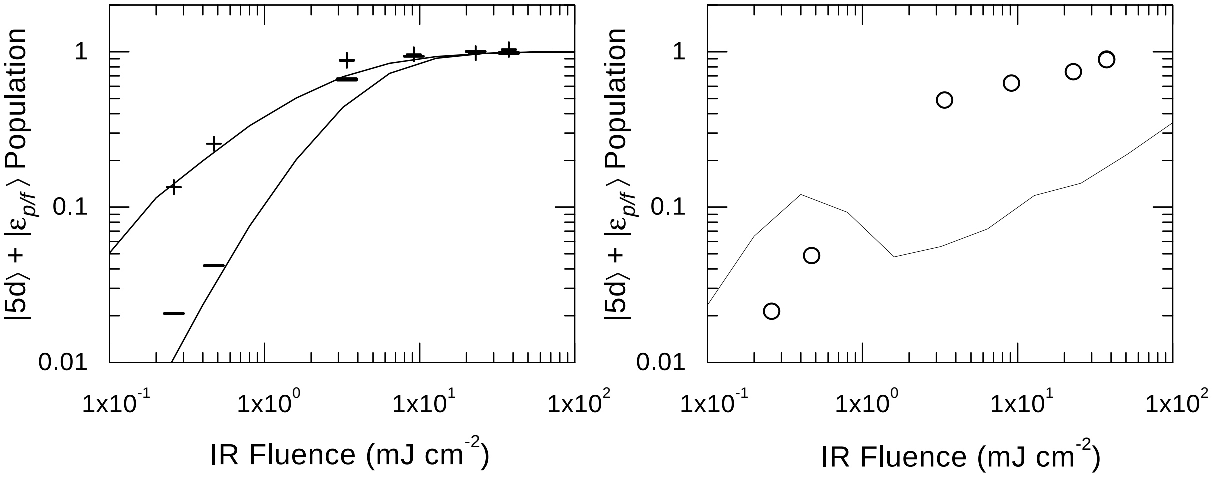

Figure 3.5: *The measured population transfer to* ($|5d\rangle + |\varepsilon_{p/f}\rangle$) *as a function of experimental fluence (see bottom axis) compared to model calculations. The symbols in the left panel represent the data recorded for two different values of the chirp:* $-$ *for* $\alpha = -7\times10^{-26}$ s^2 *and* $+$ *for* $\alpha = +7\times10^{-26}$ s^2. *The solid curves correspond to model calculations using a single Gaussian model pulse with* $\nu_c =$ 12,845 cm^{-1} *and* $\Delta\nu = 152$ cm^{-1}) *of the population transfer for* $\alpha = \pm7\times10^{-26}$ s^2. *The symbols* $\circ$ *in the right panel show the data for* $\alpha = 0$, *which is not very well reproduced by the calculations.*

for the model from chapter 2 (solid curves). The agreement of the 4-level model calculations with the data is not great. The disagreement between model calculations and data is discussed in more detail in section 3.4.3. For the low fluence perturbative regime the transfer efficiency for both $\alpha = -7\times10^{-26}$ s^2 and $\alpha = 0$ s^2 is one order of magnitude less than for $\alpha = +7\times10^{-26}$ s^2. For all three chirp values the transfer efficiency goes as the square of the fluence. For high fluence the transfer saturates at 100%. This total population inversion is confirmed by model calculations for $\alpha = \pm7\times10^{-26}$ s^2 (solid curves in Fig. 3.5). As mentioned above, the prediction for $\alpha = 0$ (dashed curve) is dissimilar from the measured data. Most importantly, data and both models show that for $\Phi \geq 20$ J cm^{-2} 100% transfer is reached for the positive and negative chirp.

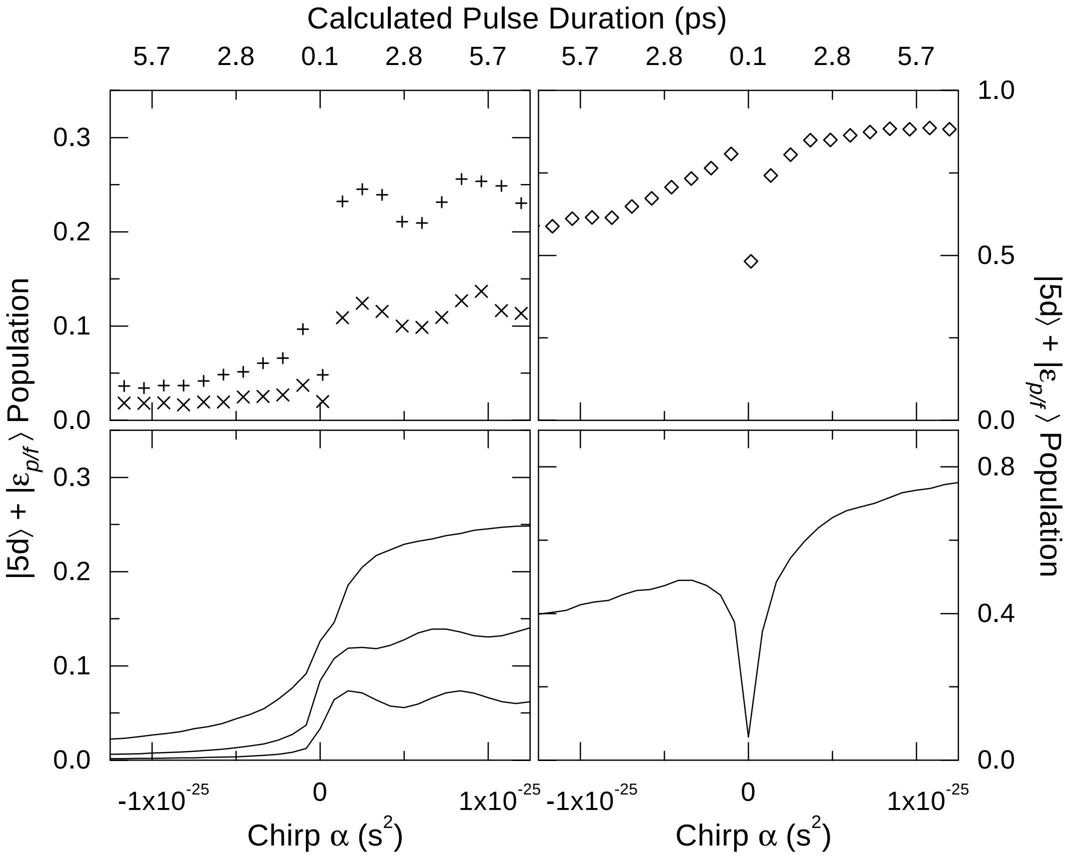

Figure 3.6: *The symbols in the upper panels of this figure display a subset of the data of Fig. 3.4. The data are recorded for IR fluences of* $\Phi = 0.26, 0.47$ *(left upper panel) and* 3.4 mJ cm^{-2} *(right upper panel). The curves in the lower panels compare the data to model calculations performed with the model from chapter 2, using a single Gaussian model pulse with* $\nu_c = 12{,}845$ cm^{-1}, $\Delta\nu = 152$ cm^{-1} *and* $\Phi = 0.125, 0.25, 0.5$ *(left lower panel) and* 3.3 mJ cm^{-2} *(right lower panel). Both theory and data show the disappearance of the interference features as a function of IR fluence.*

3.4.2 Population transport as a function of chirp

A comparison of the measured transfer efficiency to the $|5d\rangle$ state with predictions from the model that was developed in chapter 2 is discussed in this subsection. The population transfer for low, medium and high IR fluences is displayed in Fig.'s 3.6, 3.7 and 3.8, respectively. Individual data sets could be brought into much closer agreement by small adjustments of the pulse parameters for each scan. However, for a more systematic comparison of the model calculations to the data sets, the simulations are performed with one set of parameters (i.e. $\nu_c = 12{,}845$ cm^{-1} and $\Delta\nu_c = 152$ cm^{-1}) to model the electric field, while only the fluence of the pulse is varied.

The upper panels of Fig. 3.6 display the total ionization signal as a function of chirp at three fluences $\Phi = 0.26, 0.47$ and 3.4 mJ cm^{-2}. The lowest two fluence scans clearly show modulation in the population transfer for $\alpha > 0$, demonstrating the quantum interference between paths I and II. In the highest fluence scan the modulations are no longer visible. The lower panels of the same figure shows the results of theoretical modeling at four fluences. The functional form of the chirp scans is nicely reproduced by the calculations. Theory and data also agree well in absolute magnitude. The top panel of Fig. 3.7 displays the total ionization signal as a function of chirp at the fluences $\Phi = 3.4$ and 9.2 mJ cm^{-2}. In the bottom panel the calculated population is shown for $\Phi = 3.3$ and 10 mJ cm^{-2}. Again, the agreement is remarkably good. The slight discrepancy at $\alpha \approx 0$ will be discussed in section 3.4.3. For $\alpha < 0$ the decrease of the transfer for more

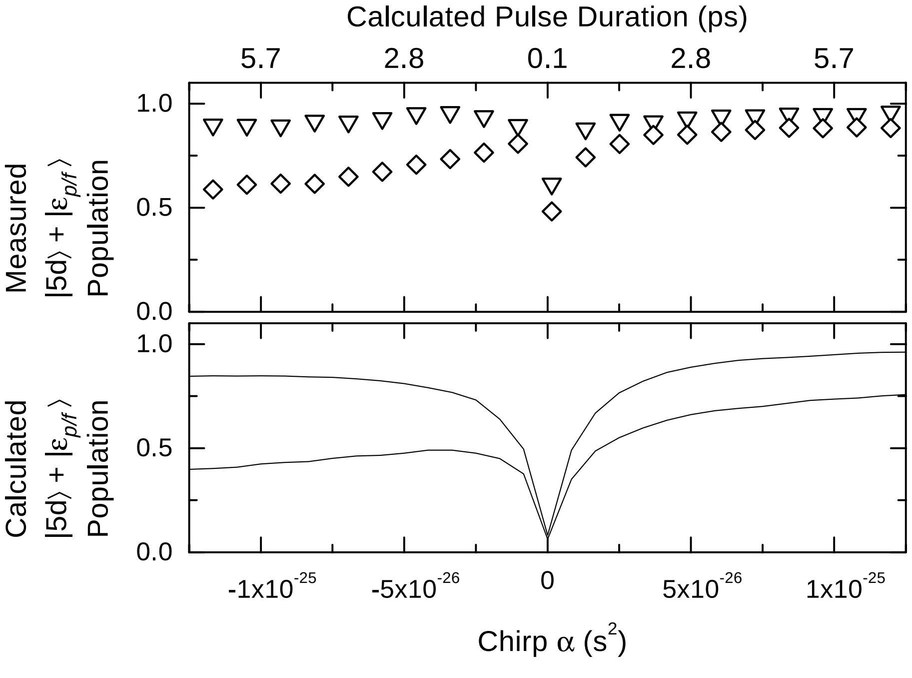

Figure 3.7: *The symbols in this figure display the same data as the middle panel of Fig. 3.4, as recorded for IR fluences of* $\Phi = 3.3$ and 9.2 mJ cm^{-2}. *The curves compare the data to model calculations, performed with the model from chapter 2, using a single Gaussian model pulse with* $\nu_c = 12{,}845$ cm^{-1}, $\Delta\nu = 152$ cm^{-1} *and* $\Phi = 3.3$ and 10 mJ cm^{-2}.

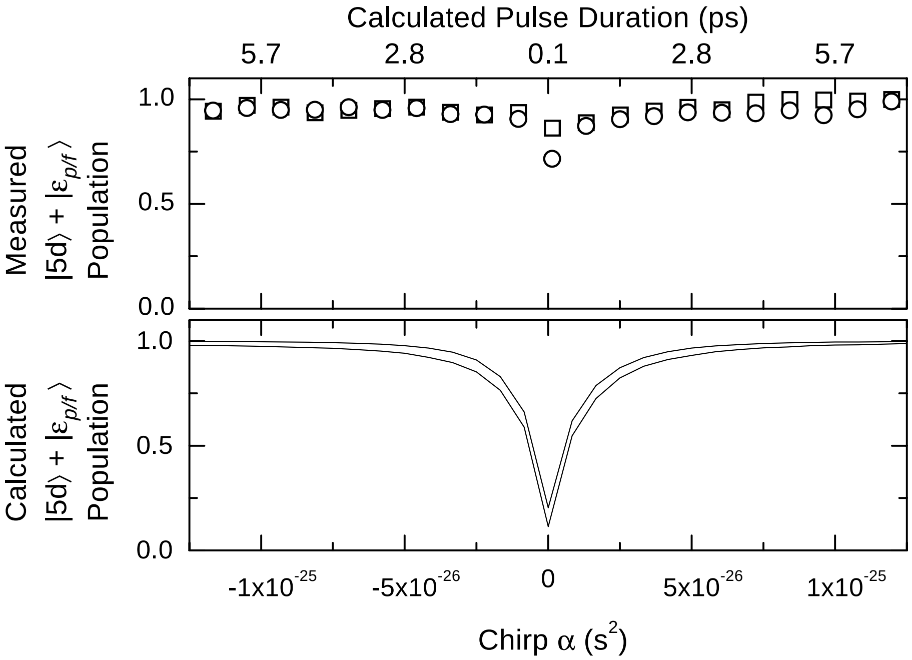

Figure 3.8: *The symbols in this figure display the same data as the top panel of Fig. 3.4, as recorded for IR fluences of* $\Phi = 23$ and 38 mJ cm^{-2}. *The curves compare these to model calculations, performed with the model from chapter 2, using a single Gaussian model pulse with* $\nu_c = 12{,}845$ cm^{-1}, $\Delta\nu = 152$ cm^{-1} *and* $\Phi = 20$ and 40 mJ cm^{-2}.

negative chirp demonstrates the dependence of the two-photon adiabaticity criterion $R_{2\nu}(\alpha)$ on the chirp. For sufficiently large positive chirp ($\alpha \geq 3 \times 10^{-26}$) the transfer remains constant, confirming the independence of the chirp for the single-photon adiabaticity criterion R_ν. At last, in Fig. 3.8 the top panel displays the total ionization signal as a function of chirp at the fluences $\Phi = 23$ and 38 mJ cm^{-2}. Clearly for these fluences and the whole experimentally accessed chirp range, the transfer is more efficient than for $\alpha = 0$. This observation is supported by the model calculations, as shown in the bottom panel for $\Phi = 20$ and 40 mJ cm^{-2}. Summarizing, minor deviations between model calculations and measurements occur for $\alpha \approx 0$. Extending the model with extra basis states improves the prediction for $\alpha = 0$. The general features of the measured transfer efficiency are confirmed by the model calculations:

I. Enhancement for $\alpha > 0$ for the entire fluence range, with the interference only present for low fluences (Fig. 3.6),
II. For both $\alpha < 0$ and $\alpha > 0$ a strong enhancement for medium-high fluences and, finally,
III. For both $\alpha < 0$ and $\alpha > 0$ transfer of 100% of the population to the upper state of the ladder.

3.4.3 On the discrepancies between data and calculations for $\alpha \approx 0$

The features of the data are reproduced well by the model calculations. Only at zero chirp the results deviate from the measurements. There are several explanations for these discrepancies.

Firstly, the measured pulse shape deviates from the *single* Gaussian used in the model calculations. As can be seen from Fig. 3.3, the real pulse fits to a *pair* of Gaussians with different pulse widths and central frequencies. The sub-peak on the red side of the spectrum contains about 15% of the total energy, which correspond to substantial contributions to the electric fields compared to those from the main peak. The field interference between the two peaks can dramatically change the time profile of the IR laser pulse, and therefore change the efficiency of population transfer. Unfortunately the power spectrum contains no phase information, prohibiting reconstruction of the actual temporal profile of the IR laser pulse. However, chirping the pulse introduces a time-ordering of the spectral components such that the two features cease to interfere. For "large" chirp the original phase information is irrelevant, and the power spectrum alone is sufficient to describe the population transfer. Determination of the magnitude of the chirp for which the effect of the side peak is negligible can be estimated from the width of the subpeak: its field profile must be *at least* 600 fs (FWHM) assuming that the incident sub-pulse is transform limited. This estimate is consistent with the observation that the model and data disagree for pulse durations of the chirped pulse $\tau_{\text{chirped}} \leq 2$ ps, corresponding to $|\alpha| \leq 3 \times 10^{-26}$. Outside this region where a Gaussian power spectrum models the pulse sufficiently, agreement to the model is very good. For instance, assume that each of the two pulses has a different amount of linear chirp. This would effectively reduce the width of the range of chirp with reduced transfer since for $\alpha_1 = 0$ (i.e. when one of the pulses is compressed), the chirp of the other pulse is $\alpha_2 \neq 0$ and already increases the transfer efficiency.

Secondly, for the high fluence regime the basis set chosen in the model calculations is probably too limited to completely describe the system. The nearest states which are not resonant with the ladder for weak IR pulses are the $|5p_{\frac{1}{2}}\rangle$ state, with $(E_{5\text{p}_{\frac{1}{2}}} - h\nu_c) \approx -275$ cm^{-1} and the $|7s\rangle$ state, with $(E_{7\text{s}} – 2h\nu_c) \approx 600$ cm^{-1}. When $\alpha \approx 0$ and the IR intensity is high (e.g. for the highest fluences of the experiment) the coupling to the levels $5p_{\frac{1}{2}}$ and $7s$ become sufficiently large to become resonant with the excitation pulse due to the large AC-Stark shift [79]. This is investigated by extension of the basis set of the model from chapter 2 with the $|7s\rangle$ state and its coupling to the $|\varepsilon_p\rangle$ continuum. The calculations of this model (dashed curve in Fig. 3.9) are compared with the results from the 4-state model (solid curve) and the data (symbol $\circ$). Including the $7s$ state does improve the prediction. For $\Phi = 38$ mJ cm^{-2}, the highest fluence of the experiment, a substantial increase of the population in the upper states of the ladder is found: $P^{\text{oldmodel}}_{5d+\varepsilon_{p/f}} = 0.18$ whereas $P^{\text{newmodel}}_{5d+7s+\varepsilon_{p/f}} = 0.39$. Although the transfer still is less than experimentally determined ($P^{\text{exp}}_{5d+7s+\varepsilon_{p/f}} = 0.87$), including the $7s$ state in the model clearly improved the modeling. Hence, as is to be expected for the high intensities of the IR pulse around $\alpha = 0$, off-resonant states are coupled to the states of the ladder (this is also found by [52]). The extension of the basis set of the model with the $7s$ state shows that this state contributes to the population transfer for high intensities (i.e. $\alpha = 0$ and $\Phi \geq 5$ mJ cm^{-2}, see Fig. 3.9). For chirped pulses with the same fluence the AC-Stark shift [79] drops quickly and the $7s$ state ceases to contribute. However, since the detuning of the laser with the $|5p_{\frac{1}{2}}\rangle$ state is less and the dipole-moments between the $5p_{\frac{1}{2}}$ and the $5s$ and $5d$ states are larger, the $5p_{\frac{1}{2}}$

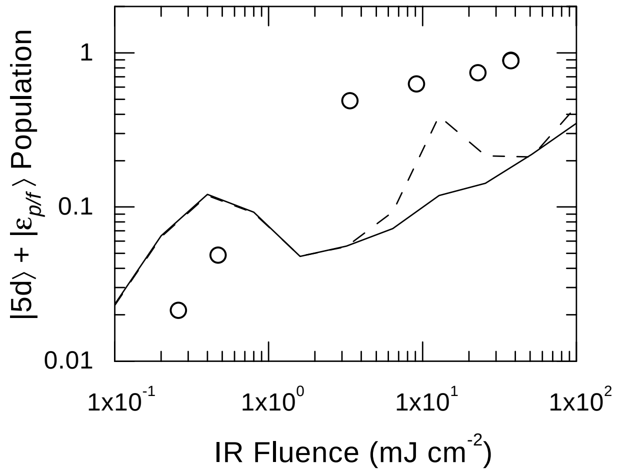

Figure 3.9: *The measured population transfer to ($|5d\rangle + |\varepsilon_{p/f}\rangle$) at $\alpha = 0$ ($\circ$) as a function of experimental fluence (see bottom axis) compared to model calculations. The solid curve is the same result from the 4-states model as in Fig. 3.5. The dashed curve is calculated with a similar model, including the* $7s$ *state in the basis set. This does improve the calculation.*

state is expected to start contributing at lower intensities and a larger range around $\alpha = 0$. It is clear that the preliminary result on the extension of the basis set with the $7s$ state ask for closer investigations of the population transfer using a new model that extends the old basis set of $|5s\rangle$, $|5p_{\frac{3}{2}}\rangle$, $|5d_{\frac{3}{2}}\rangle$, $|5d_{\frac{5}{2}}\rangle$, $|\varepsilon_p\rangle$ and $|\varepsilon_f\rangle$ with both the $|5p_{\frac{1}{2}}\rangle$ and $|7s\rangle$ levels.

3.5 Conclusions

The present experimental results show that population transport to the upper level of an anharmonic ladder system can be significantly enhanced by chirping the IR laser pulse. For the low-Rabi-cycle limit, transfer is enhanced only when the laser frequency follows the ladder anharmonicity. The interference effect found in chapter 2 disappears when the sequential absorption of two photons (path I in Fig. 3.2) starts to fulfill the adiabaticity condition at higher pulse fluences. In the high-Rabi-cycle limit, *all* population can be transported to the upper level of a ladder system for a sufficiently large chirp $|\alpha|$. In contrast with the general behaviour of multi-photon excitation, the transfer is now *least* efficient for the *most* intense pulses (i.e. for $\alpha = 0$). Compared to the experiment of Broers *et al.* [29], the present experiment shows for the first time that full transfer is obtained for both signs of the chirp of a laser pulse with all other parameters identical.

CHAPTER 4

VIBRATIONAL LADDER CLIMBING IN NO BY ULTRASHORT INFRARED LASER PULSES

In this chapter an experiment demonstrating vibrational ladder climbing in the diatomic molecule NO using the Free-Electron Laser for Infrared eXperiments (FELIX) [48, 49] is presented. The anharmonic vibrational ladder of nitric oxide (NO) is climbed by irradiating the molecule with femtosecond infrared (IR) pulses. The free-electron laser FELIX is tuned to $\lambda = 5.4$ *µm with a bandwidth of* $\Delta\lambda = 0.3$ *µm, corresponding to a pulse duration of 150 femtoseconds. Transfer to the excited states of NO is monitored by 1+1 REMPI. NO is chosen for its well-known spectroscopy and the established Resonance Enhanced Multi-Photon Ionization (REMPI) scheme to determine the ro-vibrational distribution of the electronic ground state [80]. The REMPI probe on the NO* $A\,^2\Sigma^+ {-} X\,^2\Pi$ *system has proved to be very sensitive, and resolves the distributions over the vibrational and rotational states. Population is found up to* $v'' = 5$*, the highest level within reach of the IR bandwidth. The average transfer per step of the ladder is found to be 17%.*

Firstly, the history of vibrational ladder climbing is introduced briefly in section 4.1. Then, in section 4.2, some relevant attributes of the NO molecule are reviewed. The experimental system is described in section 4.3. Several measured REMPI spectra are presented in section 4.4. The chapter ends with some brief conclusions in section 4.6.

4.1 Introduction

One of the goals in physical chemistry is to achieve control over chemical reactions [7]. The vibrational state of a molecule often determines what type of reaction occurs, and greatly influences reaction rates (chemical activation). Hence excitation or even the dissociation of a specific molecular bond is a major ingredient of state-selective chemistry. The high spectral brightness of lasers makes them outstanding tools to excite a large fraction of an ensemble of molecules bond-specifically or mode-selectively. For example, using laser light having a well defined frequency, it is possible to activate isotope-selective processes, making use of the optical shifts in the transition frequencies induced by the difference in the nuclear masses. Multi-photon (MP) dissociation of sulphurhexafluoride (SF_6) provided one of the earliest demonstrations of the applicability of lasers in mode-selective processes (see [81, 82] for a review). Here the first absorbed photon was in resonance with a vibrational overtone of the $^{32}SF_6$ isotope. Thereafter, MP dissociation into $^{32}SF_5 + F$ was possible, although all subsequent steps were off-resonant due to the anharmonicity of the vibrational ladder system. Using a similar scheme enrichment of uranium, of interest for the nuclear industry, was accomplished: by tuning a CO_2-pumped p-H_2 laser to lines which preferentially excite $^{235}UF_6$, an isotope separation factor of 1.2 was observed [83]. Such experiments involve narrow-band laser light and are only feasible because of the rare coincidence of an excitation frequency of a molecular mode with the output of a powerful laser operating in the mid-infrared ($1.5-20$ μm).

Bond-selective dissociation by vibrational ladder climbing involves a series of vibrational excitations. The anharmonic nature of vibrational ladders requires as many narrow-band lasers as the number of steps to be resonantly climbed. One alternative scheme uses MP absorption driven by intense CW IR lasers. The resonance condition is set such that N times the photon energy is resonant with the N$^{\text{th}}$ vibrational level of the molecule [32, 84]. The selection rules for MP transitions to v''=N are relaxed as compared to the very restricted single photon overtone excitation to the same v''. The number of lasers can also be reduced if one uses lasers with larger bandwidths. In order to be resonant with a large number of vibrational steps, several authors have suggested the use of broadband radiation [19, 20]. An ultrashort laser pulse necessarily has the large bandwidth containing the frequencies required to climb several steps of the ladder. Recently von Helden *et al.* demonstrated the ionization of fullerenes by the absorption of more that 200 IR photons that are resonant with a vibrational mode of the C_{60} molecule [85]. The vibrational excess energy (35-40 eV) redistributes over both the vibrational and the electronic modes, and is sufficiently large for to efficiently ionize the fullerenes. Although the large bandwidth of such pulses frustrates isotope selectivity, mode selectivity can still be achieved since the different vibrational modes in a molecule are generally well separated in frequency. Because the large bandwidth sustains short pulses, intramolecular vibrational relaxation to other modes will not have time to occur during the pulse, keeping the energy localized in the selected bond. This aspect of short-pulse excitation is of importance in preserving mode-selectivity or bond-specificity in vibrational excitation of polyatomic molecules. The efficiency of population transfer may be enhanced considerably by tailoring the IR laser pulses. Recent experiments on anharmonic electronic ladder systems in atomic rubidium [29, 30] and sodium [59] have shown that by frequency chirping a very intense laser pulse the transfer approaches 100%, and is rather insensitive to the exact pulse fluence (Rabi-cycling limit). Chelkowski *et al.* [19, 20, 86] have performed calculations on vibrational excitation of HF by intense chirped IR laser pulses. These calculations predict that, if the instantaneous IR frequency follows the anharmonicity of the ladder, the transfer to the highest vibrational level is increased by several

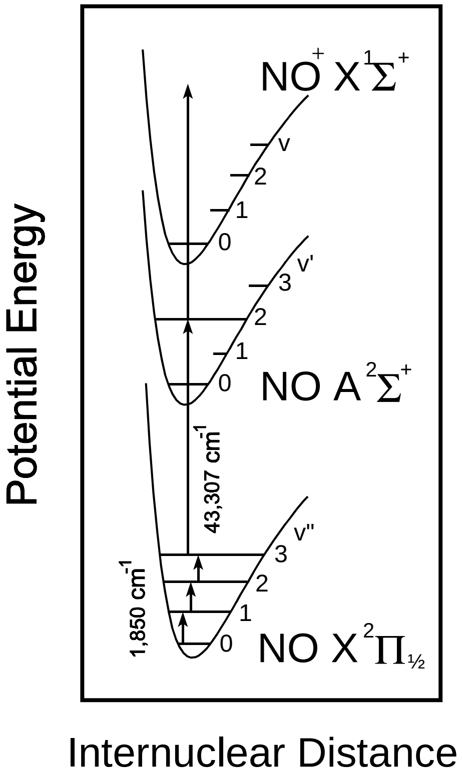

Figure 4.1: *Simplified energy level diagram of NO showing the $X\,^2\Pi$ electronic ground state and the first $A\,^2\Sigma^+$ electronic excited Rydberg state with their first few vibrational levels (denoted by v'' and v') and the ionic $X\,^1\Sigma^+$ ground state. The arrows indicate the types of driven transitions: vibrational excitation of the electronic ground state at $\nu = 1{,}850\ \mathrm{cm}^{-1}$, electronic excitation to the $A\,^2\Sigma^+$ Rydberg state by a UV photon (the NO(v', v'')γ-band), and subsequent ionization by a UV photon. For clarity neither the rotational splitting of the vibrational levels nor the spin-orbit splitting of the $X\,^2\Pi$ electronic ground state is displayed.*

orders of magnitude. So far, the lack of experiments demonstrating vibrational ladder climbing stems from the absence of tunable ultrashort sources in the infrared. The construction of Free-Electron Lasers (FEL) has made a tunable coherent radiation source available that operates at the required wavelengths in the infrared at high power. Ultrashort laser pulses produced by a FEL contain sufficient spectral width to cover several steps of a vibrational ladder.

4.2 The NO molecule

Fig. 4.1 shows a simplified schematic energy level diagram of the NO molecule. The electronic ground state is split by 119 cm^{-1}, by spin-orbit interaction, into the $X\,^2\Pi_{\frac{1}{2},\frac{3}{2}}$ doublet (not shown). The step size of the vibrational ladder is 0.23 eV, corresponding to an excitation wavelength of 5.4 μm (short arrows in Fig. 4.1). The anharmonicity of the NO ladder is $\delta \approx 1.5\%$ per step. Transfer to vibrationally excited states is monitored by 1+1 REMPI: a UV photon excites the NO molecule from the $X\,^2\Pi(v'')$ ground state to the first $A\,^2\Sigma^+(v')$

Rydberg state (the NO(v', v'') γ-band) and a second photon ionizes the molecule to the NO$^+$ $X\ ^1\Sigma^+$ ionic ground state. Ionization signal is only present if the energy of the first photon is resonant with an electronic transition from one of the $X\ ^2\Pi_{\frac{1}{2},\frac{3}{2}}$ multiplets to the $A\ ^2\Sigma^+$ state, and is proportional to the population in the $X\ ^2\Pi$ ground state. By scanning the UV wavelength the distribution of population over the rotational and vibrational levels in the $X\,^2\Pi$ electronic ground state is probed. The REMPI scheme resolves the vibrational and rotational distribution. Such detailed information can not be retrieved by simply measuring the amount of IR energy absorbed by the molecular beam. Using a bolometer, for example, one molecule present in $v''=5$ is practically indistinguishable from five molecules in $v''=1$.

4.3 Description of the experiment

The experiments were organized as follows: NO molecules were vibrationally pumped by the output of the IR free-electron laser FELIX. FELIX produced 5.5 μs long macro pulses at a repetition rate of 5 Hz with an energy of 10 mJ per macro pulse. Each macro pulse consisted of a series of unchirped, bandwidth-limited [87], micro pulses, ±150 fs long, separated by 1 ns. The pulse-train nature made it useless to apply chirp to the laser pulse. In the low-Rabi-cycle limit (the condition of the present experiment) the advantage of chirp stems mainly from ordering the spectral components in time, so that they follow the ladder anharmonicity. In a pulse train the same advantage is also provided by unchirped pulses, since the molecule will interact with many pulses each of which containing the whole bandwidth of frequencies. In the present experiment it is estimated that the molecule interacted with 130 micro pulses. Hence a long sequence of chirped pulses would hardly do better than the same train of unchirped bandwidth-limited pulses. In the high-Rabi-cycle limit a pulse train chirped pulses will also not do significantly better than a single pulse: the first pulse finishes the job already. The UV pulses ($\Delta\nu \leq 0.5$ cm^{-1}) for the REMPI probe were generated by sum-frequency generation in BBO from the third harmonic of a 8 ns Q-switched Nd:YAG (yttrium aluminum garnet) laser with the output from a dye laser, pumped by the second harmonic of the same Nd:YAG laser. A CaF$_2$ ($f=18$ cm) lens was used to focus the sum-frequency to a spotsize diameter of $d=50$ μm. After traversing 1 m of air, the IR beam entered the vacuum chamber through a CaF$_2$ window and was focused by a CaF$_2$ lens ($f=5$ cm) to a spotsize of $d=130$ μm, yielding an estimated maximum intensity of $I=7\times10^{10}$ W cm^{-2}. The IR focus was several times larger than the UV focus, therefore a region of uniform IR intensity was probed. The REMPI laser was Q-switched at 10 Hz, twice the repetition rate of the FEL, recording a background REMPI spectrum after each IR shot. The experimental set-up consisted of a vacuum chamber with a General Valve Series 9 nozzle, operated at 10 Hz, providing a pulsed molecular beam of NO with estimated pressures up to $P_{\rm NO}=0.1$ mbar in the focus. The backing pressure behind the nozzle was $P_{\rm back}=1$ bar. The 99.0% pure NO came from a lecture bottle. The velocity in the molecular beam was estimated to be $v_{\rm NO}=500$ m s^{-1}, so the maximum number of IR micro pulses to which the molecules were exposed was 130. A charged-particle detection system

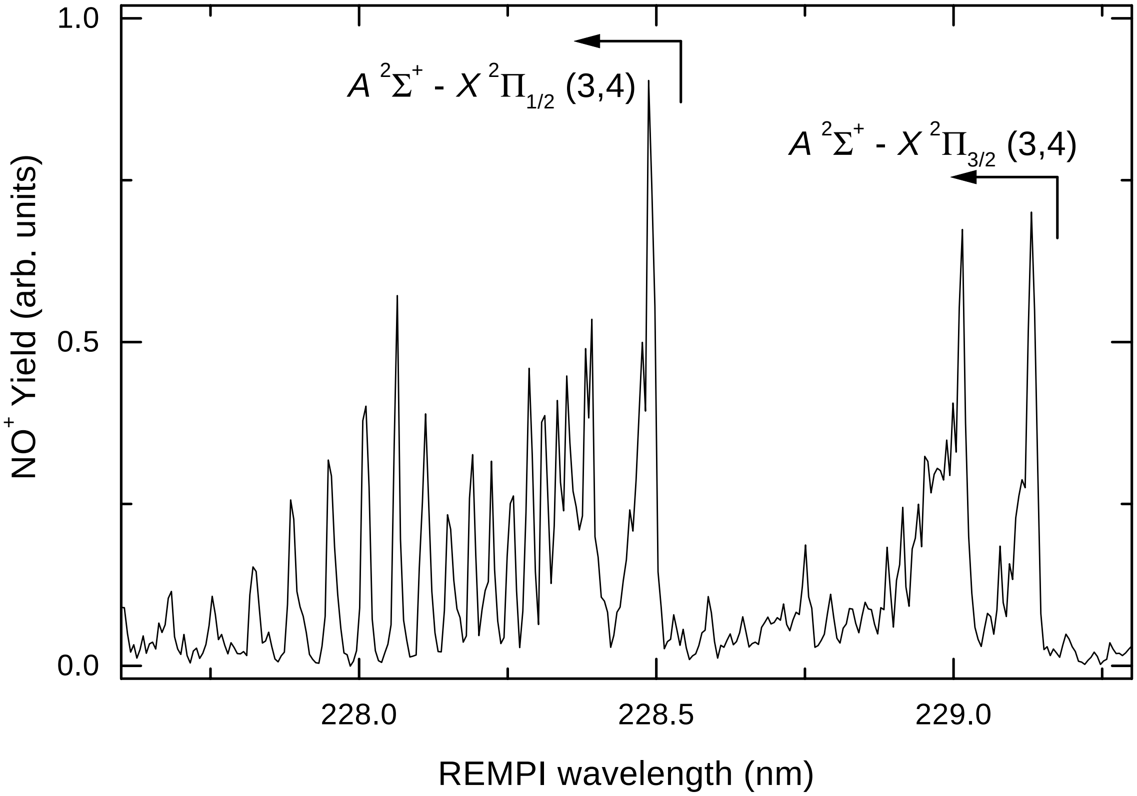

Figure 4.2: *A typical REMPI spectrum as measured after excitation by IR-FEL radiation with $\lambda = 5.4$ μm and $\Delta\lambda = 0.3$ μm. The individual peaks reflect the population of the rotational states. The presence of the NO(3,4) γ-band demonstrates population transfer to $v'' = 4$ by the IR.*

consisting of extraction field plates and an El-Mul Micro Sphere Plate (MSP) was used to detect NO$^+$ ions after a flight distance of 25 cm. A digital oscilloscope monitored the MSP output and transferred the data to a computer.

4.4 Experimental results: vibrational excitation up to $v'' = 5$

We now discuss the REMPI spectra of the NO(0,1), (3,4) and (3,5) γ-bands, probing the population pumped by the IR pulses to $v'' = 1, 4$ and 5, respectively. The curve in Fig. 4.2 displays a typical REMPI spectrum of the NO(3,4) γ-band as recorded with the FEL tuned at 5.4 μm with a bandwidth of $\Delta\lambda = 0.3$ μm. The sublevels due to the spin-orbit doublet of the $X\,^2\Pi_{\frac{1}{2},\frac{3}{2}}$ state shows up as two groups of peaks, labeled as $A\,^2\Sigma^+ - X\,^2\Pi_{\frac{1}{2}}(3,4)$ and $A\,^2\Sigma^+ - X\,^2\Pi_{\frac{3}{2}}(3,4)$, in the spectrum shown in Fig. 4.2. The separation of the peaks is caused by the large spin-orbit splitting of the $X\,^2\Pi$ ground state. Each individual multiplet consists of the sets of P-, Q- and R-lines (for $\Delta J = -1$, 0 and $+1$, respectively). The shape of the rotational envelope of this spectrum does not show rotational selectivity in the vibrational excitation. The measured NO(3,4) γ-band as displayed in Fig. 4.2 demonstrates significant population transfer to $v'' = 4$ by the absorption of four IR photons.

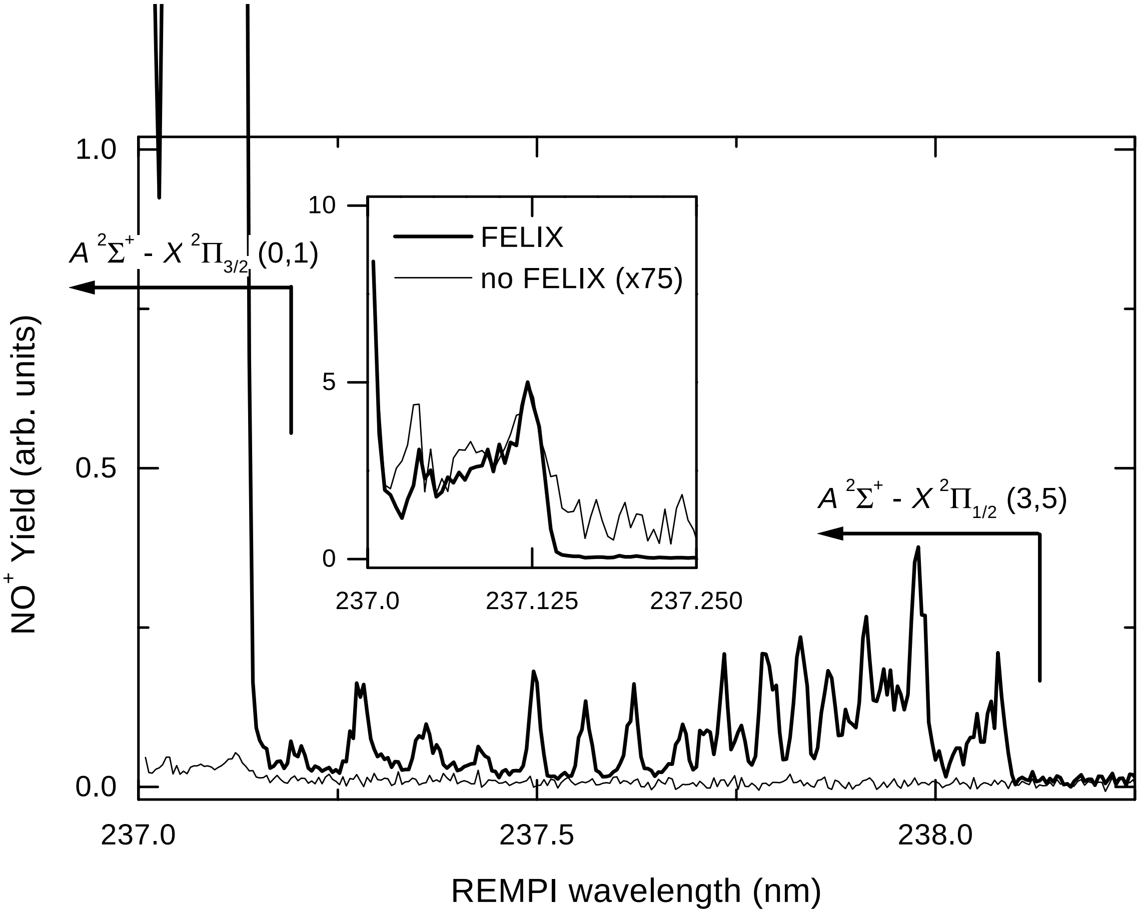

Figure 4.3: *The main panel shows the NO(3,5) γ-band after excitation with IR laser pulses (thick curve). Near 237.1 nm the NO(0,1) γ-band (going off-scale) is also present. The ratio of the $v''=5$ population over the $v''=1$ population is* $8{\times}10^{-4}$*, corresponding to a transfer efficiency per step of 17%. The small peak near 237.1 nm in the measured background (thin curve) stems from the thermally populated fraction in $v''=1$ (*$\approx 1.2\times10^{-4}$ *for* $\mathrm{T}=300$ K*). The inset shows the $v''=1$ bandhead with the background trace scaled up by* 75×.

The vibrational ladder was climbed even one step higher as is shown in Fig. 4.3. This figure shows both the (0,1) and the (3,5) band of the NO γ-system, with and without excitation of the ground state by the FEL pulses. The main panel from Fig. 4.3 displays the $A\,^2\Sigma^+{-}X\,^2\Pi_{\frac{1}{2}}$-multiplet of the NO(3,5) γ-band as well as the P_{12} bandhead of the NO(0,1) γ-band. The recorded relative intensities of the bandheads of these bands enable us to estimate the transfer efficiency of the IR-pumping. The Hönl-London factor for the NO P_{12} band is relatively small. This makes the measured P_{12} signal, as probed by the REMPI scheme, from the richly populated $v''=1$ only one order of magnitude larger than the signal from the main bandheads of $v''=5$ and therefore within the dynamic range of our measurement system. From the observed ratio of the $v''=1$ and $v''=5$ peaks in Fig. 4.3 the ratio of the $v''=5$ over the $v''=1$ population is estimated to be $\frac{\mathrm{P_{FEL}}(v''=5)}{\mathrm{P_{FEL}}(v''=1)}=8\times10^{-4}$, where the subscript FEL denotes population transferred by the IR pulses. From this ratio, the measured average transfer per step of the ladder from $v''=1$ to $v''=5$ is estimated to be $\sqrt[4]{8\times10^{-4}}=17\%$. This transfer efficiency is in qualitative agreement with the amount of population observed in $v''=2$ and 4. To convert the measured band intensities into the relative populations in $v''=1$ and $v''=5$, the Hönl-London factors as well as the Franck-Condon factors for the (0,1) and (3,5) γ-band, as calculated using the Rydberg-Klein-Rees procedure, are used.

Although relative transfer from $v''=5$ to $v''=6$ may still be $\sim 5\%$, no population in $v''=6$ could be observed with the sensitive REMPI probe, since the absolute transfer to $v''=6$ is below our detection limit of 5×10^{-7}. The $5\leftarrow4$ transition is the red-most transition still within the bandwidth of the IR laser, making the observed $v''=5$ state the highest vibrational level that can be populated via resonant ladder climbing. Populating the $v''=5$ state represents a transfer of energy into the NO bond equal to 17% of the dissociation energy to the lowest dissociation limit.

The peak in the background spectrum (thin curve in Fig. 4.3) at 237.1 nm shows the presence of thermal population in $v''=1$. For comparison, the inset in Fig. 4.3 displays a close-up of the $\mathsf{P}_{12}(0,1)$ bandhead with the background curve scaled up 75×, showing a similar shape for the FEL on/FEL off curves. Hence the ratio of the thermally present population in $v''=1$ to the excited population was determined to be $\frac{\mathrm{P_{FEL}}(\mathrm{v''=1})}{\mathrm{P_{Thermal}}(\mathrm{v''=1})}=75$.

Assuming no vibrational cooling during the expansion of the molecular beam [88], the thermally populated fraction present in the $X\ ^2\Pi$ $(v''=1)$ state is 1.2×10^{-4}. This gives a transfer efficiency to $v''=1$ after FEL-pumping of 0.9%. This low $1\leftarrow0$ transfer efficiency is attributed to the detuning of the central wavelength of the IR radiation from the $1\leftarrow0$ band of NO. The central wavelength was tuned for maximum population transfer to $v''=5$, the highest vibrational level in resonance with the large bandwidth FEL pulse. The consequent detuning from the $1\leftarrow0$ resonance frequencies reduces pumping efficiency towards $v''=1$.

By combining the measured micro pulse fluence and frequency spectrum with the transition strengths for vibrational excitation [89], the efficiency of the ladder climbing is easily estimated. Realizing that the NO molecules are irradiated by a train of approximately 130 micropulses, one can convert the above to the pulse train pumping efficiency. Ignoring any rotational complications, a 5-level ($v''=1$–5) calculation adding contributions of 130 micro pulses incoherently yielded the same ratio for $v''=1$ over $v''=5$ population as is observed, if an intensity of 6×10^{10} W cm^{-2} is assumed. This intensity is in excellent agreement with the estimated experimental IR intensity of 7×10^{10} W cm^{-2}.

4.5 Comparison of resonant pumping with overtone excitation

To demonstrate the effectiveness of resonant pumping, the transfer efficiency of the above experiment is compared with direct excitation of the fifth overtone of NO ($v''=5\leftarrow0$) by the fundamental (9,391 cm^{-1}) of a high intensity Q-switched Nd:YAG laser. The fluence of one 700 mJ 8 ns Nd:YAG pulse is five orders of magnitude larger than the total pulse fluence of 130

FELIX micro pulses. The Nd:YAG fundamental is 150 cm^{-1} off-resonant from the $v''=5 \leftarrow 0$ transition, but for these intensities ($I \approx 10^{13}$ W cm^{-2}) the AC-Stark shift is expected [79] of the $v''=5$ state energy to be sufficiently large to shift this state into resonance with the laser field, possibly allowing for direct one-photon vibrational excitation. However, no detectable fraction of the population was transferred to $v''=5$. The only perceptible signal stemmed from multi-photon ionization of NO by the absorption of at least eight Nd:YAG photons. This observation shows that the absorption of five resonant photons in the IR, even at much lower intensity, is more favorable than the absorption of a single almost-resonant photon. The present experiment has demonstrated the feasibility of multi-step vibrational excitation and state-resolved probing of the transferred population, paving the way for experiments on increasing the control of bond-selective vibrational excitation by chirping the IR laser pulse, as will be discussed in the next two chapters.

4.6 Conclusions

Summarizing, we have performed an experiment demonstrating resonant vibrational excitation of a molecule with femtosecond infrared laser pulses, while monitoring state-selectively the population transfer. After approximately 130 micro pulses a significant fraction of the NO molecules has been transferred from $v''=0$ to $v''=5$ by absorption of five IR photons. Although the present experiment was performed in NO, the tunability of free-electron lasers allows for vibrational excitation of almost any molecule.

CHAPTER 5

VIBRATIONAL LADDER CLIMBING IN NO BY (SUB)PICOSECOND FREQUENCY-CHIRPED INFRARED LASER PULSES

The anharmonic vibrational ladder of nitric oxide (NO) is climbed by irradiating the molecule with chirped intense (sub)picosecond infrared (IR) pulses ($I_{\mathrm{max}} = 1.0 \times 10^{10}$ W cm^{-2})*. The chirp of the broadband IR* ($h\nu = 1{,}850$ cm^{-1}, $\Delta h\nu = 50$ cm^{-1}) *pulse from a free-electron laser is controlled by a pulse shaper. Transfer up to the excited vibrational state* $X\,{}^2\Pi_{\frac{1}{2}}(v=3)$ *of NO shows a strong enhancement when the frequency chirp of the IR pulses follows the consecutive anharmonic vibrational transitions.*

The concepts of chirp and chirped vibrational ladder climbing are introduced in section 5.1. Then, in section 5.2, some relevant attributes of the NO molecule, the pulse chirper and the experiment are reviewed. The experimental results are presented in section 5.3. The chapter ends with some brief conclusions in section 5.5.

5.1 Introduction

Laser excitation of molecules into a specific highly-excited vibrational state is a controllable way to enhance their chemical activity. Direct population of such a highly-excited state by absorption of a single photon is very inefficient, due to the small transition dipole moment between the initial and final state. Step-wise excitation of a sequence of vibrational states is a more promising route. However, this method is frustrated by the anharmonicity of the molecular potential: an infrared (IR) laser which has the appropriate frequency to drive a molecule from the vibrational ground state $v = 0$ to $v = 1$ is non-resonant with consecutive vibrational transitions ($v = 1 \rightarrow 2$, $v = 2 \rightarrow 3$, $\ldots$). To overcome this bottleneck, the use of broadband short laser pulses that contain more frequencies in their spectrum has been suggested [19]. Such broadband pulses can be “chirped”, that is, their frequency can be made to change in time to follow the consecutive vibrational transitions. This chirping should strongly enhance the transfer to the higher states [19,20,86]. Ultrafast excitation of a specific bond in a poly-atomic molecule by chirped short pulses can outpace intramolecular relaxation processes and, hence, enables bond-selective excitation.

Up till now, laser experiments have not been very successful in driving vibrational ladder climbing for two reasons. Firstly, the required radiation to drive vibrational transitions is in the infrared (IR). In that wavelength regime, lasers which are both intense and tunable are scarce. Secondly, the bandwidth of most high power IR lasers is too small to resonantly drive consecutive transitions in the anharmonic potential. Nowadays, free-electron lasers provide tunable ultrashort infrared pulses with a sufficiently broad frequency spectrum to drive several consecutive transitions. The efficiency of population transfer to high vibrational states in such a multi-step vibrational ladder climbing process may be enhanced considerably by tailoring these IR laser pulses. The chirp α is defined as [30,64]

$$\alpha = \frac{1}{2!}\frac{\partial^2 \varphi}{\partial \nu^2} , \tag{5.1}$$

and is a measure of the amount of temporal dispersion, where ν denotes the frequency, and $\varphi(\nu)$ the frequency-dependent phase. For $\alpha < 0$ the instantaneous frequency of the laser pulse decreases in time (i.e. the color goes from blue-to-red), at $\alpha = 0$ all colors are simultaneously present (the pulse is bandwidth-limited provided that all higher order dispersion terms are zero as well), and for $\alpha > 0$ the instantaneous frequency increases in time (i.e. the color goes from red-to-blue). Chelkowski *et al.* [19, 20, 86] have calculated that for $\alpha < 0$, when the instantaneous IR frequency follows the anharmonicity of the vibrational ladder, the transfer to the highest vibrational level is increased by several orders of magnitude. When the laser field is strong enough to saturate the transitions, 100% of the population can be transferred through the vibrational ladder by employing the technique of Rapid Adiabatic Passage (RAP) [63]. Inspired by these calculations, we studied the enhancement of population transfer through the vibrational ladder of NO (see Fig. 5.1) as a function of the chirp of an ultrashort IR laser pulse. The transfer to excited vibrational states is monitored by 1+1 Resonance Enhanced Multi-Photon Ionization (REMPI) [43, 80]. This experiment demonstrates the feasibility of bond-selective excitation of molecules by chirped IR laser pulses [8].

5.2 Description of the experiment

The experiment was organized as follows. Short (0.37 ps) Gaussian bandwidth-limited IR pulses from a free-electron laser [48,49] drove the vibrational ladder climbing process in the diatomic molecule NO. The free-electron laser was tuned to the frequency ($h\nu_{\mathrm{central}} = 1{,}850\ \mathrm{cm}^{-1}$) matching the vibrational transitions in NO with sufficient bandwidth to support the $v'' = 0$ to $v'' = 1$ transition ($h\nu_{10} = 1{,}877\ \mathrm{cm}^{-1}$) up to the $v'' = 2$ to $v'' = 3$ transition ($h\nu_{32} = 1{,}820\ \mathrm{cm}^{-1}$), as indicated by the short arrows in fig 5.1. Chirping of the frequency during an ultra-short IR

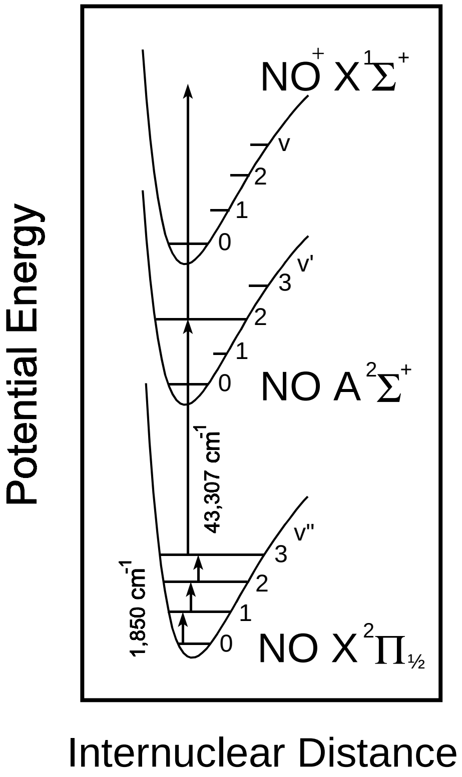

Figure 5.1: *Schematic energy level diagram of the NO molecule. The step size of the vibrational ladder of the electronic ground state is 0.23* eV, *corresponding to a vibrational excitation frequency of* 1,850cm^{-1} *(short arrows in Fig. 5.1). The anharmonicity of the NO ladder is ≈1.5% per step. Transfer to vibrationally excited states is monitored by 1+1 REMPI: a UV photon excites the vibrationally excited NO molecule from the* $X\,^2\Pi_{\frac{1}{2}}(v'')$ *electronic ground state to the first* $A\,^2\Sigma^+(v')$ *Rydberg state (the NO*(v',v'') γ*-band) and a second photon ionizes the molecule to the NO*$^+$ $X\,^1\Sigma^+$ *ionic ground state (long arrows). For clarity neither the rotational splitting of the vibrational levels nor the* $X\,^2\Pi_{\frac{3}{2}}$ *electronic ground state is displayed.*

pulse was obtained and controlled by sending the infrared radiation through a pulse shaper [87]. This optical device basically consists of a parallel grating pair. The first grating separates the frequency components spatially and the second one recombines them into a parallel beam. The frequency-dependent optical pathlength between the gratings generates a chirp that is proportional to the grating separation. The chirp results in a *linear* change of the frequency ν over the pulse duration for a Gaussian pulse [30,90]. The tailored IR pulse entered the vacuum chamber perpendicular to both the output of a narrowband UV laser and a supersonic gas jet of NO [88]. The IR pulse was focused to a spotsize of $d = 80$ μm, yielding a fluence of $\Phi = 3.7\times10^{-3}$ J cm^{-2}. The supersonic expansion of 5% NO seeded in 95% He, with gas densities up to $n = 10^{11}$ cm^{-3} in the focus, was generated using a pulsed valve with a nozzle diameter of $D = 0.8$ mm and a backing pressure of 3 bar. The velocity of the molecules, $\mathrm{v_{NO}} = 2\times10^3$ m s^{-1}, was sufficiently high to replenish the IR focus during the 40 ns that separated the micropulses from the free-electron laser. This ensured that each NO molecule interacted with a single IR pulse only. A UV laser probed the rotational and vibrational distribution of the electronic ground state, as populated by the IR pulse, by 1+1 Resonance Enhanced Multi-Photon Ionization (REMPI) [43, 80]. The UV pulses (with $\Delta\nu = 1.85$ cm^{-1}) for the REMPI probe were generated by sum-frequency generation in BBO from the third harmonic of an 8 ns Q-switched Nd:YAG laser with the output from a dye laser [91]. Ionization signal is only present if the energy of the first photon is resonant with an electronic transition from one of the $X\,^2\Pi_{\frac{1}{2},\frac{3}{2}}$ multiplets to the $A\,^2\Sigma^+$ state (see Fig. 5.1). By scanning the UV laser over the intermediate resonances, the distribution of population over the rotational J'' and vibrational v'' levels in the $X\,^2\Pi$ electronic ground state is probed. The observed NO$^+$ yield, as created in the REMPI-detection scheme, is a measure for the population of the vibrationally excited states. We aimed to determine the amount of excited vibrational population as a function of the frequency-chirp α of the IR laser pulse.

5.3 Experimental results: chirp-enhanced excitation to $v''=3$

5.3.1 Transfer efficiency as a function of the chirp α

The top panel of Fig. 5.2 displays the population in the $v''=3$ state as a function of the chirp α of the IR laser pulse. Any non-zero chirp stretches the IR pulse (see top axis of Fig. 5.2 for the pulse durations). The $v''=3$ state is the highest vibrational state having a transition frequency within the bandwidth of the IR laser. For a blue-to-red chirp ($\alpha < 0$) the instantaneous frequency of the IR radiation decreases as a function of time and, thus, follows the decreasing transition frequency of consecutive vibrational steps. The data for the $v'' = 3$ population are obtained with the UV REMPI laser at 43,307 cm^{-1}. Due to the "large" UV bandwidth of 1.85 cm^{-1} the low rotational states $J'' \in \{\frac{1}{2}, \ldots, 4\frac{1}{2}\}$ of the coinciding Q_{11} and P_{21} branches of the NO(2,3) γ-band are probed simultaneously. The top panel shows the *two main observations* reported here:

I. The broad bandwidth of the IR laser pulse enables population of the $v''=3$ vibrational state by three consecutively resonant photons.
II. A 6-fold enhancement of this population is observed when the chirp follows the consecutive steps up the vibrational ladder, while a 8-fold decrease is found when the frequency is chirped in the "wrong" direction.

The bottom panel of Fig. 5.2 shows that the $v''=1$ population is independent of the magnitude and sign of the chirp (α), as expected for a one photon process in absence of significant depletion. The population of $v''=1$ is probed for the Q_{11} and P_{21} branches of the NO(0,1) γ-band at 42,323 cm^{-1}. The thermally present population in $v''=1$ is 1.2×10^{-4}. From the increase of the $v''=1$ signal by IR pumping a transfer efficiency of 0.18% from $v''=1 \leftarrow 0$ is determined. This is in good agreement with an estimate of 0.12% transfer, based on the IR intensity and the vibrational transition dipole moment of NO. The observed transfer corresponds to an enhancement of 15 times the thermal population of $v''=1$.

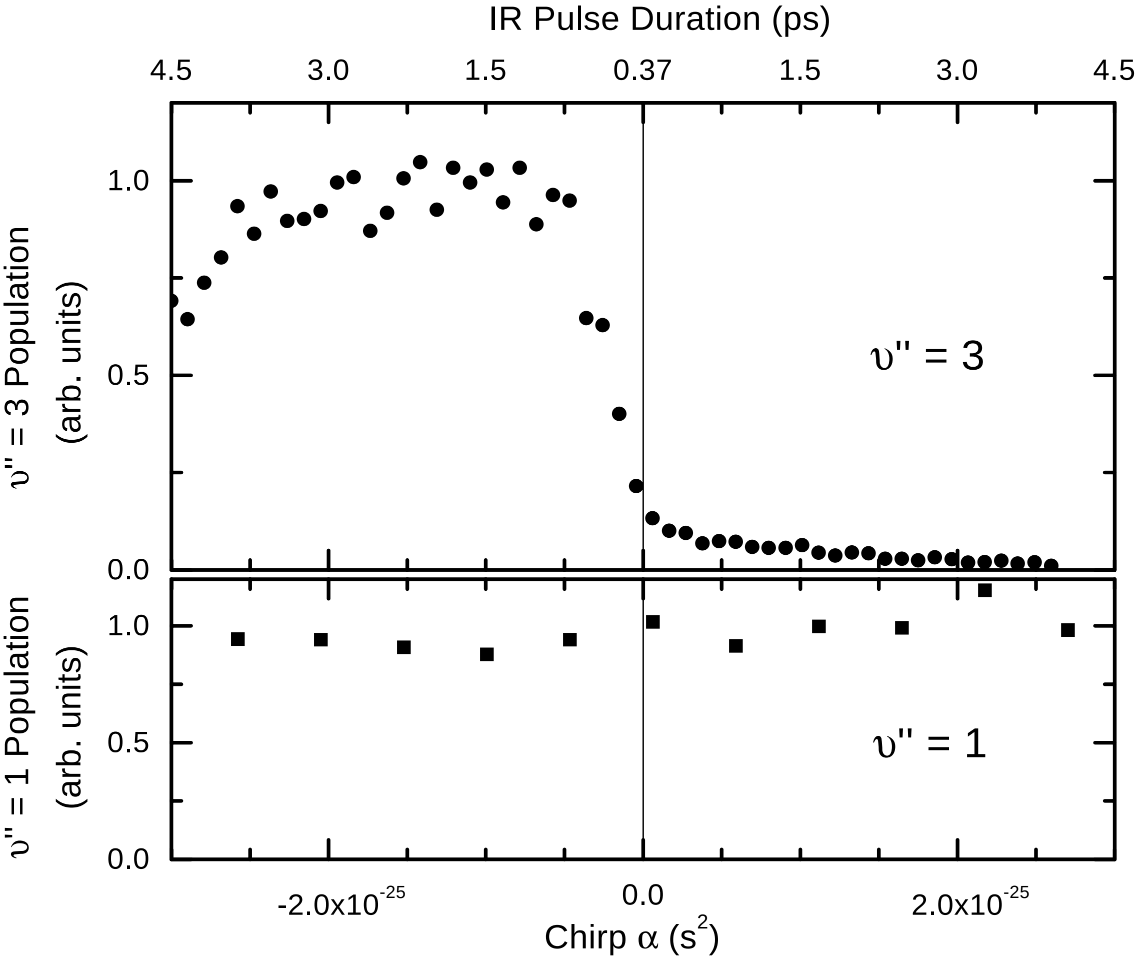

Figure 5.2: *The population in $v'' = 3$ and $v'' = 1$ as a function of chirp (α, bottom axis). The stretched pulse duration, resulting from the chirp, is shown at the top axis. The upper panel shows the population of $v'' = 3$, excited by three consecutive IR photons, as a function of the chirp α of the IR laser pulse. The data for the $v'' = 3$ population are obtained with the UV REMPI laser at* 43,307 cm^{-1}, *probing the low rotational states $J'' \in \{\frac{1}{2}, \ldots, 4\frac{1}{2}\}$ of the coinciding Q_{11} and P_{21} branches of the NO$(2,3)$ γ-band. The population of $v''=1$ (lower panel) is probed for the same branches of the NO$(0,1)$ γ-band at* 42,323 cm^{-1}.

5.3.2 Rotational redistribution

The IR laser redistributes the vibrational population of the molecule considerably, but what happens to the occupation of rotational states of the excited molecules? The REMPI spectrum for the vibrational ground state $v''=0$ (circles in the lower panel of Fig. 5.3) shows that the molecular beam has a Boltzmann-like distribution with a rotational temperature of $T_{\rm rot} = 15$ K. The dotted line in the lower panel is a fit to the data, using a Boltzmann distribution over the rotational levels for a rotational temperature of $T_{\rm rot}(v''=0) = 15$ K and a REMPI laser linewidth of 1.85 cm^{-1}. The connected bars in Fig. 5.3, indicating the position of the different branches as known from spectroscopy [44], assign the peaks in the REMPI spectrum to one,

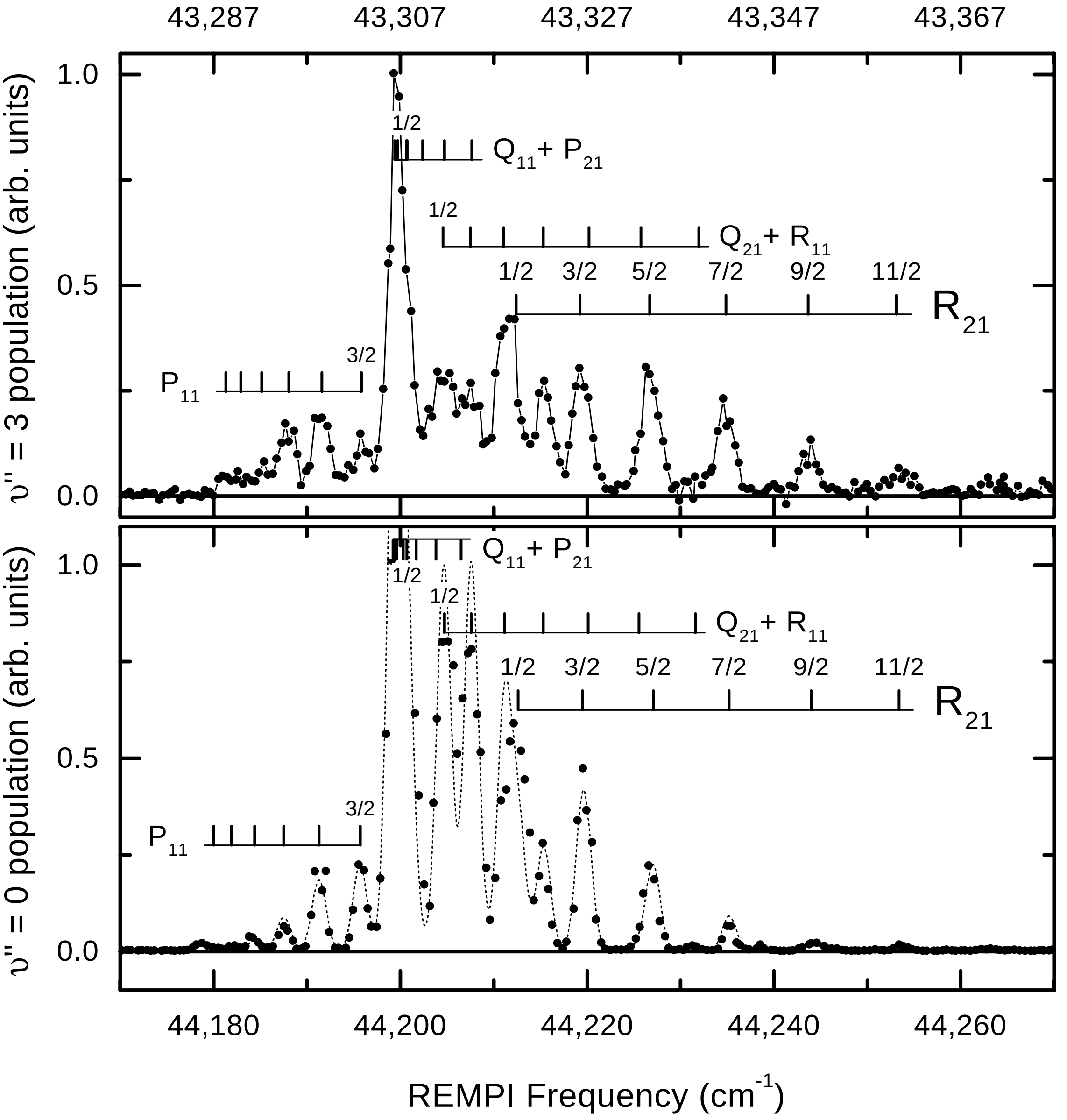

Figure 5.3: *REMPI spectra showing the rotational distribution of both the vibrational ground state ($v''=0$, lower panel) and the highest state observed ($v''=3$, top panel, recorded for $\alpha=-0.6\times10^{-25}$ s^2). The dotted line in the lower panel is a fit to the $v''=0$ data (circles). The connected bars indicate line positions for the different branches (P_{11}, Q_{11}, P_{21}, Q_{21}+R_{11}, and R_{21}), as known from spectroscopy of the NO(v',v'') γ-band [44]. The distribution over the rotational states is most easily seen from the R_{21} branch.*

or more, rotational states. The R_{21} branch reflects the distribution over the rotational states most obviously. Nearly all the NO molecules are shown to be in the five lowest rotational states (J'' values $\frac{1}{2}$ up to $4\frac{1}{2}$). The top panel displays a measured REMPI spectrum from the $v''=3$ state, for $\alpha=-0.6\times10^{-25}$ s^2. Close inspection of the REMPI spectra (Fig. 5.3), in particular of the R_{21}-branch, demonstrates that the rotational distribution of the highly-excited state

($v''=3$) is different from that of the ground state. The population is, on average, transported to higher rotational states ($\overline{J}(v''=0)=1.8$, $\overline{J}(v''=3)=3.0$) and the distribution of the $v''=3$ population is no longer Boltzmann-like. Taking into account: the Hönl-London factors for $^2\Pi-{}^2\Pi$ transitions [92]; the observed $v''=0$ ground state population ($T_{\rm rot}=15$ K); and the power spectrum of the IR pulse, the expected rotational distribution for the vibrationally excited $v''=3$ state population can be calculated. Comparison with the observed rotational distribution for $v''=3$ shows the consistency of the experiment with the selection rules for three consecutive single-photon transitions, in absence of saturation of the vibrational transitions. Despite the big gain in their vibrational energy, $[\overline{E}_{\rm vib}(v''=3)-\overline{E}_{\rm vib}(v''=0)]\approx 5{,}500$ cm^{-1}, is the average increase in rotational energy of vibrationally excited molecules relatively low: $[\overline{E}_{\rm rot}(v''=3)-\overline{E}_{\rm rot}(v''=0)]=12.3$ cm^{-1}.

5.4 Future experiments

In order to acquire precise control on a chemical reaction, one would wish to transport 100% of the population from the vibrational ground state to a specific highly-excited state. To climb the vibrational ladder efficiently, the transfer of each step must be close to 100%. It has been shown that complete population inversion can be obtained by applying a "π-pulse" to a two-level system [57,63]. The π-pulse method sets strict conditions on the laser pulse characteristics such as detuning, intensity and duration, raising serious difficulties for the experimentalist to overcome. Ladder climbing processes are complicated even more by the fact that the "π-pulse" conditions are different for every rotational state and for every step of the ladder. Any intensity fluctuation or inhomogeneity of the laser beam profile frustrates precise control over the net transfer to the excited states. Hence, usage of π-pulses is not a robust way to achieve control over chemical reactions. In their paper, Chelkowski *et al.* [19] have shown that the potential of the frequency-chirped laser excitation scheme does go beyond increasing transfer efficiency in the way as is demonstrated in the present experiment. Two additional advantages are foreseen. Firstly, adiabatic following by chirping the laser frequency over the transitions is very robust against instabilities of the pulse characteristics: provided that the intensity of the laser is sufficiently high, this excitation method produces complete population inversion [29,59,93]. Earlier work in our group has indeed demonstrated that, for a three-level electronic ladder in an atom, 100% of the electronic population can be transferred to the final state by means of chirped adiabatic passage [29, 30]. Application of this technique to molecules is promising, but will require an increase of the intensity of the IR pulses over the conditions of the present experiment. Angular momentum, in the form of molecular rotations, which is absent in the experiments on atoms, may complicate the generalization of RAP to molecules. Vibrational excitation by an IR photon is allowed only for $\Delta J=\pm1$. This splits the IR absorption band in a "red" **P**- and a "blue" **R**-branch. For $\alpha<0$, after initial inversion by a **R**-type transition is obtained, subsequent adiabatic passage over a **P**-type transition might return all the population to the vibrational ground state [93]. Whether this is a severe limitation depends strongly on both the relative magnitude of the Hönl-London factors for **P**- and **R**-transitions and on the ratio of the anharmonicity of the vibrational ladder $\omega_e x_e$ to the rotational constant B_e. This notion is explored further in chapter 6. Secondly, the use of very short laser pulses does prevent the laser-excited bond from coupling its excess-energy into other vibrational modes within a *poly*-atomic molecule. This rapid excitation is in contrast with "slow" two-color vibrational excitation schemes such as Stimulated Emission Pumping [94] and STImulated Rapid Adiabatic Passage [95], which successfully have prepared highly-excited vibrational states in small molecules making use of "long" laser pulses. By using the new excitation technique, with a characteristic time shorter than the time scale of the (usually fast) Intra molecular Vibrational Relaxation (IVR) [96] processes, *all* the laser energy will be pumped into the *selected* bond of a poly-atomic molecule. In our experiment, it took less than a picosecond to drive the NO molecule into the $v''=3$ state.

5.5 Conclusions

The presented experimental results show that ultra-short, large bandwidth, free-electron laser pulses can be frequency-tuned to a vibrational ladder of a molecule and, in addition, that the transfer of population to the upper state of a ladder is enhanced by appropriate chirping of the frequency of the laser pulse over the consecutive vibrational resonances. At higher IR intensities, 100% population transfer to a selected upper state is foreseen. Our experimental results on a diatomic molecule demonstrate the feasibility of bond-selective vibrational excitation of complex molecules on a picosecond time scale, leading to precise control of chemical reactions/reactivities.

CHAPTER 6

ROTATIONAL INTERFERENCE IN VIBRATIONAL LADDER CLIMBING IN NO BY CHIRPED INFRARED LASER PULSES

In this chapter results from model calculations and experiments on rotational interference in vibrational ladder climbing in the $X\ ^2\Pi_{\frac{1}{2}}$-state of NO are presented. In the low-fluence limit, which has been the prevailing condition for the experiment presented in the previous chapter, the predicted population in excited vibrational states shows an oscillatory behaviour as a function of the chirp of the IR laser pulse. The interference is due to the accumulated phase difference of pathways involving different intermediate rotational states. The theoretical results match the experiment on an absolute scale.

After a short introduction in section 6.1, a general expression for the expected oscillation period $\alpha_{2\pi}$ is derived in section 6.2. Then a systematic nomenclature of the various interference paths is introduced. In section 6.3 the method for the model calculation is elucidated. The predictions from these calculations are presented in section 6.4 and are compared with experimental data as recorded with the free-electron laser FELIX [48, 49] in section 6.5. Section 6.6 shows a prediction for the high-fluence regime of extremely intense pulses: the high-Rabi-cycling limit. The chapter ends with a short summary in section 6.7.

6.1 Introduction

In chapter 2 both the experimental results and the model calculations on the three-level rubidium ladder system showed an oscillatory behaviour in the $|5d\rangle$ state population as a function of chirp. These oscillations are attributed to quantum interference between two excitation paths, both contributing to the final $5d$ population:

I. Sequential transfer from $|5s\rangle$ to $|5p\rangle$, and from $|5p\rangle$ to $|5d\rangle$,
II. Direct transfer from the $|5s\rangle$ to the $|5d\rangle$ state by a two-photon process.

Each path accumulates its own phase which is determined by the time interval between the crossing of resonances and on the magnitude of the anharmonicity of the ladder. Since the above-mentioned time interval depends on the speed of the frequency-sweep (i.e. on the chirp), the accumulated phase difference between the paths is a function of the chirp. For sufficiently large chirp the instantaneous frequency of a Gaussian laser pulse increases linearly in time. Under this condition the phase difference is proportional to the chirp, and the oscillation period $\alpha_{2\pi}$ can be defined as the length of the interval between two subsequent chirp values for which the phase difference equals 2π.

For the vibrational ladder climbing in the NO molecule there are many rotationally interfering paths possible. The interferences originate from sequential transfer to the same final ro-vibrational states via different intermediate states, e.g., from $|v=0,J''=1\frac{1}{2}\rangle$ to $|v=2,J=1\frac{1}{2}\rangle$ via either $|v=1,J'=\frac{1}{2}\rangle$ or $|v=1,J'=2\frac{1}{2}\rangle$. Hence, similar interference effects are expected to be present in climbing the ro-vibrational ladder in NO.

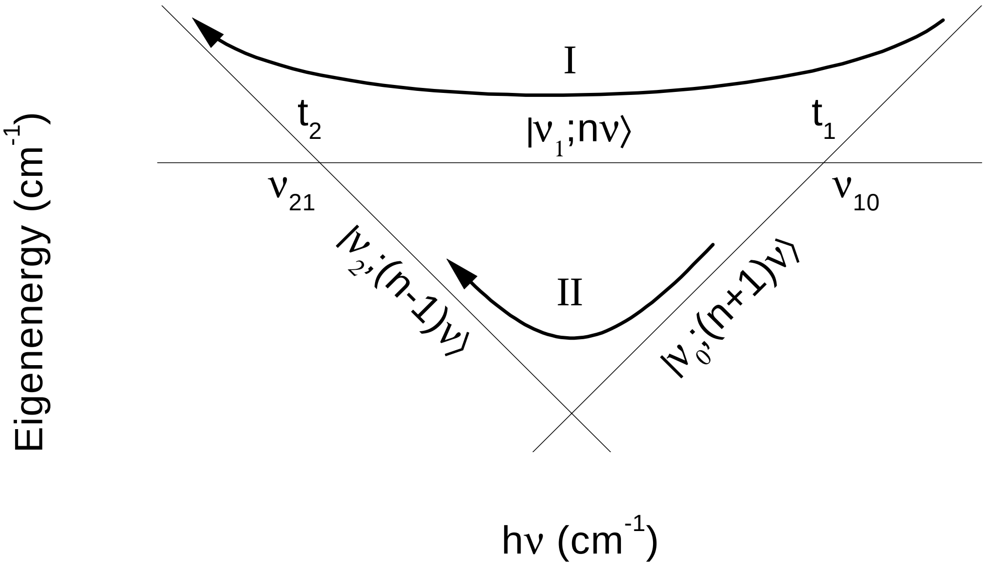

Figure 6.1: *A dressed-level energy diagram of the eigenenergies of a three-level system. The lines show the unperturbed dressed state eigenenergies as a function of laser-field frequency (ν). The levels are labeled $|\nu_0;(n+1)\nu\rangle$, $|\nu_1;n\nu\rangle$ and $|\nu_2;(n-1)\nu\rangle$. The transition frequencies are indicated by ν_{10} and ν_{21}. For a Gaussian laser pulse with chirp α, the frequency axis becomes a time axis as well, with, for large α, $t=4\pi\alpha(\nu-\nu_c)$. In the limit of weak coupling of the states, the traversion times t_1 and t_2 of the level-crossings can be calculated from the transition frequencies $\nu_{10}=\nu_1-\nu_0$ and $\nu_{21}=\nu_2-\nu_1$. The relationship between accumulated phase difference and the area enclosed by the two routes is discussed in section 6.2.1.*

6.2 Multiple rotational interference in climbing the vibrational ladder

This section starts with an explanation of a quantum interference effects in ro-vibrational ladder systems along similar lines as the discussion of the interference effect in the electronic ladder system $5s$-$5p$-$5d$ of rubidium as presented in section 2.3. Fig. 6.1 shows a diagram of the eigenenergies of the dressed states of an anharmonic three-level system. The ground state $|0\rangle$ is dressed with $(n{+}1)$ photons: $|\nu_0;(n{+}1)\nu\rangle$. The intermediate state $|1\rangle$ and the top state $|2\rangle$, dressed with respectively n and $(n{-}1)$ photons, are indicated as $|\nu_1;n\nu\rangle$ and $|\nu_2;(n{-}1)\nu\rangle$ with the ν_i the zero-field-strength eigenfrequencies of the wavefunctions. The dressed-level scheme as shown in Fig. 6.1 is drawn for a ladder system with a negative anharmonicity $\delta < 0$ [δ is defined in Eq. (1.6)], which is a general feature of vibrational ladders in molecules. For NO $\delta_{\mathrm{NO}} < 0$, consequently the orientation of the enclosed triangle in Fig. 6.1 is different from the triangle in Fig. 2.1, the dressed-level scheme for the rubidium ladder, with $\delta_{\mathrm{Rb}} > 0$. At the end of subsection 6.2.3, when the rotational structure of a molecule is included, the sign of the anharmonicity of the ro-vibrational ladder is shown to be a function of the rotational quantum number J.

6.2.1 The relation between the oscillation period $\alpha_{2\pi}$ and the enclosed area

In this subsection a relation between the area enclosed by two paths (I and II) as shown in Fig. 6.1 and the oscillation period $\alpha_{2\pi}$ of the interference is derived. The period of the interference wiggles can be explained by phase-difference arguments between the interfering paths. The two different paths correspond to different dressed state energies $\hbar W$. Since the wave function contains a factor $\exp(iWt)$, the phases of the wave functions that follow the different paths evolve differently. Both paths contribute to the population transfer from the ground state $|0\rangle$ to the final state $|2\rangle$. The magnitude of the phase difference depends on the energy difference between the paths and the time it takes to chirp from the first to the second resonance. The time interval is determined by the chirp of the laser pulse in combination with the frequency difference between the transitions. The phase difference is a linear function of the chirp, and sinusoidal oscillations in the transfer to the top level are observed. For a Gaussian pulse with a rather large chirp α and central frequency ν_c, the instantaneous frequency at time t is given by [see Eq. (2.18)]

$$\nu(t) = \nu_c + \frac{\pi}{\alpha} t \ . \tag{6.1}$$

Or, the other way round, the time t for a specific frequency ν (within the laser bandwidth) is

$$t = \frac{\alpha}{\pi}[\nu(t) - \nu_c] \ , \tag{6.2}$$

and hence

$$dt = \frac{\alpha}{\pi} d\nu \ . \tag{6.3}$$

The phase difference between the contributions by the upper path I and lower path II is

$$\Delta\phi = \int_{t_1}^{t_2} (W_{\mathrm{I}} - W_{\mathrm{II}}) dt \; , \tag{6.4}$$

and, filling in the dressed-state eigenfrequencies $W_i(t) = E_i(t)/\hbar = 2\pi[\nu_i + n_i\nu(t)]$:

$$\begin{aligned} \Delta\phi = 2\pi \Bigg[& \int_{t_1}^{(t_1+t_2)/2} \nu_1 + n\nu(t) - [\nu_0 + (n+1)\nu(t)] dt \\ & + \int_{(t_1+t_2)/2}^{t_2} \nu_1 + n\nu(t) - [\nu_2 + (n-1)\nu(t)] dt \Bigg] \; . \end{aligned} \tag{6.5}$$

One can easily see that only the relative photon number is of importance. Since the enclosed area has the shape of a right Isosceles triangle (see Fig. 6.1), both integrals give equal contributions, thus

$$\Delta\phi = 4\pi \int_{t_1}^{(t_1+t_2)/2} \nu_1 - [\nu_0 + \nu(t)] dt \; . \tag{6.6}$$

For a strongly chirped Gaussian pulse, the instantaneous frequency is a linear function of time, so, with Eq. (6.2) and Eq. (6.3),

$$\Delta\phi = 4\alpha \int_{\nu_1-\nu_0}^{(\nu_2-\nu_0)/2} (\nu_1 - \nu_0 - \nu) d\nu \; , \tag{6.7}$$

and, with the anharmonicity $\delta = (\nu_{21} - \nu_{10}) \equiv [(\nu_2 - \nu_1) - (\nu_1 - \nu_0)]$,

$$\Delta\phi = \frac{\alpha}{2}\delta^2 \; . \tag{6.8}$$

For $\Delta\phi = 2\pi$ the oscillation period $\alpha_{2\pi}$ is

$$\alpha_{2\pi} = \frac{4\pi}{\delta^2} \; . \tag{6.9}$$

The enclosed area A in the dressed-level diagram is $A = (\delta/2)^2$, hence,

$$\alpha_{2\pi} = \frac{\pi}{A} \; . \tag{6.10}$$

This expression is also valid for differently shaped enclosed areas. Eq. 6.10 may be used as as long as the instantaneous frequency increases linearly in time, which is the case for a strongly chirped laser pulse with a Gaussian temporal profile.

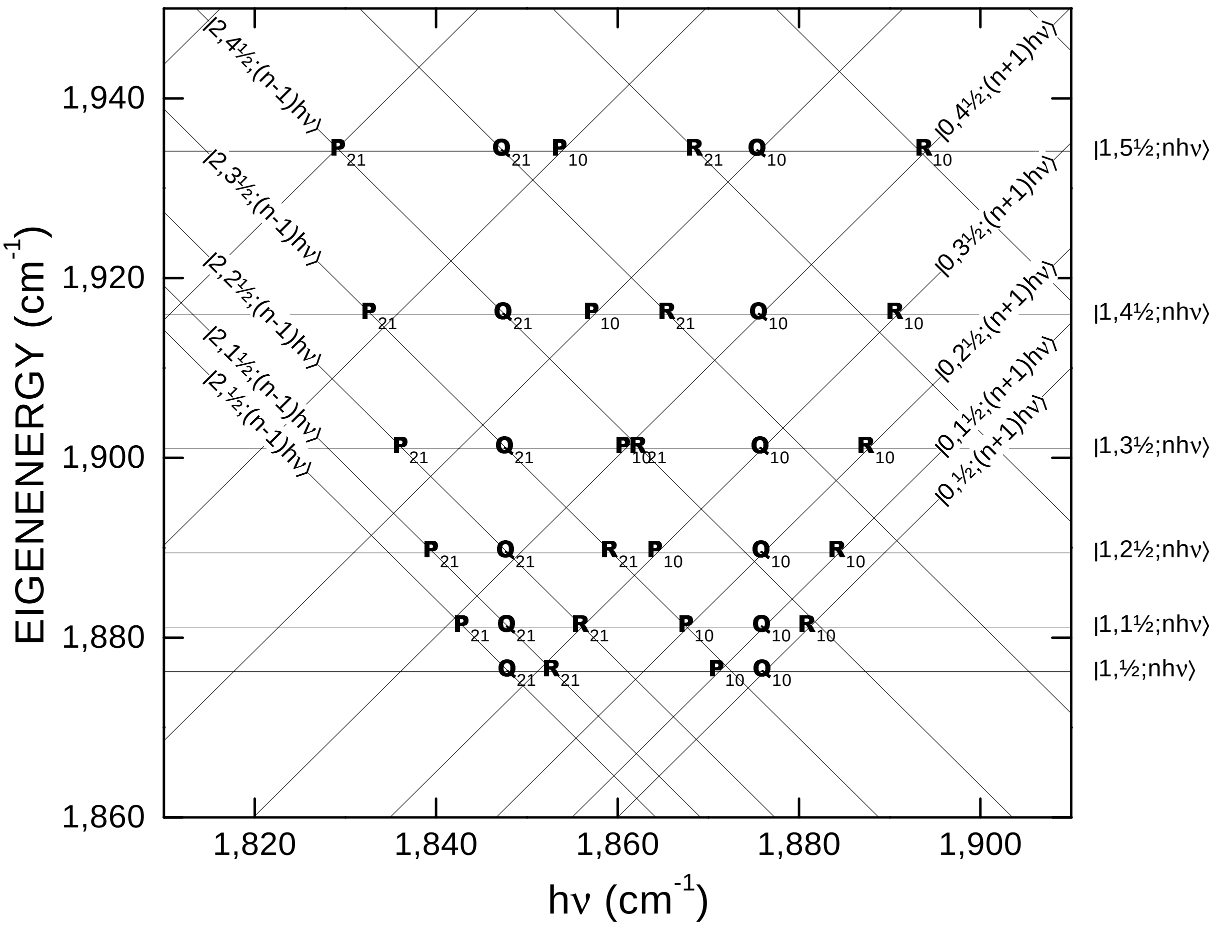

Figure 6.2: *A dressed-level energy diagram of the eigenenergies of the rotational manifold for three lowest vibrational states of the NO molecule. The lines show the unperturbed energies as a function of laser-field frequency ($h\nu$). Parallel lines belong to different rotational levels J of the same vibrational state $|v\rangle$ and are labeled $|v,J;nh\nu\rangle$. The bold-face symbols represent the dipole-allowed couplings by $\mathsf{P}_{v'v''}$-, $\mathsf{Q}_{v'v''}$- and $\mathsf{R}_{v'v''}$-type transitions.*

6.2.2 Introduction of a nomenclature for the excitation paths in a ro-vibrational ladder system

The vibrational ladder system in NO is more complicated than the simple three-level system treated in the previous section. Firstly, a large number of vibrational states ($v_{\max} = 37$) is present in the potential well (see Fig. 5.1). In addition, each vibrational state is split into a number of rotational states. This more complex situation is represented in Fig. 6.2 which displays a zero-laser-field-strength dressed-level-energy diagram of the eigenenergies $|0,J'';(n+1)h\nu\rangle$, $|1,J';nh\nu\rangle$ and $|2,J;(n-1)h\nu\rangle$ of the three lowest vibrational states of the NO molecule as a function of the photon-energy ($h\nu$). Parallel lines represent different rotational states belonging to the same vibrational level. The positions of the dipole-allowed P-, Q- and R-transitions from vibrational level v'' to v' are indicated by the symbols $\mathsf{P}_{v'v''}$, $\mathsf{Q}_{v'v''}$ and $\mathsf{R}_{v'v''}$. When the dipole coupling between the dressed ro-vibrational levels is included in the Hamiltonian, the degeneracies of the dressed states at the positions indicated by these symbols are removed for non-zero laser-field strengths. Depending on the strength of the dipole coupling (determined by the IR intensity) and the rate of frequency sweep (determined by the chirp) the avoided crossings of the dressed states are traversed more or less adiabatically. When the chirp is from blue to red, the instantaneous frequency follows the decrease in transition frequency corresponding to higher steps of the vibrational ladder. There is a large number of interfering paths that start from a specific rotational level J'' in the vibrational ground state $|0,J''\rangle$ and lead to population transfer to excited state $|2,J\rangle$. For the definition of a specific path the following nomenclature is introduced: a total difference in rotational quantum number $\Delta J=(J-J'')$ between initial and final state of $\Delta J=-1$ is called a $\mathrm{P_{YX}}(J)$-path, where $\mathrm{X,Y}\in\{\mathrm{P,Q,R,2ph}\}$, corresponding to a resonant dipole-allowed $\mathbf{P}_{v'v''}$-, $\mathbf{Q}_{v'v''}$- or $\mathbf{R}_{v'v''}$-transition or to a direct two-photon process. The subscripts X, Y identify the consecutive sequence of transitions, describing each path in a unique way. For other ΔJ, like e.g. $\Delta J=-2,0,1$ or 2, the path symbol is O, Q, R or S, respectively, after the general convention used in [34, 40]. For example, the grey triangle in Fig. 6.3 is enclosed by two paths that transfer population from $|v'',J''\rangle=|0,4\tfrac{1}{2}\rangle$ to $|2,4\tfrac{1}{2}\rangle$ either via $|1,5\tfrac{1}{2}\rangle$, labeled $\mathrm{Q_{PR}}(4\tfrac{1}{2})$, or via a two-photon transition, labeled $\mathrm{Q_{2ph}}(4\tfrac{1}{2})$. Both paths contribute to the population of $|2,4\tfrac{1}{2}\rangle$. To gain some insight in which paths can occur, the next three tables contain the label, the consecutive transitions and the intermediate states for all possible paths that populate $|2,J\rangle$ from $|0,J''\rangle$.

All possible P-paths for two-photon processes:
$\mathrm{P_{QP}}=\mathbf{Q}_{21}\mathbf{P}_{10}\equiv|2,J;(n-1)h\nu\rangle\leftarrow|1,J;nh\nu\rangle\leftarrow|0,J+1;(n+1)h\nu\rangle$
$\mathrm{P_{PQ}}=\mathbf{P}_{21}\mathbf{Q}_{10}\equiv|2,J;(n-1)h\nu\rangle\leftarrow|1,J+1;nh\nu\rangle\leftarrow|0,J+1;(n+1)h\nu\rangle$
$\mathrm{P_{2ph}}=\mathbf{P}_{20}\equiv|2,J;(n-1)h\nu\rangle\leftarrow|\text{virtual state}\rangle\leftarrow|0,J+1;(n+1)h\nu\rangle$

All possible Q-paths for two-photon processes:
$\mathrm{Q_{PR}}=\mathbf{P}_{21}\mathbf{R}_{10}\equiv|2,J;(n-1)h\nu\rangle\leftarrow|1,J+1;nh\nu\rangle\leftarrow|0,J;(n+1)h\nu\rangle$
$\mathrm{Q_{RP}}=\mathbf{R}_{21}\mathbf{P}_{10}\equiv|2,J;(n-1)h\nu\rangle\leftarrow|1,J-1;nh\nu\rangle\leftarrow|0,J;(n+1)h\nu\rangle$
$\mathrm{Q_{QQ}}=\mathbf{Q}_{21}\mathbf{Q}_{10}\equiv|2,J;(n-1)h\nu\rangle\leftarrow|1,J;nh\nu\rangle\leftarrow|0,J;(n+1)h\nu\rangle$
$\mathrm{Q_{2ph}}=\mathbf{Q}_{20}\equiv|2,J;(n-1)h\nu\rangle\leftarrow|\text{virtual state}\rangle\leftarrow|0,J;(n+1)h\nu\rangle$

All possible R-paths for two-photon processes:
$\mathrm{R_{QR}}=\mathbf{Q}_{21}\mathbf{R}_{10}\equiv|2,J;(n-1)h\nu\rangle\leftarrow|1,J;nh\nu\rangle\leftarrow|0,J-1;(n+1)h\nu\rangle$
$\mathrm{R_{RQ}}=\mathbf{R}_{21}\mathbf{Q}_{10}\equiv|2,J;(n-1)h\nu\rangle\leftarrow|1,J-1;nh\nu\rangle\leftarrow|0,J-1;(n+1)h\nu\rangle$
$\mathrm{R_{2ph}}=\mathbf{R}_{20}\equiv|2,J;(n-1)h\nu\rangle\leftarrow|\text{virtual state}\rangle\leftarrow|0,J-1;(n+1)h\nu\rangle$

The above-introduced labeling system can easily be extended for higher-order photon processes by extending the number of subscripts. For example, populating $|3,4\tfrac{1}{2}\rangle$ from $|0,1\tfrac{1}{2}\rangle$ by the three consecutive single-photon transitions $\mathbf{R}_{32}(3\tfrac{1}{2})$, $\mathbf{R}_{21}(2\tfrac{1}{2})$, $\mathbf{R}_{10}(1\tfrac{1}{2})$ is labeled by $\mathrm{T_{RRR}}(4\tfrac{1}{2})$.

Since all P-paths start in the same initial state and contribute to population in the same final state, every pair of them has its own period in α. The same is true for all Q- and all R-paths. If there are n paths, then there are $N=\frac{n!}{2!(n-2)!}$ different oscillating periods. The population in

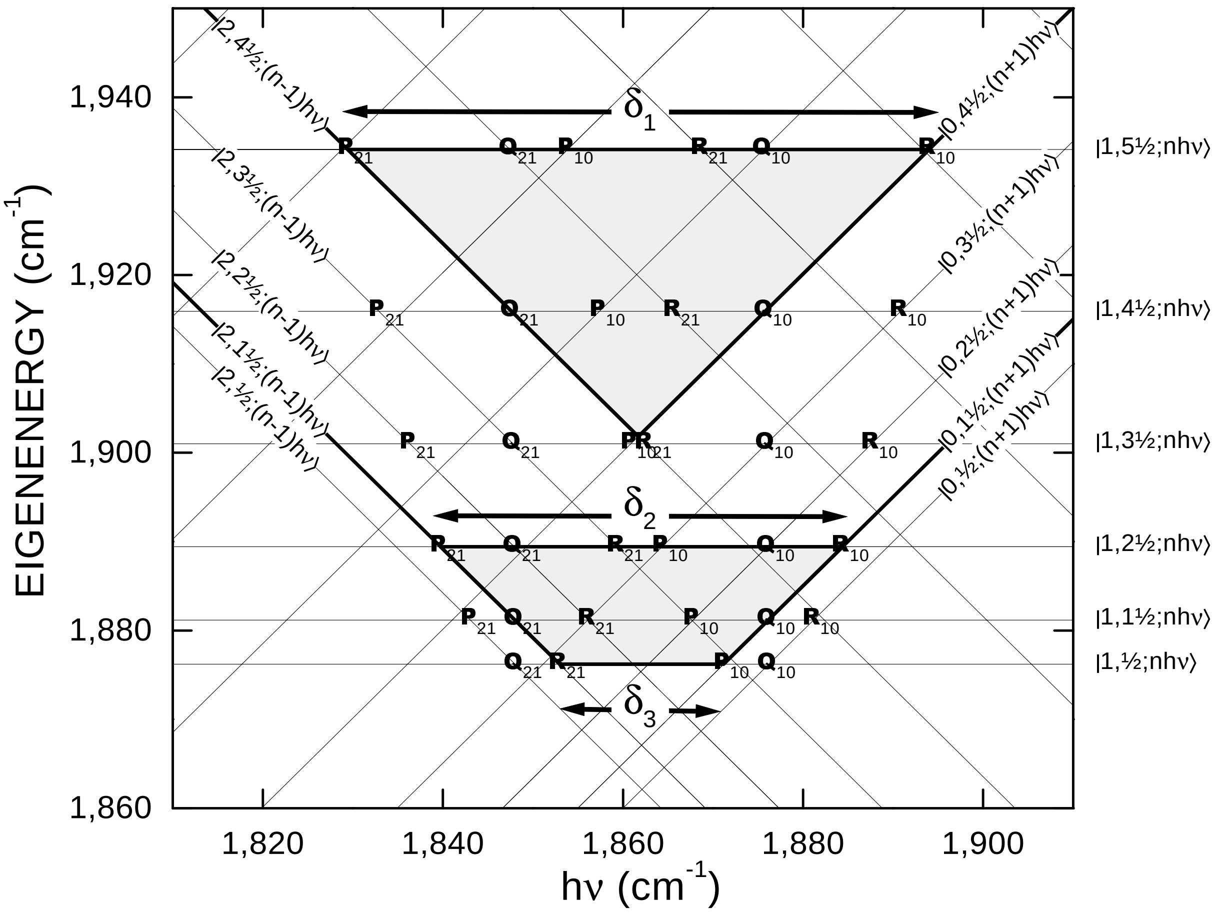

Figure 6.3: *The same dressed-level energy diagram of the eigenenergies of the rotational manifold for three lowest vibrational states of the NO molecule. The two basic interference paths are indicated. The triangle represents interference* $\mathrm{Q_{2ph}} - \mathrm{Q_{PR}}(4\frac{1}{2})$ *i.e. between the two-photon path and the path with the two resonant transitions* $\mathsf{P}_{21}(5\frac{1}{2}) \leftarrow \mathsf{R}_{10}(4\frac{1}{2})$*. One can calculate the interference frequency* $\alpha_{2\pi} = \pi/A$ *from the enclosed area* $A_{\rm tri} = (\delta_1/2)^2$*, with* $\delta_1 = -64.55\ \mathrm{cm}^{-1}$ *the anharmonicity between these transitions. The trapezium shows the interference paths* $\mathrm{Q_{PR}} - \mathrm{Q_{RP}}(1\frac{1}{2})$*, with* $A_{\rm tra} = [(\delta_2/2)^2 - (\delta_3/2)^2]$ *and* $\delta_2 = -44.66\ \mathrm{cm}^{-1}$*,* $\delta_3 = -18.22\ \mathrm{cm}^{-1}$*.*

the upper level of rubidium can be written as the square of the sum of the contributions to the probability amplitude a_1 and a_2 of the two pathways:

$$\begin{aligned} \langle 5d|5d\rangle &= |a_1 + a_2|^2 \\ &= (a_1 + a_2)^*(a_1 + a_2) \\ &= a_1^2 + a_2^2 + 2|a_1| \times |a_2| \cos(\Delta\phi)\ , \end{aligned} \tag{6.11}$$

where $\Delta\phi$ is the chirp-dependent phase difference between the two contributions. In a similar way the population in the final state $|v,J,m_J\rangle$ is given by

$$\langle v,J,m_J|v,J,m_J\rangle = |\sum_i a_i|^2$$

$$= \sum_i a_i^2 + \sum_{i,j>i} 2|a_i| \times |a_j| \cos(\Delta\phi_{ij}) \ . \tag{6.12}$$

Hence the oscillating part in this expression is simply the sum of all mutually interfering pathways.

6.2.3 Strength of interfering pathways

Returning to the grey triangle of Fig. 6.3, its enclosed area can be attributed uniquely to interference between $\mathrm{Q_{PR}}(4\frac{1}{2})$ and $\mathrm{Q_{2ph}}(4\frac{1}{2})$. The corresponding oscillation period can be calculated from Eq. (6.10) with $\delta_1(4\frac{1}{2}) = \{\nu[\mathsf{P}_{21}(5\frac{1}{2})] - \nu[\mathsf{R}_{10}(4\frac{1}{2})]\} = -64.55\ \mathrm{cm}^{-1}$ to be $\alpha_{2\pi}^{\mathrm{Q_{PR}-Q_{2ph}}}(4\frac{1}{2}) = 8.486 \times 10^{-26}\ \mathrm{s}^2$. Such a chirp is experimentally easily achievable, see e.g. chapter 5 or [87]. The grey trapezium in Fig. 6.3 shows the area enclosed by paths $\mathrm{Q_{PR}}(1\frac{1}{2})$ and $\mathrm{Q_{RP}}(1\frac{1}{2})$. Its area is $A_{\mathrm{tra}} = [(\frac{\delta_2}{2})^2 - (\frac{\delta_3}{2})^2]$ with $\delta_2(1\frac{1}{2}) = \{\nu[\mathsf{P}_{21}(2\frac{1}{2})] - \nu[\mathsf{R}_{10}(1\frac{1}{2})]\} = -44.66\ \mathrm{cm}^{-1}$ and $\delta_3(1\frac{1}{2}) = \{\nu[\mathsf{R}_{21}(\frac{1}{2})] - \nu[\mathsf{P}_{10}(1\frac{1}{2})]\} = -18.22\ \mathrm{cm}^{-1}$, corresponding to a period of $\alpha_{2\pi}^{\mathrm{Q_{PR}-Q_{RP}}}(1\frac{1}{2}) = 2.123 \times 10^{-25}\ \mathrm{s}^2$.

There are several conditions determining the contribution of a path $\mathrm{X_{YZ}}(J)$ to the population transfer to the upper state. Firstly, its contribution is proportional to the product of the Rabi frequency of the two transitions. In general, paths containing Q-transitions only play a role for the first rotational states, since their Hönl-London factor is small compared to those for P- and R-transitions ($\mathrm{HLF_Q} < 0.01$ for $J \geq 4\frac{1}{2}$) [92]. Secondly, to enhance the transfer for a given sign of the chirp of the laser pulse, the instantaneous frequency has to follow the ordering of transition frequencies $\nu[\mathsf{Y}_{21}(J')]$ and $\nu[\mathsf{Z}_{10}(J'')]$. More formally put: the sign of the anharmonicity $\delta_{\mathrm{YZ}} = \{\nu[\mathsf{Z}_{21}(J')] - \nu[\mathsf{Y}_{10}(J'')]\}$ should equal the sign of the chirp α. Of course, whether this condition is met depends on both the sign of the chirp and the rotational quantum number J, and on the spectroscopic parameters for the vibrational frequency ω_e, the anharmonic constant $\omega_e x_e$ and the rotational constant B_e of the particular molecule (see section 1.4.1 for NO and [34] for other diatomic molecules). Since the direct two-photon excitation occurs at a single frequency, the $\mathrm{Y_{2ph}}$ paths always meet this condition. From Fig. 6.2 it is clear that the paths $\mathrm{P_{PQ}}$, $\mathrm{Q_{PR}}$, $\mathrm{Q_{QQ}}$ and $\mathrm{R_{QR}}$ have a negative anharmonicity for all J-levels, and contribute for $\alpha < 0$ only. However, for the other paths ($\mathrm{P_{QP}}$, $\mathrm{Q_{RP}}$ and $\mathrm{R_{RQ}}$) the condition sets restrictions on the subset of J-values for which population transfer is allowed. This subset is different for both signs of the chirp. For example, transfer to the $v'' = 2$ state of the NO molecule with the chirp $\alpha < 0$, the path $\mathrm{P_{QP}}(J)$ is allowed for $J \in \{1\frac{1}{2}, \ldots, 6\frac{1}{2}\}$ only. For the reverse sign of the chirp, this path is allowed for $J \geq 7\frac{1}{2}$. Similarly, for $\alpha < 0$ the path $\mathrm{Q_{RP}}(J)$ is allowed for $J \in \{1\frac{1}{2}, 2\frac{1}{2}, 3\frac{1}{2}\}$ and for $\alpha > 0$ for $J \geq 4\frac{1}{2}$. Finally, for $\alpha < 0$ the path $\mathrm{R_{RQ}}(J)$ is allowed for $J \in \{1\frac{1}{2}, \ldots, 8\frac{1}{2}\}$ and for $J \geq 9\frac{1}{2}$ if $\alpha > 0$.

The anharmonicity corresponding to a specific path of the ro-vibrational ladder is the sum of the anharmonicities of the rotational and vibrational ladder: $\delta_{\mathrm{ro-vib}}(J) = \delta_{\mathrm{rot}}(J) + \delta_{\mathrm{vib}}$. The sign of $\delta_{\mathrm{ro-vib}}$ is a function of the rotational quantum number J. This can be attributed to the competition between the positive anharmonicity of the rotational ladder [$\delta_{\mathrm{rot}}(J) > 0$ and $\delta_{\mathrm{rot}}(J) \sim J$] and the negative anharmonicity of the vibrational ladder [$\delta_{\mathrm{vib}} \approx -2 \times \omega_e x_e$, see Eq.

(1.15), with for NO $\omega_e x_e = 14.187$ cm^{-1}]. Obviously, when multiple consecutive transitions to higher vibrational levels are involved, (e.g. along path T$_{\mathrm{RRR}}$) the anharmonicity can change sign, which would frustrate population transfer along such a path by a laser pulse with a linear chirp.

6.3 Dressed state description of coherent control of molecular vibrational excitation

In this section the formalism for calculating the time evolution of the molecular wavefunction in the coherent control vibrational excitation scheme will be developed. As a result of the chirped laser excitation, a coherent superposition of ro-vibrational states is formed. This superposition evolves in time both due to the laser-molecule interaction and due to the fact that the molecule is not in an eigenstate. The situation is most conveniently described using the dressed molecule approach, where the propagation of the superposition is calculated in a frame which rotates at the optical frequency of the excitation laser. In this approach, the superposition is decomposed in eigenstates of the molecule+field Hamiltonian, which are eigenstates where the laser-molecule interaction has explicitly been taken into account. The expansion coefficients of the molecular wavefunction in terms of these states are stationary as long as the laser field is constant, and only change when the amplitude of the laser field, which is a slowly varying function of time, changes. The molecular vibrational excitation can be analyzed in terms of an adiabatic or diabatic propagation over curves corresponding to individual dressed eigenstates (depending on the behaviour at a series of avoided crossings which are encountered).

The time-dependence of the molecular wavefunction is given by the Schrödinger equation as

$$i\hbar \frac{d\Psi}{dt} = H\Psi = [H_0 + V(t)]\Psi \ . \tag{6.13}$$

Here H$_0$ represents the molecular Hamiltonian and V(t) represents the interaction of the molecule, with dipole moment $\vec{\mu}(t)$ with the (chirped) laser field $\vec{E}(t)$:

$$V(t) = \vec{\mu}(t) \cdot \vec{E}(t) \ . \tag{6.14}$$

The wavefunction can be expanded in terms of the rotational and vibrational eigenfunctions of the electronic ground state $X\,^2\Pi_{\frac{1}{2}}$ according to

$$\Psi(t) = \sum_{v=0}^{v_{\max}} \sum_{J=0}^{\infty} a_{v,J}(t)\psi_{v,J} \ . \tag{6.15}$$

The laser field $\vec{E}$(t) couples rotational levels of one vibrational state $X\,^2\Pi_{\frac{1}{2}}(v'')$ with levels in the adjacent vibrational states $X\,^2\Pi_{\frac{1}{2}}(v')$, according to the selection rule $\Delta v'' = \pm 1$. All vibrational states are $^2\Pi$-states, hence the couplings are subject to the selection rule $\Delta J = 0, \pm 1$, where the relative coupling strength is calculated from the Hönl-London factors (HLF) for $^2\Pi - {}^2\Pi$

transitions [92] and the appropriate $3J$-symbols [97]. The electric field of the laser pulse is linearly polarized in the z direction and taken Gaussian in the time domain:

$$\vec{E}(t) = E_{\max}\vec{e}_z \tfrac{1}{2}[\exp(-\Gamma t^2)\exp(i\omega_c t) + \text{c.c.}] \ , \tag{6.16}$$

where Γ is given by

$$\Gamma = \left(\frac{8\ln 2}{\Delta\omega^2} + 4i\alpha\right)^{-1} \ , \tag{6.17}$$

with $\Delta\omega$ the bandwidth of the short laser pulse of central frequency $\omega_c = 2\pi\nu_c$ and α the amount of its chirp.

Substitution of the expansion of the wavefunction (6.15) into the time-dependent Schrödinger equation (6.13), left-multiplying by $\psi^*_{v,J}$ and integration over space yields the following equation for the time-dependence of the expansion coefficients $a_{v,J}(t)$

$$i\hbar\dot{a}_{v,J}(t) = E_{v,J}a_{v,J}(t) + \sum_{v'=0}^{v_{\max}}\sum_{J'=J-1}^{J'=J+1} a_{v',J'}(t)\langle\psi_{v,J}|\vec{\mu}(t)\cdot\vec{E}(t)|\psi_{v',J'}\rangle \ . \tag{6.18}$$

Next, the propagation of the wavepacket is transferred to a rotating frame, by writing the expansion coefficients as

$$a_{v,J}(t) = \sum_{n=-\infty}^{\infty} \underline{a}_{v,J,n}(t)e^{in\omega_c t} \ , \tag{6.19}$$

where the coefficients $\underline{a}_{v,J,n}(t)$ now are slowly varying functions of time. Substitution into Eq. (6.18), requiring that for each n the individual orders of $e^{in\omega t}$ are equal on both sides of Eq. (6.18) yields:

$$\begin{aligned} i\hbar\dot{\underline{a}}_{v,J,n}(t) = {} & (E_{v,J} + \hbar n\omega)a_{v,J,n}(t) \\ & + \sum_{J'=J-1}^{J'=J+1} a_{v+1,J',n-1}(t)\langle\psi_{v,J}|\vec{\mu}(t)\cdot\vec{\tilde{E}}(t)|\psi_{v+1,J'}\rangle \\ & + \sum_{J'=J-1}^{J'=J+1} a_{v-1,J',n+1}(t)\langle\psi_{v,J}|\vec{\mu}(t)\cdot\vec{\tilde{E}}^*(t)|\psi_{v-1,J'}\rangle \ , \end{aligned} \tag{6.20}$$

with

$$\vec{\tilde{E}}(t) = E_{\max}\vec{e}_z \tfrac{1}{2}\exp(-\Gamma t^2) \ . \tag{6.21}$$

Compared to Eq. (6.18) the eigenenergy $E_{v,J}$ has been replaced by a dressed state energy $E_{v,J} + \hbar n\omega$, which can be interpreted as the total energy of the molecule and the laser field. According to Eq. (6.20) different molecular and photon number states are coupled by single-photon laser transitions. In principle, Eq. (6.20) describes an infinite series of coupled differential equations. However, in the Rotating Wave Approximation (RWA), where far off-resonant couplings from $|v,J;n\nu\rangle$ to $|v',J';\hbar n'\nu\rangle$ are neglected, the mathematical treatment can be considerably simplified. In the RWA the infinite ladder of interacting dressed states is separated into finite blocks of self-contained states which only interact among themselves.

$$\begin{bmatrix}
E_{0,\frac{1}{2}} & & & \frac{1}{2}\Omega^{1,\frac{1}{2},m_J}_{0,\frac{1}{2},m_J} & \frac{1}{2}\Omega^{1,1\frac{1}{2},m_J}_{0,\frac{1}{2},m_J} & \\
 & E_{0,1\frac{1}{2}} & & \frac{1}{2}\Omega^{1,\frac{1}{2},m_J}_{0,1\frac{1}{2},m_J} & \frac{1}{2}\Omega^{1,1\frac{1}{2},m_J}_{0,1\frac{1}{2},m_J} & \frac{1}{2}\Omega^{1,2\frac{1}{2},m_J}_{0,1\frac{1}{2},m_J} \\
 & & E_{0,2\frac{1}{2}} & & \frac{1}{2}\Omega^{1,1\frac{1}{2},m_J}_{0,2\frac{1}{2},m_J} & \frac{1}{2}\Omega^{1,2\frac{1}{2},m_J}_{0,2\frac{1}{2},m_J} \\
\left(\frac{1}{2}\Omega^{1,\frac{1}{2},m_J}_{0,\frac{1}{2},m_J}\right)^* & \left(\frac{1}{2}\Omega^{1,\frac{1}{2},m_J}_{0,1\frac{1}{2},m_J}\right)^* & & E_{1,\frac{1}{2}}-\hbar\omega & & \\
\left(\frac{1}{2}\Omega^{1,1\frac{1}{2},m_J}_{0,\frac{1}{2},m_J}\right)^* & \left(\frac{1}{2}\Omega^{1,1\frac{1}{2},m_J}_{0,1\frac{1}{2},m_J}\right)^* & \left(\frac{1}{2}\Omega^{1,1\frac{1}{2},m_J}_{0,2\frac{1}{2},m_J}\right)^* & & E_{1,1\frac{1}{2}}-\hbar\omega & \\
 & \left(\frac{1}{2}\Omega^{1,2\frac{1}{2},m_J}_{0,1\frac{1}{2},m_J}\right)^* & \left(\frac{1}{2}\Omega^{1,2\frac{1}{2},m_J}_{0,2\frac{1}{2},m_J}\right)^* & & & E_{1,2\frac{1}{2}}-\hbar\omega
\end{bmatrix}$$

Figure 6.4: *Matrix of the Hamiltonian $H=[H_0+V(t)]$ of the dressed states for 3 rotational and 2 vibrational states coupled by single-photon laser transitions.*

Furthermore, the rotational-state-dependent transition matrix elements in Eq. (6.20) are replaced by the representative single-photon transition matrix elements $\Omega^{v',J',m'_J}_{v,J,m_J}(t)$. With these simplifications, Eq. (6.20) reduces to

$$\begin{aligned}
i\hbar\dot{\underline{a}}_{v,J,n}(t) = {} & (E_{v,J}+\hbar n\omega)\underline{a}_{v,J,n}(t) \\
& + \sum_{J'=J-1}^{J'=J+1} \underline{a}_{v+1,J',n-1}(t)\Omega^{v+1,J',m'_J}_{v,J,m_J}(t) + \\
& + \sum_{J'=J-1}^{J'=J+1} \underline{a}_{v-1,J',n+1}(t)\left[\Omega^{v-1,J',m'_J}_{v,J,m_J}(t)\right]^* ,
\end{aligned} \tag{6.22}$$

where $\Omega^{v',J',m'_J}_{v,J,m_J}(t)$ is the Rabi frequency for single-photon excitation:

$$\Omega^{v',J',m'_J}_{v,J,m_J}(t) = \frac{2\vec{\mu}_{v,v'}(t)\cdot\vec{E}(t)}{\hbar} \times \mathrm{HLF}(v,J,v',J') \times \begin{pmatrix} J' & 1 & J \\ m'_J & 0 & -m_J \end{pmatrix}^2 . \tag{6.23}$$

The coupled equations (6.20) for the coefficients $\underline{a}_{v,J,n}(t)$ can be written in matrix form as

$$\dot{\underline{a}}_i(t) = \sum_j H_{ij}\underline{a}_j(t) . \tag{6.24}$$

Choosing an energy scale according to $E_{0,J} \equiv -\hbar n\omega$, the Hamiltonian can be schematically represented as in Fig. 6.4. The ability to control the efficiency of molecular vibrational excitation using chirped laser pulses, enters through the presence of the chirp α in , (α) (see Eq. 2.15) in the dressed state Hamiltonian. When the Hamiltonian given in Fig. 6.4 is diagonalized, expressions are obtained for the dressed states in terms of the molecular eigenstates:

$$\psi_{\mathrm{dressed},i} = \sum_j V_{ij}\psi_j , \tag{6.25}$$

where V represents the matrix containing the eigenvectors of the dressed state Hamiltonian, and the ψ_j represent the molecular eigenstates (in the absence of the laser field). Conversely, the molecular eigenstates ψ_j can be expressed in terms of the dressed eigenstates as

$$\psi_j = \sum_i V_{ji} \psi_{\text{dressed},i} \ . \tag{6.26}$$

The total wavefunction can be written as a superposition of either the dressed molecular states or the molecular eigenfunctions. The expression in terms of the dressed eigenstates is more convenient, since these states are the eigenstates of the molecule+field Hamiltonian for a constant laser-field strength. Hence, we write:

$$\Psi_{\text{total}} = \sum_i \beta_i \psi_{\text{dressed},i} \exp(-i\lambda_i t/\hbar) \ , \tag{6.27}$$

where λ_i is the eigenvalue belonging to the dressed eigenstate i, and where the coefficients β_i follow from the initial conditions of the problem. Alternatively, using Eq. (6.25), the molecular wavefunction can be expressed as a superposition of molecular eigenstates as:

$$\Psi_{\text{total}} = \sum_{ij} \beta_i V_{ij} \psi_j \exp(-i\lambda_i t/\hbar) \ . \tag{6.28}$$

In this expression the coefficients of the individual molecular eigenstates ψ_j are a complicated function of time, containing a number of different time scales (corresponding to the eigenenergies of the various dressed eigenstates). Eq. (6.28) can be used to calculate the populations in the different ro-vibrational states and the steric properties of the molecular wavepacket as a function of the chirp and/or elapsed time.

In the present problem the laser field couples molecular eigenstates subject to the selection rules $\Delta J = 0, \pm 1$, $\Delta m_J = 0$. For each initially populated state with total rotational angular momentum J, the projection of the angular momentum m_J is restricted to $|m_J| \in \{\frac{1}{2}, \ldots, J\}$. For given laser field conditions the dressed-state Hamiltonian describes the couplings among *all* levels for a given m_J. The final population distribution after the excitation by the chirped laser pulse is computed by integrating the time-dependent Schrödinger equation over the pulse duration using the Runge-Kutta method and LU-decomposition in modified FORTRAN routines, based on the original routines LUDCMP and LUBKSB from the Fortran numerical recipes [98]. In the dressed-state picture, the molecule is in a *stationary* state, i.e. in a superposition of eigenstates of the molecule+field Hamiltonian, as long as the laser field does not change. If the variations in the laser field are rather slow, the coefficients β_i [see Eq. (6.27)] are almost constant, hence large time steps for the numerical integration are allowed. There are two equivalent ways of implementing the chirp of the laser pulse in the calculation. Firstly, the frequency of the laser can change over the pulse duration, while the couplings to the molecular state are kept constant. This implies that the diagonal elements of the laser+molecule Hamiltonian change during the laser pulse. Secondly, the laser frequency can be kept constant while including the chirp in the couplings in the off-diagonal elements of the Hamiltonian. The latter method is used for the present calculations. In order to obtain converged results, typically 5 to 10 rotational states were included for each of the 3 to 7 vibrational levels of the NO $X\ ^2\Pi_{\frac{1}{2}}$ electronic ground state that were included. Since the AC-stark shift [79] of the eigenstates is described by the mixing of the unperturbed eigenstates, a larger number of states must be used as basis set for strong-laser-field calculations. In order to obtain converged results, typically 5 to 10 rotational states were included for each of the 3 to 7 vibrational levels of the NO $X\,^2\Pi_{\frac{1}{2}}$ electronic ground state that were included. Since the AC-stark shift of the eigenstates is described by the mixing of the unperturbed eigenstates, a larger number of states must be used as basis set for strong-laser-field calculations. The calculation predicts how a the probability amplitude of every single state $|v,J,m_J\rangle$ is re-distributed over all other $|v,J,m_J\rangle$ states. To obtain the final-state population distribution over the $|v,J,m_J\rangle$ states, the incoherent sum is calculated by multiplying the computed re-distribution matrix with the vector that describes the initial population distribution over the states $|v,J,m_J\rangle$.

Summarizing, calculations in the rotating frame (i.e. using "dressed states") provide a mathematically convenient method to calculate the propagation of the molecular wavefunction under the influence of the chirped laser field.

6.4 Low IR intensity calculations

6.4.1 Most relevant interference pathways

In this subsection the appearance and origin of the rotational interferences is more closely examined. Using the model described in the previous section, calculations are performed for the vibrational excitation of the electronic ground state $X\,^2\Pi_{\frac{1}{2}}$ of the NO molecule by a chirped IR ($h\nu = 1{,}850$ cm^{-1}, $\Delta h\nu = 40$ cm^{-1}) laser pulse that is Gaussian in the time domain with a fluence $\Phi = 25$ mJ cm^{-2}. For $\alpha = 0$, the pulse duration is 0.37 ps. At the corresponding peak intensity ($I_{\max} = 68 \times 10^9$ W cm^{-2}) the single-photon Rabi frequencies are typically less than $\Omega_{v,J,m_J}^{v',J',m'_J} \leq 1 \times 10^{11}$ Hz, with $m'_J = m_J$ since the laser field is linearly polarized. The values of the set of parameters used in the simulation corresponds to the conditions of the experiment described in chapter 5.

Fig. 6.5 shows the predicted population distribution, as calculated using 3 rotational levels $J'' \in \{\frac{1}{2}, 1\frac{1}{2}, 2\frac{1}{2}\}$, and the corresponding sublevels m_J, for each of the 3 vibrational states $v'' \in \{0, 1, 2\}$, as a function of the chirp α in the excited vibrational state $|2,J,m_J\rangle$ (from top to bottom panel respectively: $|2,\frac{1}{2},\frac{1}{2}\rangle$, $|2,1\frac{1}{2},\frac{1}{2}\rangle$ and $|2,1\frac{1}{2},1\frac{1}{2}\rangle$. At first inspection it is clear from the irregular oscillatory behaviour that multiple interference periods are present, as expected from Eq. (6.12). This is in contrast with the sinusoidal behaviour of the oscillations as a function of the chirp in the simple three-level ladder system in rubidium [Eq. (6.11) and chapters 2 and 3].

For each of the individual J, m_J levels of the $v'' = 2$ state the population oscillates with a different set of periods. To identify the contributions of the different interfering pathways the results shown in Fig 6.5 are Fourier transformed after subtraction of the DC component and multiplication with a Hanning window [99]. The calculation was performed for a large

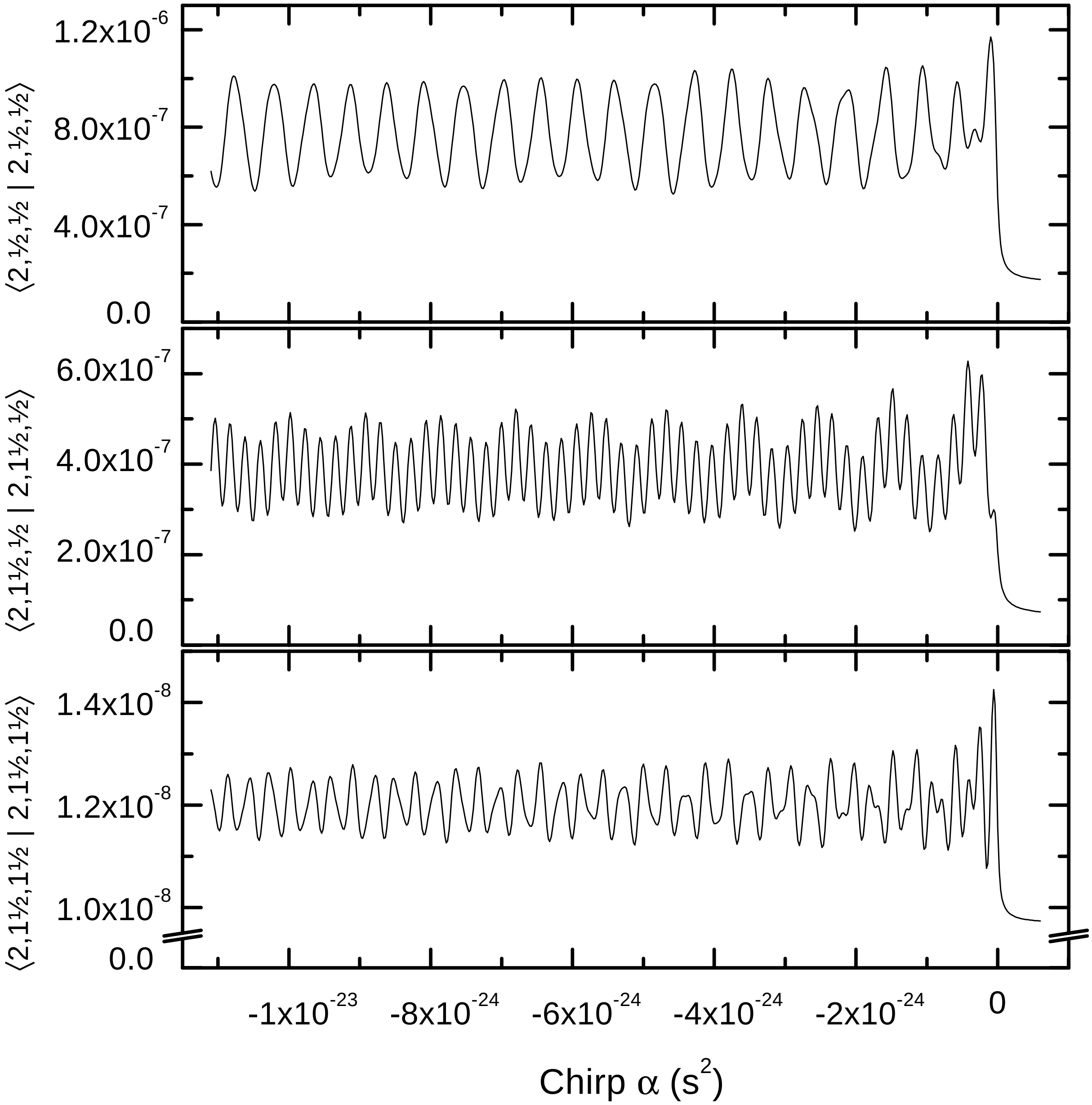

Figure 6.5: *The top panel shows the population in* $|v{,}J{,}m_J\rangle = |2{,}\frac{1}{2}{,}\frac{1}{2}\rangle$ *as a function of the chirp* α*, as calculated for an IR laser pulse with* $h\nu = 1{,}850\ \mathrm{cm}^{-1}$, $\Delta h\nu = 40\ \mathrm{cm}^{-1}$ *and a fluence of* $\Phi = 25\ \mathrm{mJ\,cm}^{-2}$. *The presence of multiple interferences is obvious. The middle and bottom panel display the population of* $|2{,}1\frac{1}{2}{,}\frac{1}{2}\rangle$ *and* $|2{,}1\frac{1}{2}{,}1\frac{1}{2}\rangle$*, respectively. Note the remarkable difference in the behaviour of the two different* m_J *sublevels in the same rotational states* J*. The initial state was a Boltzmann distribution over 3 rotational levels* ($J'' \in \{\frac{1}{2}, 1\frac{1}{2}, 2\frac{1}{2}\}$) *with all their* m''_J *sublevels of three vibrational states* ($v'' \in \{0,1,2\}$) *with* $\mathrm{T_{rot}} = 14$ K *and* $\mathrm{T_{vib}} = 300$ K.

number (2^9) of equidistant chirp values, providing a sufficient spectral resolution in a Fast-Fourier Transform (FFT) to identify interference periods with pairs of interfering paths. Fig. 6.6 shows the FFT of the population transferred to each of the $|2{,}J{,}m_J\rangle$ levels. The labels in

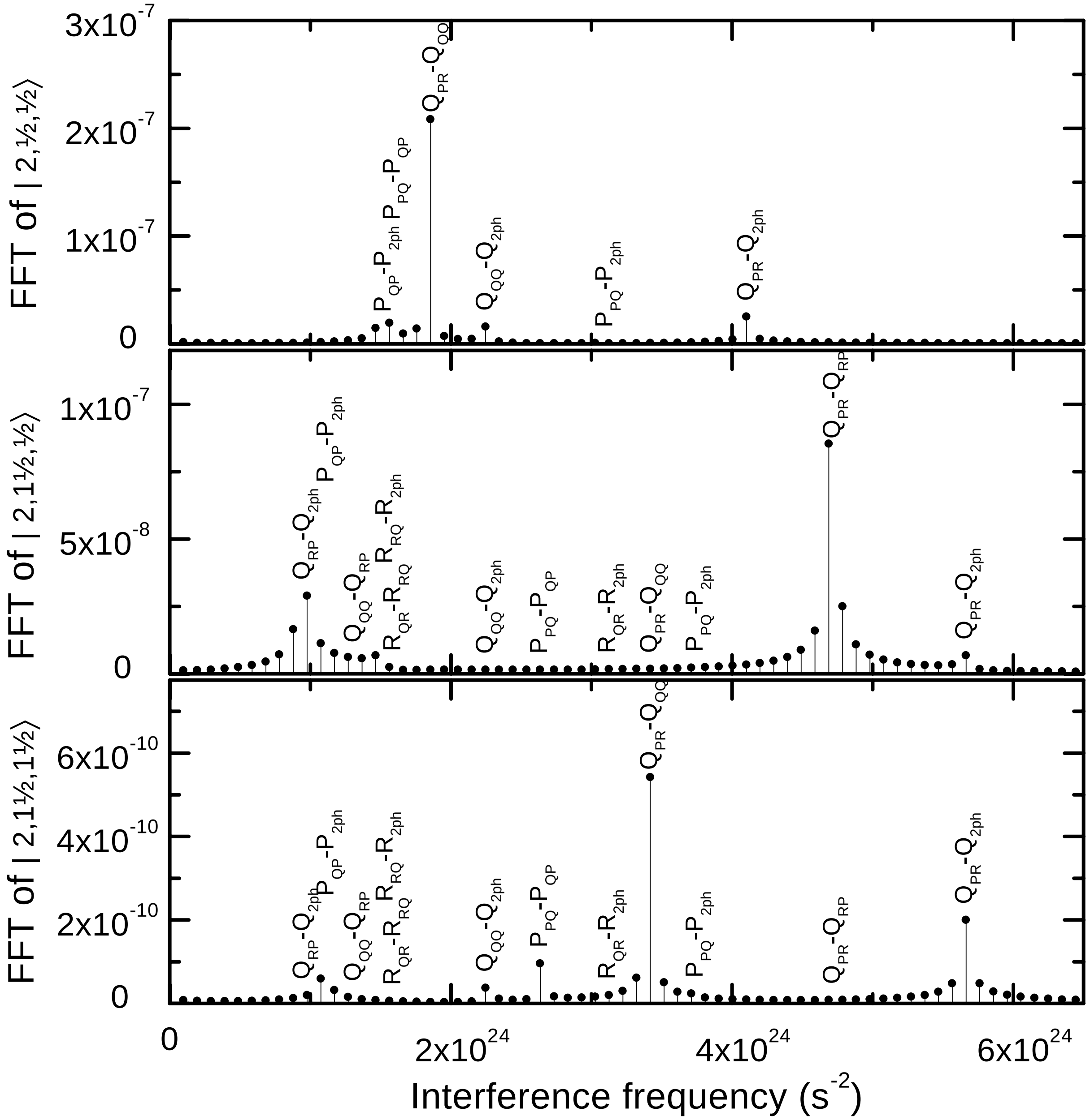

Figure 6.6: *The three panels display Fourier transforms of the population of respectively* $|2,\frac{1}{2},\frac{1}{2}\rangle$, $|2,1\frac{1}{2},\frac{1}{2}\rangle$ *and* $|2,1\frac{1}{2},1\frac{1}{2}\rangle$, *as they were shown in Fig. 6.5. The labels indicate the predicted interference frequencies as calculated from the enclosed areas (section 6.2).*

the figure indicate the frequencies $\alpha_{2\pi}$ as calculated from the different enclosed areas [using Eq. (6.10)], corresponding to the pairs of interfering paths (see also table 6.1). Obviously, each peak corresponds to a pair of interfering pathways. However, there is not always a peak present with every label. In the low intensity regime the peak height is proportional to the product of the Rabi frequencies [see Eq. (6.23)] of the two interfering paths. For certain transitions the Hönl-London factors are small, resulting in relatively small Rabi frequencies for those particular transitions. This is the case for all **Q**-transitions if $J \geq 1\frac{1}{2}$. This explains the absence (or weak presence) of the sets of pathways with a contribution via a **Q**-transition, i.e. $\mathrm{X_{XQ}}$–$\mathrm{U_{WV}}$ and $\mathrm{X_{QX}}$–$\mathrm{U_{WV}}$ peaks (with $\{\mathrm{X,U,V,W}\} \in \{\mathrm{Q,P,R}\}$) in the FFT-spectra of $|2,\frac{1}{2},\frac{1}{2}\rangle$, $|2,1\frac{1}{2},\frac{1}{2}\rangle$ and $|2,1\frac{1}{2},1\frac{1}{2}\rangle$. The absence of the several other peaks in the FFT of the $|2,1\frac{1}{2},1\frac{1}{2}\rangle$ population is explained by forbidden transitions to the intermediate state that are involved. For the following set of paths to final state $|2,1\frac{1}{2},1\frac{1}{2}\rangle$ at least one of the Hönl-London factors is zero:

I. $\mathrm{Q_{RP}}$ is forbidden since the intermediate state corresponding to this path $|1,\frac{1}{2},1\frac{1}{2}\rangle$ does not exist,

II. $\mathrm{R_{QR}}$ because transfer from the initial state $|0,\frac{1}{2},\frac{1}{2}\rangle$ to the intermediate state $|1,1\frac{1}{2},1\frac{1}{2}\rangle$ violates the selection rule $\Delta m_J = 0$,

III. $\mathrm{R_{RQ}}$ since, as for II, transfer from the intermediate state $|1,\frac{1}{2},\frac{1}{2}\rangle$ to the final state $|2,1\frac{1}{2},1\frac{1}{2}\rangle$ would violate $\Delta m_J = 0$.

Summarizing, the period of the interference in population as a function of the chirp can be identified with the enclosed areas between the interfering pathways and the most important contribution comes from the two paths with the largest product of their Rabi frequencies.

Table 6.1: *Frequencies ($1/\alpha_{2\pi}$ ps^{-2}) for interference between pairs of paths for all possible paths that transport population from $|0,J'',m''_J\rangle$ to $|2,J,m_J\rangle$.*

	$\lvert 2,\frac{1}{2},\frac{1}{2}\rangle$	$\lvert 2,1\frac{1}{2},\frac{1}{2}\rangle$	$\lvert 2,1\frac{1}{2},1\frac{1}{2}\rangle$
$\mathrm{P_{QP}} - \mathrm{P_{PQ}}$	1.58	2.63	2.63
$\mathrm{P_{PQ}} - \mathrm{P_{2ph}}$	3.09	3.73	3.73
$\mathrm{P_{QP}} - \mathrm{P_{2ph}}$	1.51	1.11	1.11
$\mathrm{Q_{PR}} - \mathrm{Q_{QQ}}$	1.86	3.41	3.41
$\mathrm{Q_{PR}} - \mathrm{Q_{RP}}$	-	4.71	-
$\mathrm{Q_{PR}} - \mathrm{Q_{2ph}}$	4.10	5.65	5.65
$\mathrm{Q_{QQ}} - \mathrm{Q_{RP}}$	-	1.30	-
$\mathrm{Q_{QQ}} - \mathrm{Q_{2ph}}$	2.24	2.24	2.24
$\mathrm{Q_{RP}} - \mathrm{Q_{2ph}}$	-	0.94	-
$\mathrm{R_{QR}} - \mathrm{R_{RQ}}$	-	1.58	-
$\mathrm{R_{QR}} - \mathrm{R_{2ph}}$	-	3.11	-
$\mathrm{R_{RQ}} - \mathrm{R_{2ph}}$	-	1.53	-

6.4.2 Interference in the population as a function of chirp

With the model discussed in section 6.3 the population distribution over the ro-vibrational states of the electronic ground state of NO $X\ ^2\Pi_{\frac{1}{2}}$ is computed. For the low intensity limit a calculation is performed with laser pulse parameters that equal those for experiments performed at FELIX. In Fig. 6.7 the total population in the vibrational states $v''=1,2,3,$ and 4 is shown as a function of chirp for a laser pulse with $\nu = 1{,}845\ \mathrm{cm}^{-1}$, $\Delta\nu = 50\ \mathrm{cm}^{-1}$ and a fluence of $\Phi = 25\ \mathrm{mJ\,cm}^{-2}$. For the calculation a total of 45 states is used: $v'' \in \{0,\ldots,4\}$, $J \in \{\frac{1}{2},\ldots,8\frac{1}{2}\}$ and m_J is restricted to $|m_J| \in \{\frac{1}{2},\ldots,J\}$. The calculation weights the contribution of each initial state to the final states with the thermal population of that initial state. The thermal population is calculated for two different cases:

I. a Boltzmann distribution with $\mathrm{T_{rot}} = 14$ K and $\mathrm{T_{vib}} = 1$ K, i.e. for only $v''=0$ as initial state,
II. as I., but now $\mathrm{T_{vib}} = 300$ K (circles at $\alpha = -1\times10^{-25}\ \mathrm{s}^2$).

The temperature values represent the experimental conditions: $\mathrm{T_{rot}}$ is obtained from the REMPI spectrum of Fig. 5.3, and $\mathrm{T_{vib}}$ equals room temperature since no vibrational cooling in the supersonic expansion is assumed [88]. The final state population distribution is shown in Fig. 6.7 for both case I (dashed curves) and for case II (solid curves). The range of chirp for which the population is shown is much smaller than for Fig. 6.5.

The top panel shows that the population transfer to $v''=1$ by the IR laser is several times the thermally present population (circle at $\alpha = -1\times10^{-25}\ \mathrm{s}^2$). As expected for the first excited state in a ladder system in the low intensity limit (no depletion of the $v''=0$ state), the population in $v''=1$ (top panel) only is a function of the fluence and *not* of the chirp. One panel down, the final population in $v''=2$ is displayed, which shows a strong enhancement for negative chirp, i.e. when the instantaneous frequency follows the consecutive steps up the vibrational ladder. The weak bends in the dashed and solid curves show interference between several pathways. For each vibrational state the population is summed over all 9 J-levels. Since the summing causes the oscillations in the populations of individual rotational to (partially) average out, and because the $v''=2$ population is gathered mostly in the low J-levels, (for these lowest J-levels the period of interference $\alpha_{2\pi}$ is large compared to the the experimentally accessed range of chirp), the appearance of the oscillations is less pronounced, although clearly modulations are present. For positive chirp the $v''=2$ population is expected to go to zero, since the molecule is irradiated with the required frequencies for transferring population from $v''=2 \leftarrow 1$ *before* the frequencies that transfer population from $v''=1 \leftarrow 0$. Consequently there would be no population in $v''=1$ that can be passed on to $v''=2$. This notion is confirmed by the prediction for case I (dashed curve). For case II, however, there always is a non-zero population transfer to $v''=2$. This is attributed to transfer of population that is thermally present in $v''=1$. The lowest two panels show the population in $v''=3$ and $v''=4$ as a function of chirp. The curves have the same features as the curve for $v''=2$, but they are showing up more pronounced. This is due to the consecutive nature of the transfer up on the vibrational ladder: since both the

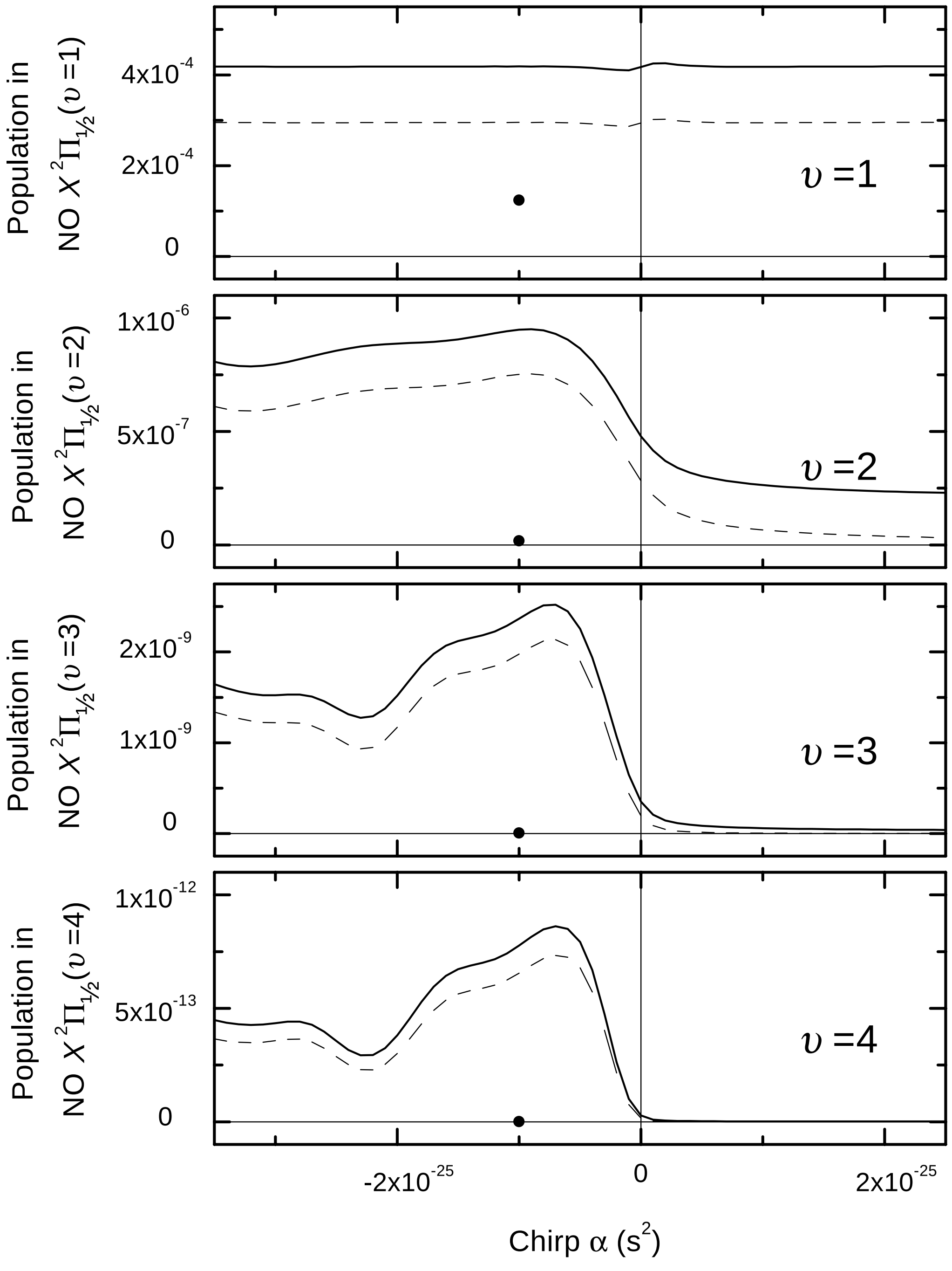

Figure 6.7: *The predicted population for respectively* $v''=1,2,3$ *and* 4 *as a function of the chirp, for a Gaussian laser pulse with* $\nu_c=1{,}845\ \mathrm{cm}^{-1}$ *and* $\Delta\nu=50\ \mathrm{cm}^{-1}$ *for a pulse fluence of* $\Phi=25\ \mathrm{mJ\,cm}^{-2}$. *For the calculation* 9 *rotational levels with all their* m_J *sublevels in* 5 *vibrational states of NO* $X\,^2\Pi_{\frac{1}{2}}$ *were included. The prediction for the final population distribution is calculated for an initial Boltzmann distribution of the population with I.* $\mathrm{T_{rot}}=14$ K *and* $\mathrm{T_{vib}}=1$ K *(dashed curves) and for II.* $\mathrm{T_{rot}}=14$ K *and* $\mathrm{T_{vib}}=300$ K *(solid curves). The circles at* $\alpha=-1{\times}10^{-25}\ \mathrm{s}^2$ *indicate the initial thermal population of the vibrational states for case II.*

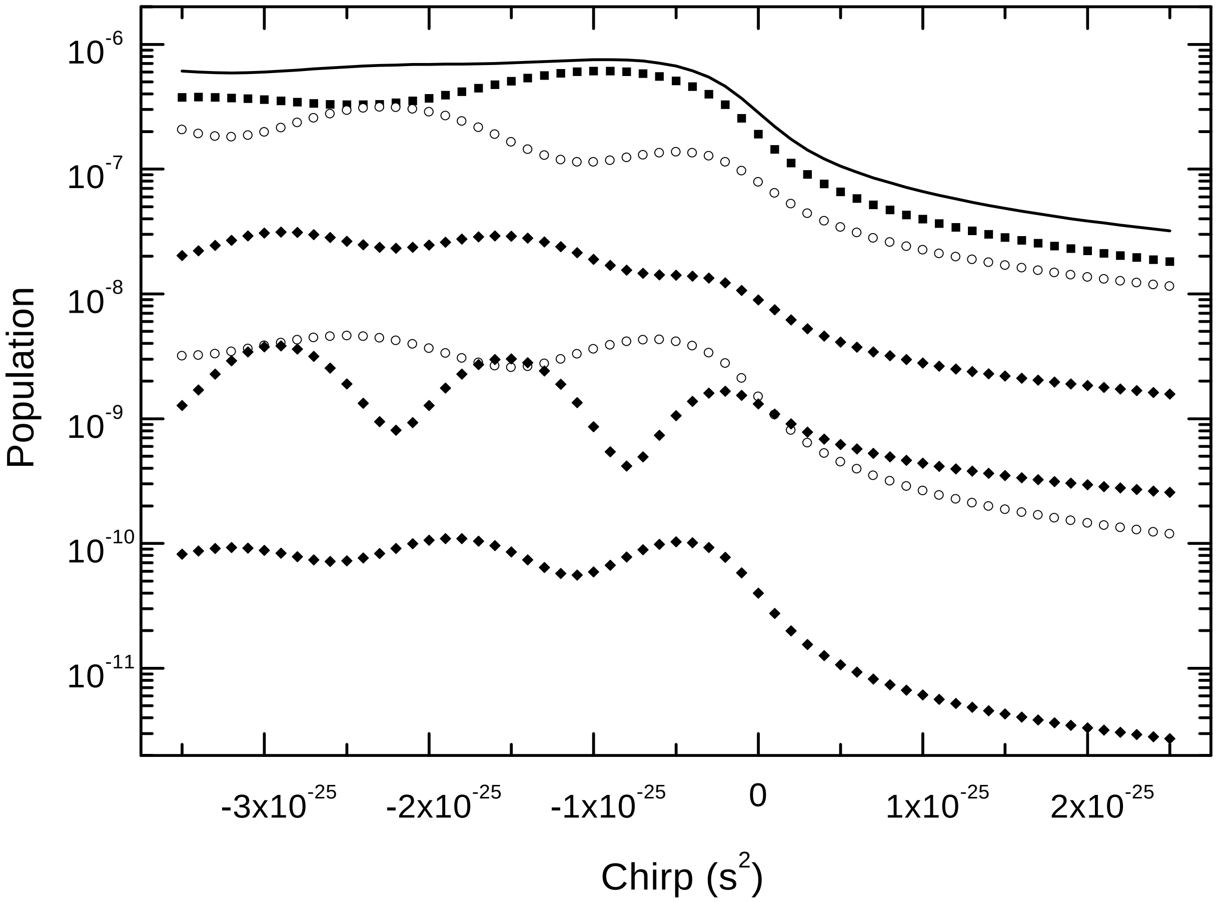

Figure 6.8*: The final population distribution over the states $|2,J,m_J\rangle$ as a function of the chirp, calculated for temperature case I. The squares, circles and diamonds denote the population in the states $|2,\frac{1}{2},m_J\rangle$, $|2,1\frac{1}{2},m_J\rangle$ and $|2,2\frac{1}{2},m_J\rangle$, respectively. Different values of m_J belonging to the same J are denoted by the same symbol, with m_J increasing from the top to the bottom data sets (i.e. the sublevel with $m_J = \frac{1}{2}$ is most efficiently populated for each J-level). The total population in $|2\rangle$ is shown as a solid curve [and is identical to the dashed curve shown in the second panel from the top in Fig. 6.7 (temperature case I.)]*

distribution of the population over the rotational states and the interference periods $\alpha_{2\pi}$ do not change very much for the next steps up on the ladder, the transfer efficiency is enhanced (or reduced) for the same values of the chirp as for the transfer to $v'' = 2$. Hence the wiggly structure in the transfer to intermediate vibrational states, as caused by the interference effects, is augmented as it is passed on to higher vibrational states.

Fig. 6.8 displays the calculated $v''\!=\!2$ population as a function of the chirp for the individual $|2,J,m_J\rangle$-levels for $J \in \{\frac{1}{2}, \ldots, 2\frac{1}{2}\}$ and the total population (solid curve, same data as in Fig. 6.7). Firstly, the calculations show that sublevels with $m_J = \frac{1}{2}$ are most efficiently excited to the $|2\rangle$ level. This is a general feature of population that is transferred to higher vibrational states. This selection of $m_J\!=\!\frac{1}{2}$ sublevels means that the excited molecules become more aligned with the polarization direction of the IR laser with every step up on the vibrational ladder.

Secondly, the different oscillatory structure in the calculations for different m_J with the same J demonstrates that each individual m_J-sublevel is populated via its own specific subset of paths. Finally, comparison of the calculated population of the individual $|2,J,m_J\rangle$ states to the total population in $|2\rangle$ shows that the interference structure that is present in the rotational state populations is largely smoothed out by their addition to the total population of a vibrational state.

Summarizing, the difference in the final population between the calculations without or with thermal population of vibrational states as initial states (temperature case I and II, respectively) is evident. The two prominent differences are

1. the overall reduction of the final population in $|v\rangle$-levels for temperature case I as compared to case II,
2. the population in $|2\rangle$ does *not* go to zero for $\alpha > 0$ when thermal population of the higher $|v\rangle$-levels is taken into account.

The subset of molecules that is excited to higher vibrational states shows the propensity of alignment along the polarization direction of the laser field. The prediction that the population of the higher vibrational states ($v'' \geq 2$) shows a large enhancement in transfer efficiency for the intuitive ordering of the frequencies, i.e. for chirp $\alpha < 0$, is the most important conclusion from Fig. 6.7.

6.5 Comparison of calculations with experimental results

In this section a comparison of the calculation from the previous section with experimental data is presented. The experimental data that are discussed in this section are recorded with two slightly different IR pulse spectra. For each calculation the appropriate set of laser pulse parameters is used. The data on the population distribution are retrieved using the REMPI technique (see section 1.4.2). Therefore the calculated final population of a certain level $|v,J,m_J\rangle$ is multiplied with the appropriate Hönl-London factors and $3J$-symbols [80, 97, 100] for the NO $A\ ^2\Sigma(v') - X\ ^2\Pi_{\frac{1}{2}}(v'')$ transition. In the experiment (see also Chapter 5) the population of vibrational state $|v\rangle$ is measured by tuning a UV laser with a bandwidth of 1.85 cm^{-1} to the coinciding Q_{11} and P_{21} branches of the NO $A\,^2\Sigma(v')$–$X\,^2\Pi_{\frac{1}{2}}(v'')$ or NO(v', v'') γ-bands (see Fig. 5.3. Due to the large bandwidth of the UV laser, the rotational levels with $J'' \in \{\frac{1}{2}, \ldots, 4\frac{1}{2}\}$ are probed simultaneously. For the rotational temperature of $\mathrm{T}_{\mathrm{rot}} = 14$ K almost all population is present in these rotational states. Since the distribution over the J-levels does not shift dramatically after absorption of a few IR photons, also for the vibrationally excited states most of the population is probed via the same manifold of lines of the low J-levels via Q_{11} and P_{21} branches of the NO(v', v'') γ-band.

6.5.1 Population transfer as a function of chirp

In section 6.4.2 the predicted population distribution has been presented as calculated for the parameters of the experiment performed at FELIX. As explained above, these results were calculated for each $|v,J,m_J\rangle$ for $v''\in\{0,\ldots,4\}$ and $J\in\{\frac{1}{2},\ldots,8\frac{1}{2}\}$. To compare the experimental data with the predicted population distributions, a simulated REMPI signal has been calculated from the predicted population of state $|v,J,m_J\rangle$ by multiplying by the appropriate Hönl-London factor and 3-J symbol for the NO $A\,^2\Sigma(v')-X\,^2\Pi_{\frac{1}{2}}(v'')$ transition. It is assumed that the ionization probability from the $A\,^2\Sigma(v',J'')$-state is independent of the quantum numbers in the $A\,^2\Sigma(v',J'')$-state [47]. The simulated REMPI signal from the individual states $|v,J,m_J\rangle$ are summed over the Q_{11}- (for $J''\in\{\frac{1}{2},\ldots,4\frac{1}{2}\}$) and P_{21}-branches (for $J''\in\{1\frac{1}{2},\ldots,4\frac{1}{2}\}$), yielding the calculated REMPI signal from the NO(v',v'') γ band. Fig. 6.9 displays both the measured and calculated REMPI signal (for $\mathrm{T_{vib}}=300$ K) as a function of the chirp. The Y-axis scaling is justified for each individual v''. The agreement between the simulation and the measurement is excellent, despite the small mismatch between the shape of the FELIX pulse spectrum and the model Gaussian pulse. The importance of taking the thermal population in the higher vibrational states into account is stressed by the agreement between experimental data and simulation for $v''=2$, which both do *not* go to zero for $\alpha>0$ and $\mathrm{T_{vib}}=300$ K.

For large negative values of α both the experiment and the theory show a reduction in the $v''=3$ and $v''=4$ population due to destructive interference between different rotational pathways. What pathways are contributing most to the population transfer is not easily assessed from the interference shown by the data, since the experimentally assessed range of chirp is not sufficiently large to identify periods that correspond to specific paths. Additionally, the number of relevant interference periods is increased even more since the REMPI signal stems from five different rotational states ($J''\in\{\frac{1}{2},\ldots,4\frac{1}{2}\}$). As demonstrated in the previous section the model calculations the most important paths can be identified, explaining the interference features of the data.

6.5.2 Population transfer as a function of IR intensity

The intensity dependency of the IR multi-photon excitation process has been investigated by probing the population in the vibrationally excited states the same way as described in the previous section as a function of IR laser fluence Φ. The IR pulse spectrum is somewhat narrower than that in the previous spectrum, with $\nu=1{,}850$ cm^{-1}, $\Delta\nu=40$ cm^{-1}. The spectrum fitted less well to a Gaussian: the spectral intensity on the far-infrared (FIR) side of the bandwidth was much lower than for the Gaussian used in the model calculations.

In the experiment the intensity of the IR pulses was varied by placing wire-meshes from the "LASNIX" IR attenuator with variable transmission in the beampath. The measured REMPI signal was recorded as a function of the IR laser fluence. This fluence was measured with a HgCdTe-detector, which monitored the fluence of the IR laser pulse. All data are recorded at a chirp of 0.6×10^{-25} s^2, where a maximum of the transfer to $v''=3$ was observed.

Fig. 6.10 shows the REMPI signal from the population in $v''=1$ as a function of the IR

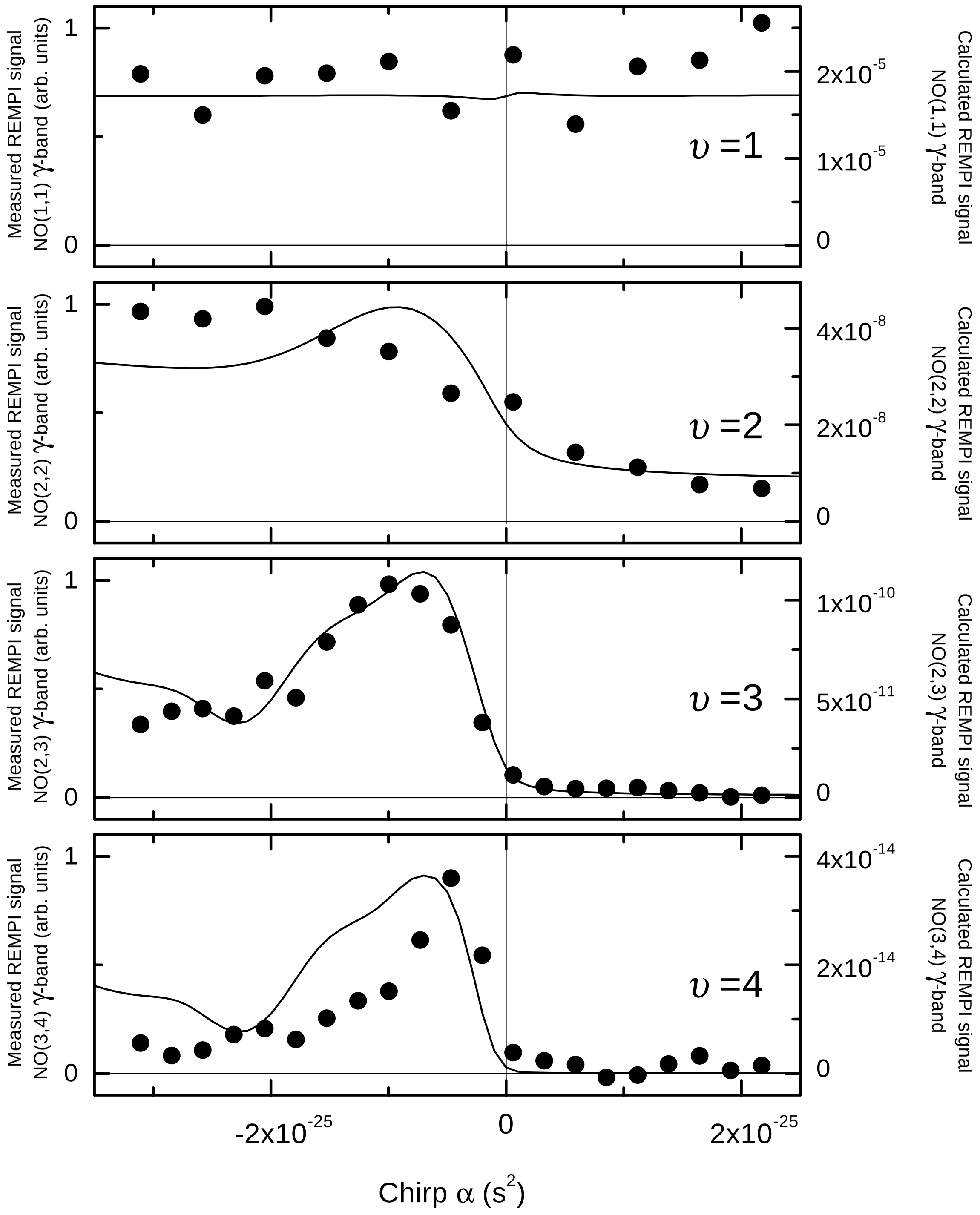

Figure 6.9: *The REMPI signal (curves) corresponding to the prediction of the population of* $v'' = 1, 2, 3$ *and* 4 *as a function of the chirp, as shown in Fig. 6.7. The dots display the measured REMPI signal, probing the low rotational states* $(J'' \in \{\frac{1}{2}, \ldots, 4\frac{1}{2}\})$ *of the coinciding* Q_{11} *and* P_{21} *branches of the NO*(v', v'') γ*-bands.*

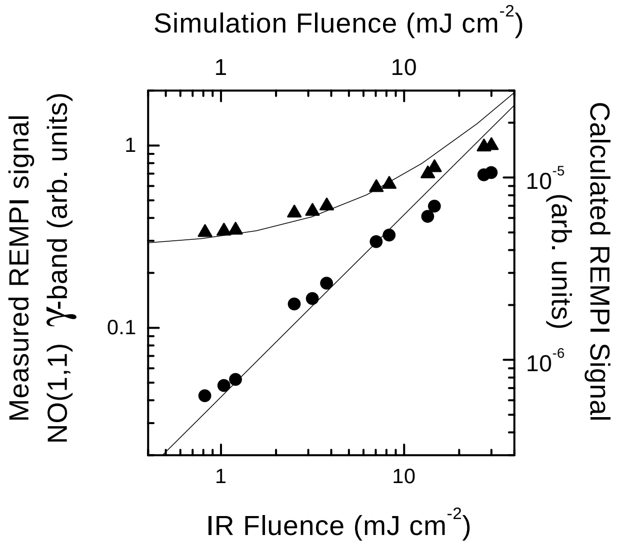

Figure 6.10: *A comparison of the rate of population of NO X* $^2\Pi_{\frac{1}{2}}(v''=1)$ *as a function of intensity between experimental results (points) and predicted by model calculations (solid curves). To obtain the transfer by the IR laser field (circles), the background signal from thermal population of* $v''=1$ *(*$\mathrm{T_{vib}}=300$ K*) is subtracted from the recorded signal (triangles). The model calculations are performed with* $\mathrm{T_{vib}}=300$ K. *Both experimental results and simulation are probing the lowest rotational states (*$J''\in\{\frac{1}{2},\ldots,4\frac{1}{2}\}$*) of the coinciding* $\mathsf{Q}_{11}+\mathsf{P}_{21}$ *branches of the NO*$(1,1)$ γ*-band.*

fluence (triangles). The contribution to the population from the IR laser (circles) is obtained by subtraction of the thermal background from the total REMPI signal. In the low-fluence limit the observed yield is expected to be proportional to F^N, where N is the number of photons involved in the excitation process. The observed order of the excitation to $v''=1$ is found to be $N_1=0.86(20)$. The solid curves are calculated REMPI signals, in- and excluding the contribution from the thermal background. The model calculations fit the data very well.

Fig. 6.11 shows the REMPI signal from the population in $v''=2$ as a function of the IR fluence (triangles) and the same signal, after subtraction of the thermal background (circles). The order of the excitation to $v''=2$ is found to be $N_2=1.75(20)$. The solid curves are calculated REMPI signals, in- and excluding the contribution from the thermal background. Again, the prediction fits the data very well.

Fig. 6.12 shows the REMPI signal from the population in $v''=3$ as a function of the IR fluence (triangles) and the same signal, after subtraction of the thermal background (circles). The order of the excitation to $v''=3$ is found to be $N_3=2.85(20)$. The solid curves are calculated REMPI signals, in- and excluding the contribution from the thermal background. Except for the scaling by a factor 3 in the intensity between theory and experiment, the prediction fits the data very well. The factor of three is probably due to reduced power in the low frequency part of the spectrum of the IR pulse. These low-frequency components are essential to drive the $v''=2$ to $v''=3$ transition. The observed orders N_v equal the number of the excitation process within experimental error. Both from the measured and computed intensity dependencies it is

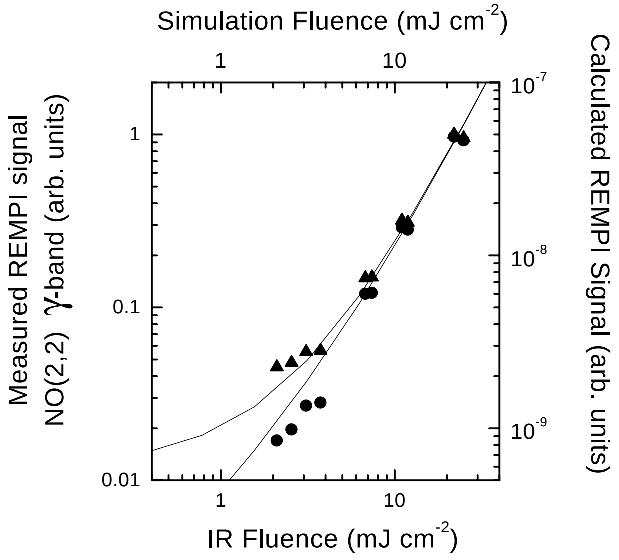

Figure 6.11: *A comparison of the rate of population of NO* $X\,^2\Pi_{\frac{1}{2}}(v''\!=\!2)$ *as a function of intensity between experimental results (points) and predicted by model calculations (solid curves). To obtain the transfer by the IR laser field (circles), the background signal from thermal population of* $v''=2$ *(*$\mathrm{T_{vib}}=300$ K*) is subtracted from the recorded signal (triangles). The model calculations are performed with* $\mathrm{T_{vib}}=300$ K. *Both experimental results and simulation are probing the lowest rotational states (*$J''\in\{\frac{1}{2},\ldots,4\frac{1}{2}\}$*) of the coinciding* $\mathsf{Q}_{11}+\mathsf{P}_{21}$ *branches of the NO*$(2,2)$ γ*-band.*

clear that the present experiment has been performed in the low fluence regime.

6.6 Forecast on vibrational ladder climbing in the Rabi-cycling regime

Fig. 6.13 shows the intensity dependency of the population of $v''=0,\ldots,4$ as calculated for large fluence range for chirp $\alpha=-0.6\times10^{-25}$ s^2 and a Gaussian laser pulse with $\nu=1{,}850$ cm^{-1} and $\Delta\nu=40$ cm^{-1}. The number of state in the basis set used for the calculation is enlarged for convergence of the calculation: $J''\in\{\frac{1}{2},\ldots,19\frac{1}{2}\}$ and all the corresponding m_J sublevels and $v''\in\{0,\ldots,6\}$. The total population in $|v\rangle$ is shown as the solid curves, the contribution of the IR laser as the curves with symbols. Compared to similar curves for $\alpha=0$ (not shown) the population in each state $|v\rangle$ is enhanced by about one order of magnitude. As in the previous figures the onset of significant contributions to the population by the IR laser pulse is at a fluence of $\Phi\approx5$ mJ cm^{-2}. Significant depletion of the ground state $v''=0$ is predicted for a fluence of $\Phi\approx10^4$ mJ cm^{-2}, indicating that non-linear population dynamics are starting. A typical Rabi frequency for this fluence is $\Omega_{\mathrm{Rabi}}\approx2\times10^{12}$ Hz, which, combined with the pulse duration of 0.9 ps makes the pulse area $A_{\mathrm{Rabi}}\approx1.8$. At a fluence of $\Phi\approx2\times10^4$ mJ cm^{-2} the population of $|2\rangle$ is suddenly enhanced, while transfer to higher vibrational states is stalking. A possible explanation is that, due to the strong coupling by the laser field, the enclosed areas

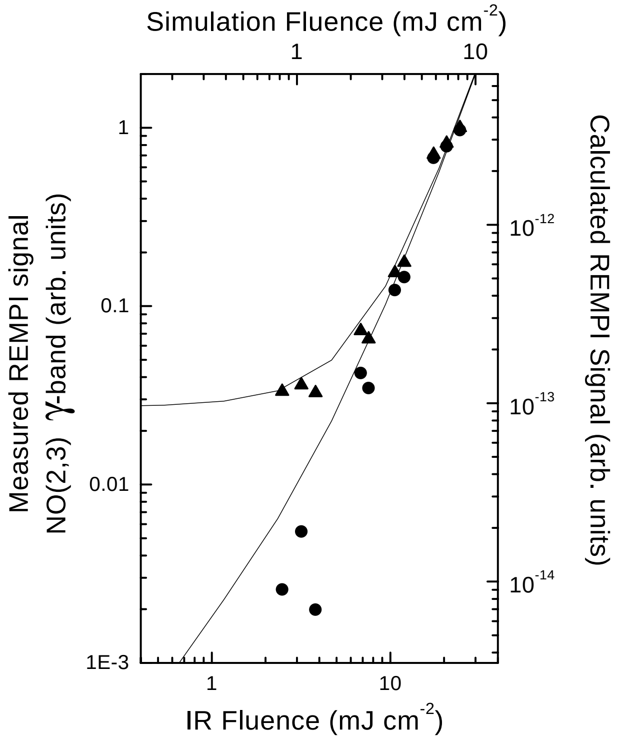

Figure 6.12: *A comparison of the rate of population of NO* $X\,^2\Pi_{\frac{1}{2}}(v''=3)$ *as a function of intensity between experimental results (points) and predicted by model calculations (solid curves). To obtain the transfer by the IR laser field (circles), the background signal from thermal population of* $v''=3$ ($\mathrm{T_{vib}}=300$ K) *is subtracted from the recorded signal (triangles). The model calculations are performed with* $\mathrm{T_{vib}}=300$ K. *Both experimental results and simulation are probing the lowest rotational states* ($J''\in\{\frac{1}{2},\ldots,4\frac{1}{2}\}$) *of the coinciding* $\mathsf{Q}_{11}+\mathsf{P}_{21}$ *branches of the NO*$(2,3)$ γ*-band.*

between different paths change. The particular value of the chirp ($\alpha=-0.6\times10^{-25}$ s^2) has been chosen because in the low fluence limit a constructive interference showed the population transfer to $v''=3$ to be optimal. Consequently, any change in enclosed areas then would change the interference periods, which could cause a reduction the total transfer efficiency.

Finally, for the highest intensities, the population of the highest vibrational states not only become of the same order of magnitude as the ground state population. Even population inversion can be seen: for fluences above $\Phi>5\times10^4$ mJ cm^{-2} the population in $v''=3$ is larger than the population of $v''=2$.

A closer inspection of the population distribution over the excited states, shows that with increasing intensity and with increasing vibrational quantum number, a larger fraction of the population resides in the lowest m_J states. Consequently, for the residual population in the vibrational ground state the contrary is true. This demonstrates the propensity of the excitation process to select that subset of molecules that have their dipole moment (anti-)parallel to the polarization vector of the laser field.

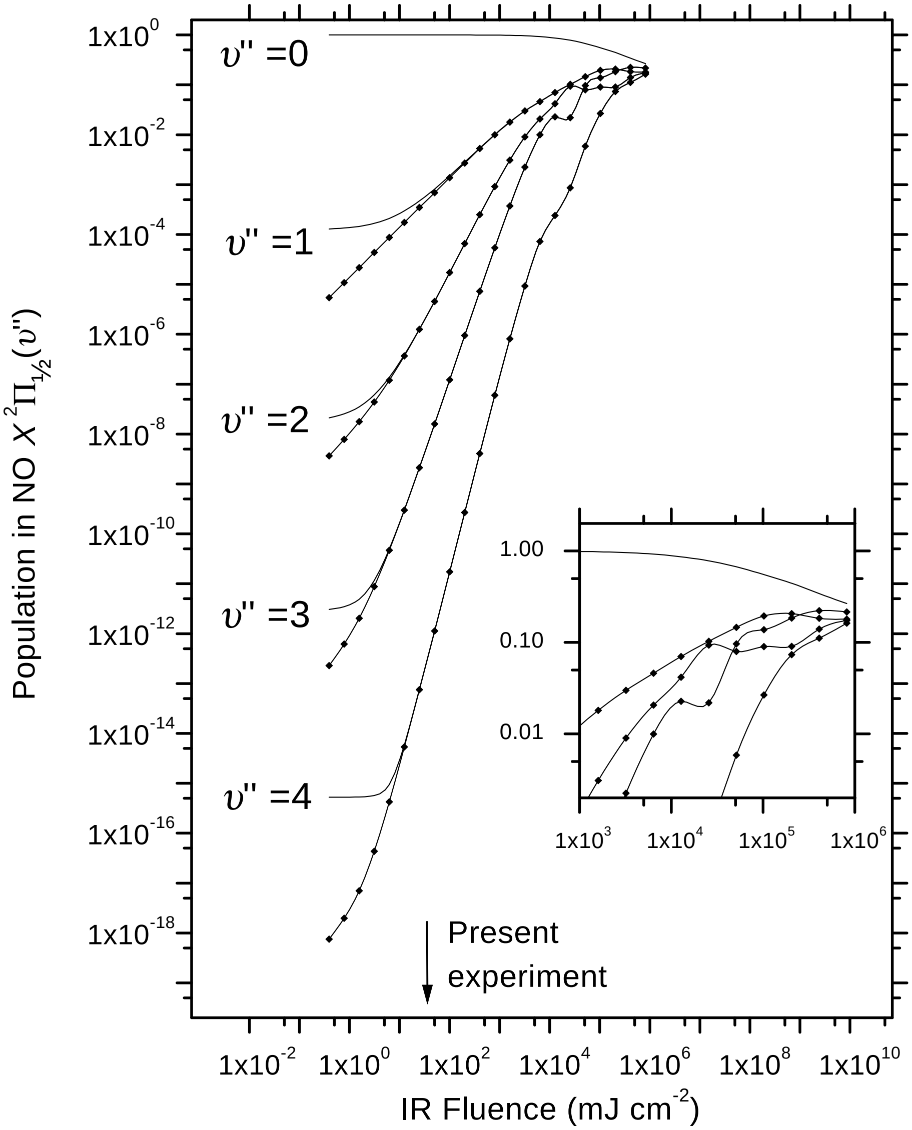

Figure 6.13: *Population distribution over the vibrational states* $v''=0,\ldots,4$ *of the NO* $X\,^2\Pi_{\frac{1}{2}}$ *ground state as a function of IR laser intensity* ($\nu=1{,}850$ cm^{-1}, $\Delta h\nu=40$ cm^{-1})*, starting with a Boltzmann distribution with* $\mathrm{T}_{\mathrm{rot}}=14$ K *and* $\mathrm{T}_{\mathrm{vib}}=300$ K *(typical supersonic beam conditions). The solid curves display the final population, the solid curves with symbols show the population transfer by the IR laser field (for* $v''=1,\ldots,4$ *only). The inset shows a close-up of the high-intensity range for the same data as in the main panel.*

6.7 Summary

In this chapter a more general notion on the quantum interference has been developed, relating the area enclosed by two interfering paths with the oscillation period in chirp. A nomenclature for the interfering paths is introduced. It is the first time that these rotational interferences are observed. The above-mentioned notion explains the observed rotational interferences completely. Although generally the anharmonicity of a vibrational ladder of a molecule is negative, it is found that the anharmonicity of the ro-vibrational ladder depends on the rotational quantum number J, and can very well become positive. This implies that the sign of the chirp that is required to follow the ladder anharmonicity depends on both the rotational level and the pathway in the dressed-level diagram that is followed. Next, a model is described for the calculation of the population distribution over the ro-vibrational states as created by a resonant chirped IR laser pulse. The model is applied to the electronic ground state of NO. It is the first time that calculations are performed on population transfer in a single electronic state of a molecule by a chirped laser pulse that take rotational J-levels and m_J-sublevels fully into account. For the low fluence regime excellent agreement is found between experiment and theory. Finally, some predictions have been made of the efficiency of vibrational population transfer in the high-fluence regime.

References

---

[1] J. A. Moulijn, P. W. N. M. van Leeuwen, and R. A. van Santen, editors, *Catalysis: an integrated approach to homogeneous, heterogeneous and industrial catalysis*, Elsevier, Amsterdam, first edition, 1993.

[2] R. A. van Santen and J. W. Niemantsverdriet, *Chemical kinetics and catalysis*, Fundamental and applied catalysis, Plenum Press, New York, 1995.

[3] G. A. Somorjai, *Introduction to surface Chemistry and catalysis*, John Wiley & Sons, New York Chichester Brisbane Toronto Singapore, 1995.

[4] T. H. Maiman, *Stimulated optical radiation in Ruby*, Nature **187**, 493 (1960).

[5] B. D. Josephson, *Possible new effects in superconductive tunnelling*, Phys. Lett. **1**, 251 (1962).

[6] K. von Klitzing, G. Dorda, and M. Pepper, *New method for high-accuracy determination of the fine-structure constant based on quantized Hall resistance*, Phys. Rev. Lett. **45**, 494 (1980).

[7] L. R. Khundkar and A. H. Zewail, *Ultrafast molecular reaction dynamics in real-time: Progress over a decade*, Annu. Rev. Phys. Chem. **41**, 15 (1990).

[8] J. Maddox, *Towards real-time molecular demolition?*, Nature **360**, 103 (1992).

[9] W. S. Warren, H. Rabitz, and M. Dahleh, *Coherent control of quantum dynamics: The dream is alive*, Science **259**, 1581 (1993).

[10] D. G. Truhlar and A. D. Isaacson, *Statistical-diabatic model of state-selected reaction rates. Theory and application of vibrational-mode correlation analysis to* $OH(n_{OH})+H_2(n_{HH})\rightarrow H_2O+H$, J. Chem. Phys. **77**, 3516 (1982).

[11] A. Sinha, M. C. Hsiao, and F. F. Crim, *Bond-selected bimolecular chemistry:* $H+HOD(4\nu_{OH})\rightarrow OD+H_2$, J. Chem. Phys. **92**, 6333 (1990).

[12] A. Sinha, M. C. Hsiao, and F. F. Crim, *Controlling bimolecular reactions: Mode- and bond-selected reaction of water with hydrogen atoms*, J. Chem. Phys. **94**, 4928 (1991).

[13] M. J. Bronikowski, W. R. Simpson, and R. N. Zare, *Effect of reagent vibration on the H+HOD reaction: An example of bond-specific chemistry*, J. Chem. Phys. **97**, 2194 (1993).

[14] M. J. Bronikowski, W. R. Simpson, and R. N. Zare, *Comparison of reagent stretch vs bend excitation in the* $H+D_2O$ *reaction: an example of mode-selective chemistry*, J. Chem. Phys. **97**, 2204 (1993).

[15] R. B. Metz, J. D. Thoemke, J. M. Pfeiffer, and F. F. Crim, *Selectively breaking either bond in the bimolecular reaction of HOD with hydrogen atoms*, J. Chem. Phys. **99**, 1744 (1993).

[16] W. S. Benedict, N. Gailar, and E. K. Plyler, *Rotation-vibration spectra of deuterated water vapor*, J. Chem. Phys. **24**, 1139 (1956).

[17] J. Franck, *Elementary processes of photochemical reactions*, Trans. Faraday Soc. **21**, 536 (1925).

[18] E. U. Condon, *Nuclear motions associated with electron transitions in diatomic molecules*, Phys. Rev. **32**, 858 (1928).

[19] S. Chelkowski, A. D. Bandrauk, and P. B. Corkum, *Efficient molecular dissociation by a chirped ultrashort infrared laser pulse*, Phys. Rev. Lett. **65**, 2355 (1990).

[20] S. Chelkowski and A. D. Bandrauk, *Control of vibrational excitation and dissociation of small molecules by chirped intense infrared laser pulses*, Chem. Phys. Lett. **186**, 264 (1991).

[21] K. Bergmann and B. W. Shore, *Coherent population transfer*, volume 4 of *Adv. Phys. Chem.*, chapter 9, pp. 315–373, World Scientific, Singapore New Jersey London Hong Kong, 1995.

[22] R. B. Vrijen, G. M. Lankhuijzen, D. J. Maas, and L. D. Noordam, *Adiabatic population transfer in multiphoton processes*, Comments At. Mol. Phys. **33**, 67 (1996).

[23] R. Loudon, *The quantum theory of light*, Clarendon Press, Oxford, second edition, 1983.

[24] L. Landau, *Zur Theorie der Energieübertragung bei Stössen*, Phys. Z. Sowjetunion **1**, 88 (1932).

[25] L. Landau, *Zur Theorie der Energieübertragung II*, Phys. Z. Sowjetunion **2**, 46 (1932).

[26] C. Zener, *Non-adiabatic crossing of energy levels*, Proc. R. Soc. London A **137**, 696 (1932).

[27] F. Bloch, *Nuclear induction*, Phys. Rev. **70**, 460 (1946).

[28] B. W. Shore, *The theory of coherent atomic excitation*, John Wiley & Sons, New York Chichester Brisbane Toronto Singapore, 1990.

[29] B. Broers, H. B. van Linden van den Heuvell, and L. D. Noordam, *Efficient population transfer in a three-level ladder system by frequency-swept ultrashort laser pulses*, Phys. Rev. Lett. **69**, 2062 (1992).

[30] P. Balling, D. J. Maas, and L. D. Noordam, *Interference in climbing a quantum ladder system with frequency-chirped laser pulses*, Phys. Rev. A **50**, 4276 (1994).

[31] Y. B. Band and P. S. Julienne, *Molecular population transfer, alignment, and orientation using chirped pulse absorption*, J. Chem. Phys. **97**, 9107 (1992).

[32] C. Liedenbaum, S. Stolte, and J. Reuss, *Inversion produced and reversed by adiabatic passage*, Phys. Rev. **178**, 1 (1989).

[33] E. C. G. Stueckelberg, *Theorie der unelastische Stösse zwischen Atomen*, Helv. Phys. Acta **5**, 369 (1932).

[34] G. Herzberg, *Molecular spectra and molecular structure*, volume I. Spectra of diatomic molecules, Van Nostrand Reinhold Company, second edition, 1966.

[35] G. Herzberg, *Molecular spectra and molecular structure*, volume II. Infrared and Raman spectra of polyatomic molecules, Van Nostrand Reinhold Company, thirteenth edition, 1986.

[36] G. Herzberg, *Molecular spectra and molecular structure*, volume III. Electronic spectra of polyatomic molecules, Van Nostrand Reinhold Company, first edition, 1966.

[37] H. Lefebvre-Brion and R. W. Field, *Perturbations in the spectra of diatomic molecules*, Academic Press Inc., San Diego, New York, Boston, London, Sydney, Tokyo, Toronto, first edition, 1986.

[38] A. P. Thorne, *Spectrophysics*, Chapman and Hall Ltd, London, second edition, 1982.

[39] J. T. Hougen, *The calculation of rotational energy levels and rotational line intensities in diatomic molecules*, NBS Monograph (1970).

[40] F. A. Jenkins, *Report of subcommitee f (notation for the spectra of diatomic molecules)*, J. Opt. Soc. Am. **43**, 425 (1953).

[41] Joint comission for Spectroscopy of the International Astronomical Union and the International Union of Pure and Applied Physics, *Report on notation for the spectra of polyatomic molecules*, J. Chem. Phys. **23**, 1997 (1955).

[42] A. A. Radzig and B. M. Smirnov, *Reference data on atoms, molecules and ions*, chapter 10, Number 31 in Chemical Physics, Springer-Verlag, first edition, 1980.

[43] W. G. Mallard, J. H. Miller, and K. C. Smyth, *Resonantly enhanced two-photon photoionization of NO in an atmospheric flame*, J. Chem. Phys. **76**, 3483 (1982).

[44] R. Engleman, Jr. and P. E. Rouse, *The β- and γ-bands of Nitric Oxide observed during the flash photolysis of Nitrosyl Chloride*, J. Mol. Spectrosc. **37**, 240 (1971).

[45] D. T. Biernacki, S. D. Colson, and E. E. Eyler, *High resolution laser spectroscopy of NO: The A, v=1 state and a series of nf, v=1 Rydberg states*, J. Chem. Phys. **89**, 2599 (1988).

[46] G. Reiser, W. Habenicht, K. Müller-Dethlefs, and E. W. Schlag, *The ionization energy of nitric oxide*, Chem. Phys. Lett. **152**, 119 (1988).

[47] H. Zacharias, F. de Rougemont, T. F. Heinz, and M. M. T. Loy, *Ionization probabilities of* $A\,^2\Sigma^+(v'{=}0,1,2)$ *and* $B\,^2\Pi(v'{=}0,2)$ *states of NO*, J. Chem. Phys. **105**, 111 (1996).

[48] D. Oepts, A. F. G. van der Meer, and P. W. van Amersfoort, *The free-electron-laser user facility FELIX*, Infrared Phys. Technol. **30**, 297 (1995).

[49] G. M. H. Knippels, R. F. X. A. M. Mols, A. F. G. van der Meer, D. Oepts, and P. W. van Amersfoort, *Intense far-infrared free-electron-laser pulses with a length of six optical cycles*, Phys. Rev. Lett. **75**, 1755 (1995).

[50] A. A. Radzig and B. M. Smirnov, *Reference data on atoms, molecules and ions*, Number 31 in Chemical physics, Springer-Verlag, first edition, 1980.

[51] A. Lindgård and S. V. Nielsen, *Transition probabilities for the alkali isoelectronic sequences Li I, Na I, K I, Rb I, Cs I, Fr I*, Atomic Data and Nuclear Data Tables **19**, 533 (1977).

[52] R. B. Vrijen, D. I. Duncan, and L. D. Noordam, *Limitations on quantum ladder climbing in complex systems*, Phys. Rev. A **56**, 2205 (1997).

[53] R. B. Vrijen, *Rydberg atoms in intense electromagnetic radiation*, PhD thesis, Universiteit van Amsterdam, 1997.

[54] J. H. Hoogenraad, *Rydberg atoms in picosecond optical and far-infrared laser pulses*, PhD thesis, Universiteit van Amsterdam, 1996.

[55] R. N. Zare, *Reactions á la mode*, Nature **365**, 105 (1993).

[56] For general references see the feature issue, *Femtosecond chemistry, the Berlin conference*, 1993.

[57] B. W. Shore, K. Bergmann, A. Kuhn, S. Schiemann, J. Oreg, and J. H. Eberly, *Laser-induced population transfer in multistate systems: A comparative study*, Phys. Rev. A **45**, 5297 (1992).

[58] J. S. Melinger, A. Hariharan, S. R. Gandhi, , and W. S. Warren, *Adiabatic population inversion in* I_2 *vapor with picosecond laser pulses*, Chem. Phys. Lett. **95**, 2210 (1991).

[59] J. S. Melinger, S. R. Gandhi, A. Hariharan, J. X. Tull, and W. S. Warren, *Generation of narrowband inversion with broadband laser pulses*, Phys. Rev. Lett. **68**, 2000 (1992).

[60] A. N. Buijserd, H. B. van Linden van den Heuvell, W. J. van der Zande, and H. G. Muller, *Opent de ontwikkeling van de Ti:saffier laser een nieuw tijdperk in de fs en ps lasertechnologie?*, van A tot Q **4**, 27 (1993).

[61] J. Agostinelli, G. Harvey, T. Stone, and C. Gabel, *Optical pulse shaping with a grating pair*, Applied Optics **18**, 2500 (1979).

[62] A. M. Weiner, J. P. Heritage, and E. M. Kirschner, *High-resolution femtosecond pulse shaping*, J. Opt. Soc. Am. B **5**, 1563 (1988).

[63] L. Allen and J. H. Eberly, *Optical resonance and two-level atoms,* Interscience monographs and texts in physics and astronomy, volume XXVIII, John Wiley & Sons, New York London Sydney Toronto, first edition, 1975.

[64] E. B. Treacy, *Optical pulse compression with diffraction gratings*, IEEE J. of Quantum Electronics **5**, 454 (1969).

[65] A. E. Siegman, *Lasers*, University Science Books, Mill Valley, California, 1986.

[66] R. R. Freeman and P. H. Buckbaum, *Investigations of above-threshold ionization using subpicosecond laser pulses*, J. Phys. B **24**, 325 (1991).

[67] J. Parker and C. R. Stroud, Jr., *Population trapping in short-pulse laser ionization*, Phys. Rev. A **41**, 1602 (1990).

[68] P. Balling, *The structure and dynamics of atomic negative ions*, PhD thesis, University of Århus, 1995.

[69] I. I. Sobelman, *Atomic spectra and radiative transitions*, volume 1 of *Chemical Physics*, Springer Verlag, Berlin Heidelberg New York, first edition, 1979.

[70] H. G. Muller, *Photoionisation of atoms in strong radiation fields*, PhD thesis, Vrije Universiteit, 1985.

[71] M. Aymar, E. Luc-Koenig, and F. Combet Farnoux, *Theoretical investigation on photoionization from Rydberg states of lithium, sodium and potassium*, J. Phys. B **9**, 1279 (1976).

[72] L. Allen and C. R. Stroud, *Broadening and saturation in n-photon absorption*, Phys. Rep. **91**, 1 (1982).

[73] R. C. Constantinescu, *Generation of soft X-radiation and application to multiphoton processes*, PhD thesis, Vrije Universiteit, 1997.

[74] C. E. Moore, *Atomic energy levels as derived from the analysis of optical spectra. Volume II*, U. S. Government Printing Office, Washington D. C. first edition, 1952.

[75] M. Berek, *Zur Messung der Doppelbrechung hauptsächlich mit Hilfe des Polarisationsmikroskops*, Zbl. Miner. Geol. Paläont. **1**, 388 (1913).

[76] M. Berek, *Zur Messung der Doppelbrechung hauptsächlich mit Hilfe des Polarisationsmikroskops (Fortsetzung)*, Zbl. Miner. Geol. Paläont. **1**, 427 (1913).

[77] M. Berek, *Zur Messung der Doppelbrechung hauptsächlich mit Hilfe des Polarisationsmikroskops (Schluß)*, Zbl. Miner. Geol. Paläont. **1**, 464 (1913).

[78] M. Berek, *Berichtigung und Nachtrag zu meiner Mitteilung "Zur Messung der Doppelbrechung usw."*, Zbl. Miner. Geol. Paläont. **1**, 580 (1913).

[79] T. W. B. Kibble, *Mutual refraction of electrons and photons*, Phys. Rev. **150**, 1060 (1966).

[80] D. C. Jacobs, R. J. Madix, and R. N. Zare, *Reduction of 1+1 resonance enhanced MPI spectra to populations: Application to the NO* $A\,^2\Sigma^+ - X\,^2\Pi$ *system*, J. Chem. Phys. **85**, 5469 (1986).

[81] V. N. Bagratashvili, V. S. Letokhov, A. A. Makarov, and E. A. Ryabov, *Multiple photon absorption and excitation of lower vibrational molecular levels*, chapter 5, and references therein, Harwood, first edition, 1985.

[82] P. A. Schulz, Aa. S. Sudbø, D. J. Krajnovich, H. S. Kwok, Y. R. Shen, and Y. T. Lee, *Multiphoton dissociation of polyatomic molecules*, Annu. Rev. Phys. Chem. **30**, 379 (1979).

[83] P. Rabinowitz, A. Kaldor, A. Gnauck, R. L. Woodin, and J. S. Gethner, *Two-color infrared isotopically selective decomposition of* UF_6, Opt. Lett. **7**, 212 (1982).

[84] C. Liedenbaum, S. Stolte, and J. Reuss, *Multiphoton excitation of molecules by single mode CW lasers*, Infrared Phys. **29**, 397 (1989).

[85] G. von Helden, I. Holleman, G. M. H. Knippels, A. F. G. van der Meer, and G. Meijer, *Infrared resonance enhanced multiphoton ionization of fullerenes*, Phys. Rev. Lett. **79**, 5234 (1997).

[86] S. Chelkowski and A. D. Bandrauk, *Control of molecular vibrational excitation and dissociation by chirped intense infrared laser pulses. Rotational effects*, J. Chem. Phys. **99**, 4279 (1993).

[87] G. M. H. Knippels, A. F. G. van der Meer, R. F. X. A. M. Mols, P. W. van Amersfoort, R. B. Vrijen, D. J. Maas, and L. D. Noordam, *Generation of frequency-chirped pulses in the far-infrared by means of a sub-picosecond free-electron laser and an external pulse shaper*, Opt. Commun. **118**, 546 (1995).

[88] G. Scoles, D. Bassi, U. Bick, and D. Laine, editors, *Atomic and molecular beam methods*, volume 1, Oxford University Press, New York, Oxford, 1988.

[89] F. P. Billingsley II, *Calculated vibration-rotation intensities for NO(X* $^2\Pi$*)*, J. Mol. Spectrosc. **61**, 53 (1976).

[90] A. E. Siegman, *Linear pulse propagation*, chapter 9, In Lasers [65], 1986.

[91] D. J. Maas, D. I. Duncan, A. F. G. van der Meer, W. J. van der Zande, and L. D. Noordam, *Vibrational ladder climbing in NO by ultrashort infrared laser pulses*, Chem. Phys. Lett. **270**, 45 (1997).

[92] R. Engleman, Jr., P. E. Rouse, H. M. Peek, and V. D. Baiamonte, *Beta and Gamma band systems of Nitric Oxide*, Los Alamos Scientific Lab Report **LA-4364**, 1 (1970).

[93] J. S. Melinger, S. R. Gandhi, A. Hariharan, D. Goswami, and W. S. Warren, *Adiabatic population transfer with frequency-swept laser pulses*, J. Chem. Phys. **101**, 6439 (1994).

[94] C. E. Hamilton, J. L. Kinsley, and R. W. Field, *Stimulated emission pumping: New methods in spectroscopy and molecular dynamics*, Annu. Rev. Phys. Chem. **37**, 493 (1986).

[95] S. Schiemann, A. Kuhn, S. Steuerwald, and K. Bergmann, *Efficient coherent population transfer in NO molecules using pulsed lasers*, Phys. Rev. Lett. **71**, 3637 (1993).

[96] K. H. Lehmann, G. Scoles, and B. H. Pate, *Intramolecular dynamics from eigenstate-resolved infrared spectra*, Annu. Rev. Phys. Chem. **45**, 241 (1994).

[97] R. N. Zare, *Angular momentum. Understanding spatial effects in chemistry and physics*, John Wiley & Sons, Inc., New York, Chichester, Brisbane, Toronto, Singapore, 1988.

[98] W. H. Press, S. A. Teukolsky, W. T. Vetterling, and B. P. Flannery, *Numerical recipes in Fortran*, Cambridge University Press, Cambridge, New York, second edition, 1992.

[99] A. V. Oppenheim, A. S. Willsky, and I. T. Young, *Signals and systems*, Prentice-Hall, London Sydney Toronto, 1983.

[100] D. C. Jacobs and R. N. Zare, *Reduction of 1+1 resonance enhanced MPI spectra to populations and alignment factors*, J. Chem. Phys. **85**, 5457 (1986).

[101] M. Planck, Verh. dt. phys. Ges. **2**, 202 (1900).

[102] M. Planck, Verh. dt. phys. Ges. **2**, 237 (1900).

[103] J. Ferguson-Lees and I. Willis, *Tirions vogelgids*, Tirion, Baarn, 1987.

SAMENVATTING

De wens om chemische reacties te kunnen sturen, heeft geleid tot pogingen om toestands-selectieve chemie te ontwikkelen. De idee is de uitkomst van een reactie de gewenste kant op gestuurd kan worden door één der reagentia naar een specifieke toestand te exciteren. Drie karakteristieken van die toestands-selectieve chemie zijn:

1. toestands-selectieve excitatie van op zijn minst één van de reagentia moet mogelijk zijn,
2. de aangeslagen toestand moet de reactiesnelheid van het geëxciteerde deel van het molecule verhogen,
3. het surplus aan energie moet binnen het geëxciteerde deel van het molecule gelokaliseerd blijven.

Of een bepaalde chemische reactie aan al deze eisen voldoet hangt sterk af van de eigenschappen van de reactie en de reagentia. Bovendien is er ook nog een geschikte excitatiemethode nodig. De experimenten die in dit proefschrift worden beschreven maken duidelijk dat excitatie van een vibratie-ladder in een molecule met behulp van getjilpte infrarode laserpulsen zich kan ontwikkelen tot zo'n excitatie methode.

In dit proefschrift worden de gevolgen van de wisselwerking van een sterk elektromagnetisch veld (bijvoorbeeld licht of warmtestraling) met een quantum-mechanisch "ladder-systeem" beschreven. Kenmerkend voor ladder-systemen is een opeenvolgend aantal toestanden in een atoom of molecule met een (bijna) gelijk energieverschil. In de figuur wordt de vibratie-ladder van een molecule vergeleken met de sporten van een ladder. In de muziek komt ook een ladder-systeem voor: de eerste sport kan worden vergeleken met de grondtoon, de tweede met een octaaf, de derde met het duo-decime (=octaaf+kwint), enzovoorts. In dit geval is de afstand tussen de sporten van de ladder telkens exact gelijk: een harmonische ladder. Echter, de ladder-systemen in het rubidiumatoom en stikstofmonoxide (NO) molecule die in dit proefschrift bestudeerd zijn, hebben een langzaam toe- of afnemend energieverschil tussen de sporten: ze zijn "vals" ofwel anharmonisch.

Zo'n ladder-systeem kan in een aangeslagen toestand worden gebracht door een elektron in het atoom of molecule heen-en-weer te slingeren. Eenmaal in zo'n aangeslagen toestand gebracht, vibreren de atomen in een molecule harder, of beschrijft het elektron grotere banen om de atoomkern. Hier komt het sterke elektromagnetische veld om de hoek kijken: het oefent krachten uit op de elektrisch geladen elektronen en atoomkernen waaruit atomen en moleculen bestaan. Volgens de quantummechanica heeft het elektromagnetische veld zowel een golf- als een deeltjeskarakter. De deeltjes waaruit het elektromagnetische veld opgebouwd wordt gedacht, heten fotonen. Max Planck postuleerde al in 1900 [101, 102] de idee dat deze "pakketjes straling" elk een bepaalde hoeveelheid energie bevatten die recht evenredig is met de frequentie waarop het elektromagnetische veld oscilleert. Wanneer de fotonenergie gelijk is aan het energieverschil tussen twee sporten van de ladder wordt de absorptie van zo'n foton opeens een stuk waarschijnlijker. Men spreekt dan van een resonant absorptieproces.

Een voorbeeld van een door resonantie versterkt "proces" is de toename van de uitwijking van een schommel wanneer je er met de resonantiefrequentie tegenaan duwt. Door resonante excitatie met de karakteristieke frequentie die bij een bepaalde schommel-lengte hoort komt de toegevoegde energie in de slingerbeweging terecht. Om de vergelijking met een atomair of moleculair ladder-systeem door te zetten zou je een schommels aan kabels van elastiek moeten ophangen. Deste harder de schommel slingert, deste langer de kabels worden, met als gevolg dat de "slingertijd" toeneemt. Om toch meer energie in de slingerbeweging te kunnen blijven stoppen moet de "duw-frequentie" afnemen.

Soortgelijke effecten treden ook op wanneer je met een zeer korte (en harde) stoot elektromagnetische straling aan een atoom of molecule schudt. Voor alle experimenten die in dit proefschrift beschreven worden, is hiervoor gebruik gemaakt van een zeer korte (pulsduur tot 10^{-13} seconde) en zeer intense lichtflits (intensiteit tot 10^{12} W cm^{-2}) afkomstig uit gepulste lasers. Een bijkomstigheid van de snelheid waarmee het elektromagnetische veld wordt aan- en uitgezet is dat de kleur (=frequentie) van de laserpuls niet langer scherp gedefinieerd is. De breedte van de frequentieband kan oplopen tot een paar procent van de centrale frequentie. Zulke pulsen zijn zeer geschikt om anharmonische ladder-systemen mee aan te slaan: ze zijn resonant met meerdere sporten van de ladder, terwijl de centrale frequentie voldoende selectief is om resonant te zijn met een specifieke ladder. Dit laatste is van belang bij de excitatie van moleculen die uit meerdere atomen bestaan: nu kunnen de atomen op verschillende manieren

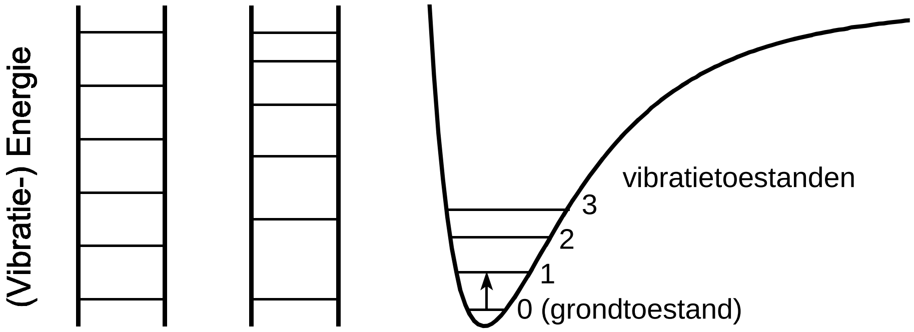

Figuur: *De linker figuur laat een "harmonische" ladder zien: alle sporten zitten even ver uit elkaar. De middelste ladder is anharmonisch: bij het bestijgen van de ladder neemt de afstand tussen de opeenvolgende sporten steeds verder af. De rechter figuur is een schematische weergave van een vibratie-ladder in een molecule. Zo'n ladder bestaat uit een reeks toestanden die beschrijven hoe hard de atomen waaruit een molecule bestaat ten opzichte van elkaar trillen. Ook deze ladder is anharmonisch: vibratietoestanden hoger op de ladder liggen steeds dichter bij elkaar. Een vibratietoestand is een toegestane toestand van het molecule. Des te hoger het molecule zich op de ladder begeeft des te meer vibratie-energie het bevat. De pijl geeft aan hoe een foton van een bepaalde frequentie (=hoeveelheid energie) een molecule kan aanslingeren.*

ten opzichte van elkaar vibreren. Elk van deze vibratie-manieren heeft een eigen resonantiefrequentie. Men hoopt dat de pulsen zo kort zijn dat resonante excitatie de extra energie kan toevoegen aan één bepaalde vibratie-ladder van het molecule.

In bijna alle hoofdstukken van dit proefschrift worden experimenten beschreven die zijn verricht met behulp van “getjilpte” laserpulsen. Het woord tjilp is geleend uit de biologie (zie Mus en Dwerguil [103]); het beschrijft een in de tijd veranderende toonhoogte. In de optica spreekt men van de tjilp van een laserpuls; ruwweg gesproken de kleurverandering als functie van de tijd, of, meer exact, de fase-relatie tussen de verschillende frequenties binnen de frequentieband. Voor een puls zonder tjilp komen alle frequenties gelijktijdig bij het atoom of molecule aan. Een negatieve tjilp correspondeert met een dalende frequentie, oftewel het laserlicht verkleurt van blauw naar rood tijdens de puls. Doordat de kleuren na elkaar komen duurt de flits langer, en is het licht minder intens. Voor de experimenten is een speciaal stuk optiek, een zogenaamde “puls-vervormer”, gebruikt om de precieze tjilp van de laserpuls te kunnen instellen. Omdat de conventionele puls-vervormer slechts in het zichtbare deel van het spectrum werkt is, in samenwerking met het FOM-instituut “Rijnhuizen”, een nieuw ontwerp voor gebruik in het infrarode deel van het spektrum ontworpen, getest en met succes in gebruik genomen. De zeer intense, ultrakorte laserpuls kan met behulp van de puls-vervormer zó getjilpt worden dat de verlopende frequentie over de opeenvolgende sporten van de anharmonische ladder schuift. Op deze manier wordt het atoom of molecule van de onderste sport van de ladder via sport 1, 2, enzovoorts, naar de hoogst bereikbare sport doorgeschoven. Het werk in dit proefschrift laat zien dat deze wijze van aanslingeren van het atoom of molecule brengt veel meer excitatie tot stand dan bestraling met alle energie van de laserpuls ineens (dus zonder tjilp).

Het genereren van zo’n klap optische of infrarode straling is de laatste jaren een stuk eenvoudiger geworden. Maar echt eenvoudig is het nog steeds niet: voor de experimenten beschreven in hoofdstuk 2 en 3 is gebruik gemaakt van de FOMFLITS-2 laser op AMOLF, de experimenten in hoofdstukken 4, 5 en 6 zijn mogelijk gemaakt door de gebruikersfaciliteit van de vrije-elektronen laser FELIX [48, 49]. Deze prachtige laser kan extreem korte pulsen infrarood licht maken op vrijwel elke moleculaire vibratie-overgangsfrequentie.

Nu volgt een korte beschrijving van de onderzochte ladder-systemen en de belangrijkste effecten die gevonden zijn.

Als eerste is een elektronische ladder in atomair rubidium (atoomgetal $Z = 37$) bekeken. Deze ladder heeft maar drie sporten: de grondtoestand $5s$, en de aangeslagen toestanden $5p$ en $5d$. Dit maakt het tot een ideaal “simpel-complex” modelsysteem. In hoofdstuk 2 is gekeken naar de efficiëntie van de excitatie van de grondtoestand $5s$ naar de boventoestand $5d$ als functie van de tjilp van de laserpuls. Bij de juiste tjilp neemt de excitatie-efficiëntie sterk toe. Ook worden oscillaties in de gecreëerde $5d$ populatie als functie van de tjilp waargenomen. Deze oscillaties worden toegeschreven aan interferentie tussen twee verschillende manieren van excitatie van de $5d$ toestand. De meest voor de hand liggende manier is het opeenvolgend bestijgen van de sporten van de ladder: eerst van $5s$ naar $5p$ en dan van $5p$ door naar $5d$.

Dit kan alleen wanneer de tjilp van de laserpuls de anharmoniciteit van de ladder volgt: het gaat immers twee keer om een resonant proces, en dan moet de fotonfrequentie passen op het energieverschil tussen de sporten van de ladder. De tweede wijze van excitatie van de $5d$ toestand is instantane absorptie van twee fotonen. Dit is in zekere zin ook een resonant proces: de som van de energie van twee fotonen past op het verschil tussen de eerste en derde sport van de ladder. Doordat de excitatietijdstippen voor de twee manieren van populatieoverdracht naar de boventoestand verschillen, is de fase van de twee bijdragen aan de totale populatie in de boventoestand verschillend. De precieze waarde van het faseverschil wordt bepaald door de grootte van de anharmoniciteit (het frequentieverschil tussen de twee overgangen) en de grootte van de tjilp. Dit interferentie-effect verklaart precies de waargenomen oscillatieperiode in de excitatie-efficiëntie als functie van de tjilp. Verder wordt in hoofdstuk 2 een model gepresenteerd op basis van integratie van de tijdsafhankelijke Schrödingervergelijking over de duur van de laserpuls. De voorspellingen uit dat model ondersteunen (bijna) alle kenmerken van de metingen.

In hoofdstuk 3 is hetzelfde ladder-systeem in het rubidiumatoom onderzocht, nu met nog intensere pulsen (tot 4×10^{11} W cm^2). De verschijnselen die zich in dit intensiteitsregime manifesteren kunnen worden verklaard met behulp van “Adiabatische Passage”: wanneer de frequentie van een voldoende intense laserpuls langzaam genoeg *over* de atomaire resonantiefrequenties heen wordt getjilpt, kan de golffunctie van het ladder+laser -systeem in een eigentoestand blijven. Adiabatische Passage treedt op wanneer de wisselwerking tussen twee toestanden A en B, met bijna dezelfde energie, langzaam in de tijd verandert. Door de sterke koppeling van toestand A met toestand B mengt het karakter van A met dat van B. Door het trage tempo van de verandering van de wisselwerking is het mogelijk *alle* elektronen die in toestand A zaten over te brengen naar toestand B. Een analogon uit het dagelijks leven is het passeren van een wissel, die is ingesteld om een trein van spoor A naar spoor B te laten wisselen, door een trein (= elektron). Wanneer de trein met een flinke vaart over de wissel rijdt merkt hij daar nauwelijks iets van en gaat hij rechtdoor (Diabatische Passage). Bij langzaam “passeren” vervolgt de *gehele* trein zijn reis netjes op het andere spoor: Adiabatische Passage. Bij tussenliggende snelheden gaat een deel van de trein door op spoor A en de rest op spoor B: er worden brokken gemaakt... Een elektron demonstreert in dat geval zijn golf-karakter: het kan zich verdelen over beide toestanden A én B.

Er bestaat een “criterium voor Adiabatische Passage”, dat voorspelt in hoeverre een bepaalde set laserpuls-parameters voor populatie-inversie kan zorgen. Het blijkt dat dit criterium voor één-foton processen onafhankelijk is van de tjilp, terwijl het criterium voor twee-foton processen omgekeerd evenredig is met de tjilp van de laserpuls.

Als er zo hard aan het ladder-systeem wordt geschud blijken er drie verrassende effecten op te treden. Uit de data blijkt dat de excitatie-efficiëntie als functie van de tjilp een *minimum* vertoont voor niet-getjilpte laserpulsen. Ten eerste is het ongebruikelijk dat niet-getjilpte laserpulsen, welke de *hoogste* intensiteit hebben, een proces minder efficiënt kunnen drijven dan getjilpte laserpulsen met dezelfde energie-inhoud. Ten tweede blijkt het ook mogelijk om de gehele populatie naar de boventoestand te transporten met laserpulsen welke een tjilp hebben die *tegen* de ladder-anharmoniciteit in gaat. Dit betekent dat het twee-foton proces dusdanig hard gedreven wordt dat, voor niet al te negatieve tjilp, aan het criterium voor Adiabatische Passage voor twee-foton processen is voldaan. Ten derde blijkt het interferentie-effect dat in hoofdstuk 2 is gevonden te verdwijnen wanneer de laserpuls-parameters voldoen aan het "criterium voor Adiabatische Passage" voor één-foton processen. In dat geval wordt de totale populatie via het sequentiele excitatiemechanisme overgebracht naar de boventoestand. Dus is er geen populatie in $5s$ over voor een bijdrage van het twee-foton proces. Dientengevolge is interferentie niet langer mogelijk.

De resterende hoofdstukken van dit proefschrift (4–6) gaan over vibratie-excitatie van het NO molecule door (on-)getjilpte infrarode pulsen. Verscheidene zaken compliceren het ladderklimmen in moleculen in vergelijking met de hierboven beschreven elektronische ladder in het rubidiumatoom. Ten eerste is de vibratie-ladder van de elektronische grondtoestand van NO 38 sporten hoog. Ten tweede kan een molecule behalve vibreren ook roteren. De rotatie-energie is voor de laagste 12 rotatietoestanden (veel) kleiner dan de gemiddelde energie die bij kamertemperatuur hoort (de Boltzmann-energief). Dus in plaats van een enkele grondtoestand, zoals bij het rubidiumatoom, hebben we nu met een groot aantal grondtoestanden te maken. Ten derde gaat excitatie van een vibratie vaak gepaard aan een verandering in de rotatie van het molecule. Dit zorgt voor een tamelijk complex geheel van koppelingen tussen de ro-vibrationele toestanden (de hoeveelheid interferenties die dit met zich meebrengt is geïnventariseerd in hoofdstuk 6). Tot slot is de sport-hoogte van de vibratie-ladder van het NO molecule vrij klein, met als gevolg dat de vibratie-overgangsfrequenties in het InfraRood (IR) liggen. Om toch in staat te zijn resonante excitatie van de ladder te bestuderen zijn deze experimenten uitgevoerd bij FELIX.

In elk van de hoofdstukken 4–6 is de populatieherverdeling, zoals die veroorzaakt is door de IR laser, vastgesteld met behulp van Resonantly Enhanced Multiphoton Ionization (REMPI), een methode waarbij de distributie van de populatie over zowel de rotatie- als de vibratietoestand van de NO moleculen kan worden vastgesteld.

In hoofdstuk 4 is het NO molecule bestraald met een pulstrein van ongeveer 130 pulsen. Populatie is getransporteerd tot aan $v''=5$ toe, de hoogste vibratietoestand die bereikt kan worden via overgangen binnen de bandbreedte van de IR laserpuls. De gemiddelde excitatie-efficiëntie bedraagt 17% per vibratie-overgang van $v''\!=\!1$ tot $v''\!=\!5$.

In hoofdstuk 5 worden de resultaten van metingen aan de tjilpafhankelijkheid van populatietransport naar aangeslagen vibratietoestanden gepresenteerd. Wanneer de frequentie van de getjilpte IR puls de anharmoniciteit in de vibratie-ladder volgt wordt de efficiëntie van de excitatie naar $v''=3$ tot een factor 6 verhoogd ten opzichte van ongetjilpte IR pulsen. Voor IR pulsen met een tegenovergestelde tjilp is juist een efficiëntie-reductie van 8 keer gemeten. In hetzelfde hoofdstuk wordt eveneens onderzocht hoe de populatie in aangeslagen vibratietoestanden zich verdeelt over de rotatietoestanden. De NO moleculen blijken een toename in de vibratie-energie van $\Delta\mathrm{E}_{\mathrm{vib}} \approx 5{,}500\ \mathrm{cm}^{-1}$ te combineren met een zeer geringe toename van $\Delta\mathrm{E}_{\mathrm{rot}} \approx 12.3\ \mathrm{cm}^{-1}$ in de rotatie-energie.

In de vibratie-ladder van een molecule zijn er veel verschillende manieren om het molecule van een specifieke grondtoestand naar een bepaalde eindtoestand op te slingeren. Het grote aantal excitiemanieren wordt door twee complicaties veroorzaakt: er zijn veel meer sporten in de vibratie-ladder (zoals gezegd, wel 38) dan in de rubidium-ladder, en bij elke sport van de vibratie-ladder kan het molecule ook nog eens met een groot aantal verschillende snelheden roteren. Zoals in hoofdstuk 2 is vastgesteld, kunnen twee verschillende manieren om een atoom van de grondtoestand te exciteren naar een aangeslagen toestand al zorgen voor een interferentie-effect. In hoofdstuk 6 wordt eerst de relatie vastgesteld tussen de ladder-anharmoniciteit en de oscillatieperiode die behoren bij interferentie tussen twee specifieke excitatiemanieren. Het hoofdstuk vervolgt met de introductie van een systematische nomenclatuur die een eenduidig symbool toekent aan elke excitatiemanier die een bepaalde begin- en eindtoestand met elkaar verbindt. Dan wordt een formalisme geïntroduceerd om de vibratie-excitatie van een molecule, zoals een getjilpte laserpuls die veroorzaakt, uit te rekenen. Dit model is, net als dat uit hoofdstuk 2, gebaseerd op numerieke integratie van de Schrödingervergelijking over de duur van de getjilpte laserpuls. Met dit model zijn voor het eerst voorspellingen gedaan over de herverdeling van de populatie over de rotatie- en vibratietoestanden waarbij de rotatietoestanden tot op zowel J- als m_J-niveau in acht zijn genomen. De uitkomsten vertonen inderdaad oscillaties als functie van de tjilp van de laserpuls, waarbij de periodes van de oscillaties exact overeenkomen met de voorspelling op grond van de ladder-anharmoniciteit. Vervolgens is het model toegepast op het NO molecule om de vibratieexcitatie door een laserpuls, zoals die door FELIX gegenereerd wordt, te voorspellen. De gevonden overeenkomst tussen het experimentele resultaat en de berekening is zeer goed. Zowel het model als het experiment laten zien dat het dusdanig tjilpen van de laserpuls, zodat de frequentie de sporten van de ladder volgt, de excitatie-efficiëntie aanzienlijk verhoogt: met een factor 10 voor $v'' = 3$. Hoofdstuk 6 besluit met een berekening van de efficiëntie van vibratie-excitatie door getjilpte IR laserpulsen met veel hogere pulsenergieën. Deze berekening voorspelt dat voor zeer hoge intensiteiten de grondtoestand (sport No. 0) “leeg” gepompt kan worden, terwijl het grootste deel van de moleculen, via enkele tussentoestanden (sporten 1, 2, enzovoorts), naar een hoog aangeslagen toestand getransporteerd kan worden.

In het begin van de samenvatting is de noodzaak van een snelle, toestands-selectieve excitatiemethode, naar voren gekomen. Gebleken is dat beklimmen van de vibratie-ladder wordt gecompliceerd door de rotatie-eigenschappen van een molecule. Uit de experimenten die in dit proefschrift worden beschreven wordt duidelijk dat vibratie-excitatie met behulp van getjilpte IR laserpulsen zich kan ontwikkelen tot zo’n excitatiemethode. Echter, om de vibratie-ladder efficiënt te beklimmen is het wel nodig dat de IR laserpulsen zo’n 10.000 keer sterker worden. Het nieuw ontwikkelde model kan de gevolgen van deze complicatie exact berekenen. Kortom, excitatie van moleculaire vibraties met behulp van intense getjilpte laserpulsen is een veelbelovende experimentele techniek. Bijvoorbeeld ten behoeve van het bedrijven van toestands-selectieve chemie, die nog in de kinderschoenen staat.